The Preparation of Silicon Nanocrystal-Based Materials for Biomedical Applications

by

Xiyu Zhang

A thesis submitted in partial fulfillment of the requirements for the degree of

Master of Science

Department of Chemistry
University of Alberta

Abstract

Silicon nanocrystals (SiNCs) are a biocompatible and elemental abundant sub-class of quantum dots. Since SiNCs were prepared, many efforts have been made to get a tunable size and rich surface chemistry that greatly expanded their applications from electronic devices to target treatments. Among all the potential applications, SiNCs have distinct advantages over fluorescent organic dyes in biomedical applications (e.g. bioimaging), such as high stability against photobleaching, long photoluminescence (PL) lifetime, and the ability of conjugating with other molecules to achieve dual-imaging or theranostics. However, their limited compatibility with water restrained their applications. Therefore, this thesis mainly focuses on preparing SiNCs with high water solubility without compromising their PL properties to extend their abilities for future use in biomedical applications.

The thesis starts with an introduction about two kinds of nanomaterials (SiNCs and dendrimers) used in the experimental parts, including properties, synthetic approaches, and applications. Chapter 2 focuses on building dendrimer structures (poly(amidoamine) and commercialized dendrons) on SiNCs to combine the complementary advantages of each material. In the divergent method, a series of stepwise reactions was performed on functionalized SiNCs, providing a promising path to build dendrimer structures on SiNCs. Some preliminary results of conjugating commercialized dendrons and SiNCs also are presented. Chapter 3 introduces a method to prepare amphiphilic SiNCs (AP-SiNCs) by thermal hydrosilylation of H-SiNCs with the mixed ligands. By studying the stabilities of SiNCs in buffer solutions, it is found that the stability of AP-SiNCs could be tuned by changing the duration of thermal hydrosilylation to adapt the needs of various applications. Chapter 4 presents the conclusions of each chapter and some future work related to water soluble SiNCs.

Preface

This thesis is an original work by Xiyu Zhang. The research was conducted under the supervision of Professor Jonathan G. C. Veinot at the Department of Chemistry, University of Alberta. No part of this thesis has been published previously.

In Chapter 2, I was responsible for designing the project, performing the experiments, carrying out material characterization, analyzing the data, and writing the material. Dr. Jonathan G. C. Veinot supervised the project and was involved with the thesis composition.

In Chapter 3, Dr. Muhammad Amirul Islam developed the method of preparing AP-SiNCs via mixed ligands. I designed the experiment to test the stability of SiNCs obtained from different reaction times, carried out material characterization, analyzed the data, and wrote the material. Dr. Jonathan G. C. Veinot supervised the project and was involved with the thesis composition.

Acknowledgments

My sincere thanks and gratitude to those who have helped and supported me throughout my MSc studies.

First, I would like to thank my supervisor, Dr. Jonathan G. C. Veinot, for his support and guidance. I will always be grateful for the opportunity you offered me so that I could learn and grow in this amazing university, University of Alberta.

I would like to thank my committee members, Dr. Arthur Mar, Dr. Mariusz Klobukowski, and Dr. Steven H. Bergens, for their valuable insight and comments.

I would like to thank all the past and present group members Dr. Muhammad Amirul Islam, Dr. Regina Sinelnikov, Dr. Maryam Aghajamali, Dr. Morteza Javadi, Dr. Philipp Kitschke, Dr. Angelique Faramus, Christopher Jay Robidillo, Haoyang Yu, Alyx Thiessen, Subha Jana, Md Asjad Hossain, Sarah Milliken, Yingjie He, I Teng Cheong, for their help and support throughout this process.

I would like to thank support and technical staff members, Dr. Wayne Moffat, Dr. Gareth Lambkin, Dr. Nathan Gerein, Peng Li, Dr. Shihong Xu, Dr. Anqiang He, for their assistance.

Special thanks to Dr. Anna Jordan for editing this thesis.

At last, I want to thank the most important people in my life, my family, for everything they have done for me.

Table of Contents

List of Figures

List of Schemes

List of Symbols, Nomenclature, and Abbreviations

a.u.	Arbitrary unit
AP-SiNC(s)	Amphiphilic silicon nanocrystal(s)
CB	Conduction band
dendron-G5-acetylene-OH	Polyester-32-hydroxyl-1-acetylene bis-MPA dendron, generation 5
dendron-G5-carboxyl-OH	Polyester-32-hydroxyl-1-carboxyl bis-MPA dendron, generation 5
DI-water	Deionized water
DLS	Dynamic light scattering
DMSO	Dimethyl sulfoxide
EDC	N-(3-dimethylaminopropyl)-N′-ethylcarbodiimide
FDA	Food and drug administration
FTIR	Fourier transform infrared
FWHM	Full widths at half-maximum
H-SiNC(s)	Hydride-terminated silicon nanocrystal(s)
HF	Hydrofluoric acid
HRXPS	High-resolution X-ray photoelectron spectroscopy
HSQ	Hydrogen silsesquioxane
in vitro	Studies performed with microorganisms, cells, or biological molecules outside their normal biological context
in vivo	Studies performed on whole, living organisms or cells
LED(s)	Light-emitting diode(s)
Milli-Q water	Purified water with resistivity of 18.2 MΩ·cm at 25 °C
NC(s)	Nanocrystal(s)
NMR	Nuclear magnet resonance spectroscopy
NP(s)	Nanoparticle(s)
PAMAM	Poly(amidoamine)
PBS	Phosphate-buffered saline
PEG	Polyethylene glycol
PEG ligands	Allyloxy (polyethylene oxide)
PL	Photoluminescence
PPE	Personal protective equipment
PPI	Poly(propyleneimine)

PTFE	Polytetrafluoroethylene
QD(s)	Quantum dot(s)
QLED	Quantum-dot light-emitting diodes
rpm	Revolutions per minute
SBF	Simulated body fluid
SiNC-ammonium	Organic ammonium ion terminated SiNCs
SiNC-ammonium-G0.5	PAMAM G0.5 terminated SiNCs starting from SiNC-ammonium
SiNC-ammonium-G1	PAMAM G1 terminated SiNCs starting from SiNC-ammonium
SiNC-ester	Ester terminated SiNCs
SiNC-ester-G0	PAMAM G0 terminated SiNCs starting from SiNC-ester
SiNC-ester-G0.5	PAMAM G0.5 terminated SiNCs starting from SiNC-ester
SiNC-ester-G1	PAMAM G1 terminated SiNCs starting from SiNC-ester
SiNC-ester-G1.5	PAMAM G1.5 terminated SiNCs starting from SiNC-ester
SiNC-ester-PAMAM	PAMAM terminated SiNCs starting from SiNC-ester
SiNC(s)	Silicon nanocrystal(s)
SiNC@dendrimer	SiNCs coated with dendrimer structures
SiNC@PAMAM	SiNCs coated with PAMAM dendrimer structures
SiNC@PPI	SiNCs coated with PPI dendrimer structures
SiNC/SiO2	Silicon nanocrystals embedded in a silica matrix
SOP	Standard operating procedure
Sulfo-NHS	N-hydroxysulfosuccinimide sodium salt
TBS	Tris-buffered saline
TGA	Thermal gravimetric analysis
UV	Ultraviolet
VB	Valence band
XPS	X-ray photoelectron spectroscopy

Chapter 1

Introduction

1.1 Nanomaterials and Nanoparticles

Nanomaterials, according to the European Commission, are materials that have nanoscale (1–100 nm) external dimensions or an internal/surface nanoscale structure.[1] Compared with their bulk counterparts, nanomaterials show different mechanical, optical, electric, and magnetic properties as well as chemical reactivity[2] because of surface and quantum effects.[3] Size dependent properties make nanomaterials potential candidates in numerous applications, such as catalysis,[4–6] sensors,[7-9] electronic devices,[10–12] bio-imaging,[13,14] and therapeutics.[14–16] Broadly speaking, nanomaterials are classified often into three categories: nanoparticles (zero-dimensional nanostructures), one-dimensional nanostructures (e.g., nanorods and nanowires), and two-dimensional nanostructures (e.g., nanosheets).[17] In this thesis, different types of nanoparticles will be introduced and studied.

1.2 Quantum Dots

Quantum dots (QDs) are semiconductor nanoparticles whose radii are smaller than the bulk material Bohr exciton radius, and have size-dependent optical response (e.g., photoluminescence (PL)).[18] In bulk semiconductors, continuous conduction and valence bands are formed by an infinite density of energy states. When material dimensions are decreased (< 10 nm), the density

of their electronic energy states correspondingly decreases, and discrete energy levels emerge, resulting in an increase in the band gap (Figure 1.1a[19]);[20,21] this phenomenon is known as quantum confinement.[22] If the band gap falls in the energy range of visible light, QD PL occurs through a radiative recombination of excitons (photogenerated electron-hole pairs).[23] An example of size dependent PL from CdSe QDs is shown in Figure 1.1b.[24] This QD property is being exploited in consumer products, such as Samsung QLED displays.

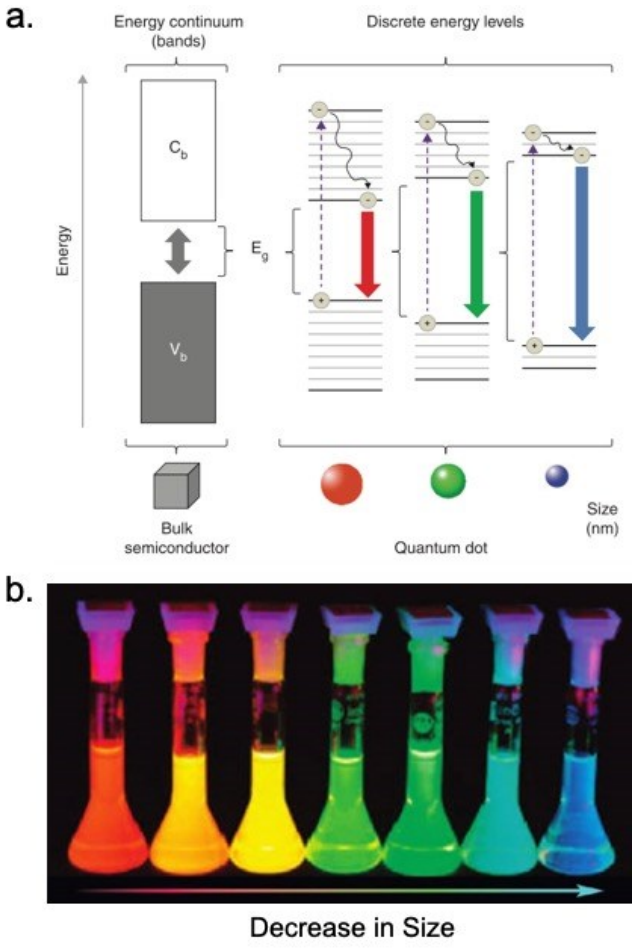

Figure 1.1. (a) A schematic representation of the relationship between the QD size and the QD band gap. Reprinted with permission from Reference 19. (b) A photograph showing size-dependent photoluminescence of CdSe/ZnS core-shell nanocrystals. Adapted with permission from Reference 24.

In the years following the discovery of the quantum size effects in CdS nanocrystals by Louis E. Brus and his colleagues in 1983,[25] there have been substantial efforts to develop different kinds of QDs, for example, group II-VI compounds (e.g., CdSe,[26] ZnS[27]), III-V compounds (e.g., InP,[28] GaAs[29]), Group 14 (e.g., Si,[30] Ge[31]), lead/tin halide perovskite (e.g., $CsPbX_3$, X = Cl, Br, and I[32]), and core-shell structures (e.g., CsSe@ZnS[33]), and to understand their fundamental properties. Although these QDs have potential applications in light-emitting diodes,[34] sensors,[35] and bioimaging,[36] etc., most suffer from the important drawback that they contain toxic (e.g., Cd, As)[37,38] or rare elements (e.g., Ga, In, Se)[39] that limits their applications; one exceptional class of QDs stands alone, Group 14 QDs (e.g., silicon nanocrystals).[40]

1.3 Silicon Nanocrystals

Silicon (Si) is the second most abundant element in the Earth's crust (about 28% by mass) and has been used widely in electronic devices.[41] The pioneering investigations on nanosized Si were carried out by Canham in 1990; by HF-etching a silicon wafer, he observed the visible photoluminescence from porous silicon.[42] Subsequently, different types of silicon QDs have been prepared and studied. When the dimensions of silicon QDs are decreased to near the bulk Bohr exciton radius (~ 5 nm), the band gap energy increases, discrete energy levels emerge, and PL shifts into the visible spectrum.[30] One subclass of QDs, silicon nanocrystals (SiNCs), show attractive optical properties, such as tunable PL within full visible light range, rich surface chemistry, emission in the solid-sate, and compatibility with existing electronics industry.[43,44]

Moreover, compared with other QDs, silicon nanocrystals have advantages, such as abundance, low toxicity, and long PL life time (tens of μs).[45–47] These properties make SiNCs attractive candidates for applications, such as LEDs,[48] photovoltaics,[49] sensors,[50,51] and biomedical fields.[47,52–54]

1.3.1 Silicon Nanocrystals Synthesis

Free standing SiNCs have been prepared using various physical and chemical approaches over the past three decades. As with all nanomaterials, the various approaches may be classified as physical, gas-phase, solution-phase, and solid-state methods. A detailed discussion of these methods is beyond the scope of this document; however, some key references are provided for context.

Physical methods, also known as "top-down" procedures, normally are involved in chemical/electrochemical etching,[55,56] laser ablating,[57] or ball milling[58] of a bulk silicon material (e.g., a silicon wafer). Significant drawbacks of these methods are poor size control and inefficient separation of particles. Gas-phase methods are performed by decomposing silane (silicon source) with a pulsed laser[59–62] or plasma.[63–65] These methods normally suffer from a broad size distribution caused by uncontrolled crystal growing. Solution-phase methods include two general strategies: the first is based on the decomposition of silanes/silane derivatives under high pressure and high temperature conditions in a suitable solvent;[66–68] the other involves reduction of $SiCl_4$ or $RSiCl_3$ using a reducing agent (e.g., Na,[69] Zintl salts,[70,71] and $LiAlH_4$[72,73]). A major limitation of

these methods is that the resulting SiNCs emit blue PL regardless of size (i.e., contrary to quantum confinement prediction).

Solid-state methods are performed by thermal processing of silicon-rich precursors (e.g., silicon-rich oxides[74–76] and silicon-rich polymers[77,78]). Under high temperature thermal processing (with slightly reducing atmosphere), these precursors undergo a disproportionation reaction to yield SiNCs embedded in a silica matrix; the resulting SiNCs can be liberated by HF etching. The Veinot group has reported a method to synthesize SiNCs via thermal annealing of hydrogen silsesquioxane (HSQ) (Scheme 1.1), a commercially available silicon-rich polymer with the empirical chemical formula $[HSiO_{3/2}]_n$. Thermal processing of HSQ under a reducing atmosphere (5% H_2, 95% Ar) yields SiNCs embedded in a silica matrix (SiNC/SiO_2 composite),[75] and the sizes (and shapes) of SiNCs can be tuned by varying the annealing temperature (1100–1400 °C) and/or the duration of annealing.[79–81]

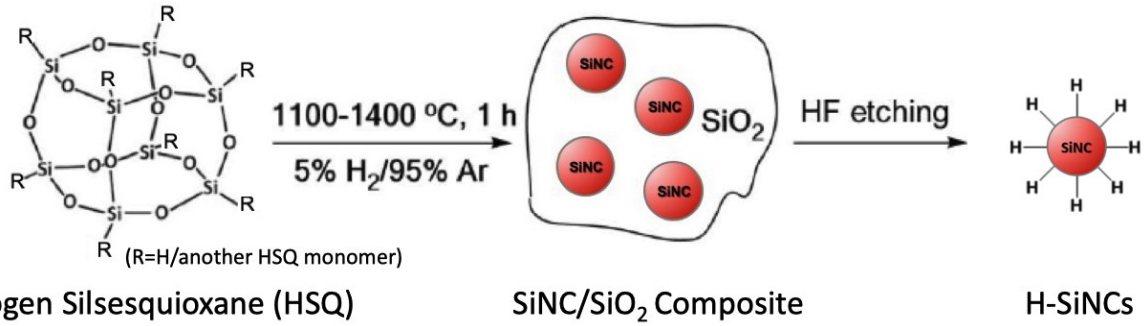

Scheme 1.1. Synthesis of SiNCs via the disproportionation of hydrogen silsesquioxane (HSQ). R=H/another HSQ monomer in the structure of HSQ.

1.3.2 Surface Chemistry of SiNCs

After HF-etching of a SiNC/SiO_2 composite to liberate the embedded SiNCs, the resulting free-standing hydride-terminated SiNCs (H-SiNCs) are incompatible with solution processing and tend to oxidize when exposed to air or moist atmosphere; therefore, passivating their surfaces becomes crucial.[82–84] Moreover, appropriate functionalization also can tune/enhance their PL properties[85,86] and provide tailorable surfaces to adapt the needs of varies applications.[87] To date, many functionalization methods have been reported, most of which are derived from the surface chemistry of bulk silicon.[30,40,43,88]

Hydrosilylation is the most common approach and involves reactions of surface Si-H bonds with unsaturated functional groups (e.g., alkene, alkyne) to form a stable Si-C bond.[88] A variety of conditions have been employed (e.g., heat,[89,90] UV light,[91] catalyst,[92] and radical initiator[93]) to trigger hydrosilylation reactions. Thermally induced hydrosilylation is used widely because it is straightforward and efficient. In a typical procedure, a mixture of H-SiNCs and a neat ligand are heated to 100–190 ℃. The ligand serves as both the solvent and reactant, and the elevated temperature induces cleavage of the Si-H bond to initiate the reaction. This reaction has been reported to yield ligand oligomers on the surfaces of SiNCs and provide a high surface coverage.[89] In this thesis, SiNCs with red/near-infrared PL were targeted because of their potential bio-medical application, and thermally induced hydrosilylation was used in Chapters 2 and 3 to modify NC surfaces.

1.3.3 Optical Properties of SiNCs

1.3.3.1 Quantum Confinement

Semiconductors can be classified in the context of their band gaps generally into two categories (direct and indirect), based upon whether the minimum of the conduction band (CB) and the maximum of the valence band (VB) are aligned in reciprocal space (k-space) (Scheme 1.2a-b). In a direct band gap semiconductor (e.g., CdSe) where the CB and VB are aligned, the radiative recombination of excitons (electron-hole pairs) is much faster than that in an indirect band gap semiconductor (e.g., Si) where the CB and VB are not aligned. This difference arises because to make an optical transition possible in an indirect band gap semiconductor, phonons (lattice vibrations) must be involved in the formation and recombination processes of exitons.[94,95] The probability of these events occurring is much higher for Si nanoparticles (< 5nm).[96–99] The origin of this behavior is the subject of much controversy and study. One explanation is that the wavefunctions of excitons in Si nanoparticles are broadened because of quantum confinement, leading to an increased possibility of overlap between the exciton wavefunctions (Scheme 1.2c), thereby achieving a higher chance of exciton formation and radiative recombination.[100–102]

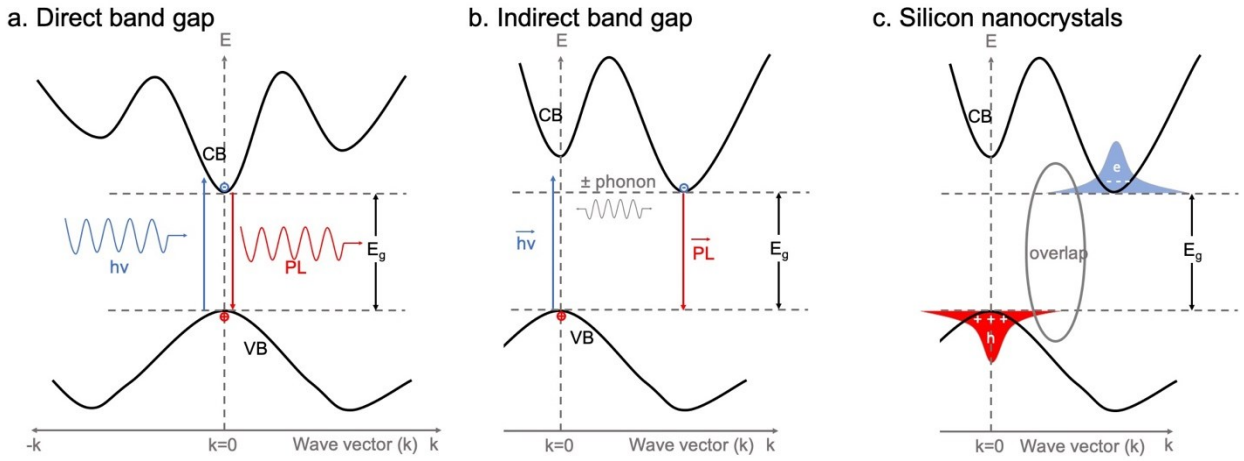

Scheme 1.2. Simplified band structure diagram of **(**a) a direct band gap semiconductor, (b) an indirect band gap semiconductor, and (c) Si nanoparticles with broaden wavefunction of excitons.

1.3.3.2 Surface effects

In addition to quantum confinement (size effect, Figure 1.2a),[75] the nature of the SiNC surfaces (surface defects and surface ligands) also plays important roles in their optical responses. Surface defects (silicon dangling bonds) and the silicon suboxide structure on the surfaces of SiNCs can influence optical properties.[103] Surface defects provide fast non-radiative traps for electrons and reduce the PL intensity.[104,105] However, the nature and effect of the silicon suboxide structure on the PL properties (blue or red-shift of the PL maxima) is still controversial. The formation of suboxide surface states, which lead to the recombination of excitons at the interface of a SiNC core and silicon suboxide shell, has been invoked to explain PL red-shifts,[106–109] while the reduction of silicon core size due to the surface oxidation is reported to explain the blue-shift in PL maxima.[110,111] Based on work by Sinelnikov et al., the effect of oxidation on the PL response of

SiNCs is size-dependent. The PL of larger SiNCs (d > 2.5 nm) blue-shifted after being exposed to moisture, while that of smaller SiNCs (d < 2.5 nm) red-shifted under the same conditions.[112]

Surface functionalization also can impact the PL properties of SiNCs. By passivating SiNCs of the same size (~ 3 nm) with different ligands, a series of colour emissions in the visible range was obtained (Figure 1.2b).[86] The resulting particles (except for dodecene functionalized SiNCs under inert conditinons) show fast radiative recombination rates (nanoseconds liftime), indicating that the PL comes from surface states.

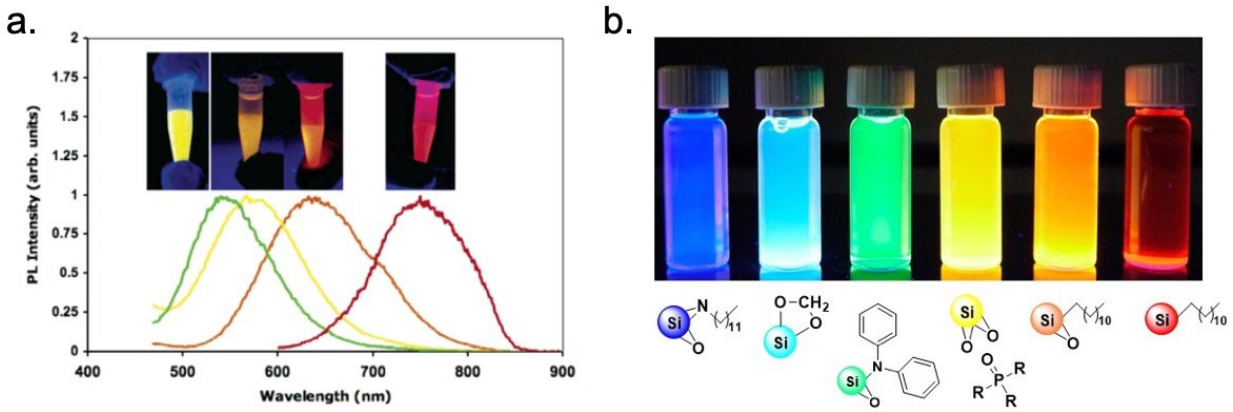

Figure 1.2. (a) PL emission of SiNCs with different sizes prepared by the solid-state method. Reprinted with permission from Reference 75. (b) PL emission of SiNCs passived by different ligands. Adapted with permission from Reference 88.

1.3.4 Biomedical Applications of SiNCs

Besides "shining" in numerous optical applications, such as LEDs,[48] photovoltaics,[49] sensors,[50,51] the exploration of bio-medical application of SiNCs[53,54] has gained attention because: i) the small sizes of SiNCs (<10 nm) make them easy to be transported in body fluid and/or into cells;[113] ii)

the bright red/near-infrared PL from SiNCs is distinguished readily from the autofluorescence of tissues;[114,115] iii) SiNCs have relatively high quantum yields (60–70 %) and high stability against photobleaching;[116] iv) silicon-based nanoparticles are biodegradable and show low toxicity (porous silicon based drug delivery products from pSivida Corp., MA, USA, have been approved by the FDA);[117] v) the long photoluminescence lifetime (microseconds) makes SiNCs ideal materials for time-gated imaging;[118] vi) the surface chemistry of SiNCs has been studied well, making it possible to build bioconjugable surfaces on SiNCs;[87,89,119] and vii) SiNCs show potential as magnetic resonance imaging contrast agents[120] and induction heating agents,[121,122] which leads to their application in dual-imaging and/or theranostics.

SiNCs have been applied in bioimaging (*in vitro* and *in vivo*) and treatment of cancer,[123–125] however, their limited compatibility with water restrained further applications. Although water soluble SiNCs have been reported, they all have suffered from key drawbacks. SiNCs functionalized with ligands containing ionic/polar terminal groups, such as carboxylic acids,[126] amines,[72] diols,[127] amino acids,[128] and sugars[129] (Scheme 1.3a), show poor water solubility or cytotoxicity. Hydrophobic SiNCs encapsulated in phospholipid or polymer micelles[130,131] (Scheme 1.3b) show poor stability under biological conditions and aggregate. Finally, SiNCs functionalized with water soluble polymers (e.g., polyethylene glycol)[132] show blue PL. The preparation of red/near-infrared emitting SiNCs that are compatible with water and biological media is crucial to expanding the application of SiNCs to biomedical fields.

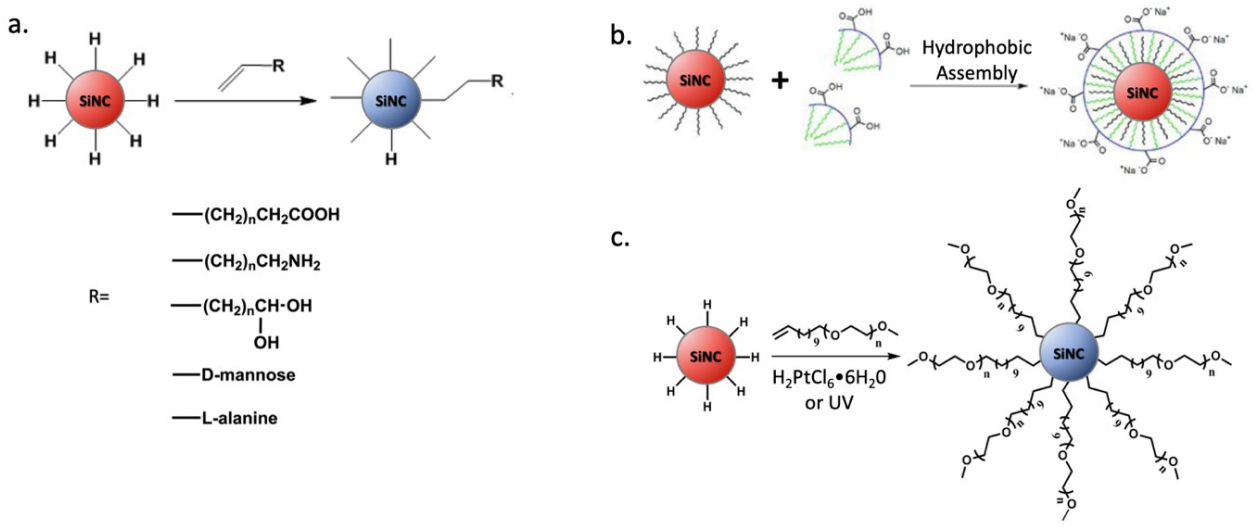

Scheme 1.3. Water soluble SiNCs prepared by (a) functionalization with ionic/polar ligands, (b) encapsuling with hydrophobic chains, adapted with permission from Reference 130, and (c) functionalization with polymers.

1.4 Dendrimers

Dendrimers are highly branched spherical polymers with tunable and uniform size. A typical dendrimer (Scheme 1.4[133]) is made up of four components: i) a core (e.g., small molecules,[134] nanoparticles,[135] and polymers[136]) that provides a starting point from which to grow branches; ii) branches formed through stepwise reactions that provide robust covalent bonds to stabilize the whole structure and provide stimulus-response properties in some cases;[133] iii) void spaces, constructed from branches, that provide loadable spaces (for drugs,[137] molecules,[138] and nanoparticles[139,140]); and iv) surface groups that hold the potential of conjugating with multiple molecules to adapt various applications.[141–143]

Countless types of dendrimers have been reported since the first published preparation in 1978 by Buhleier et al.;[133] they have been applied in sensors,[144,145] catalysts,[146,147] photonics,[148,149] adsorbents,[150] bio-imaging,[151,152] and gene/drug delivery.[153–156] In this section, dendrimer synthesis, biomedical applications, and some dendrimer-nanoparticle conjugated structures will be discussed.

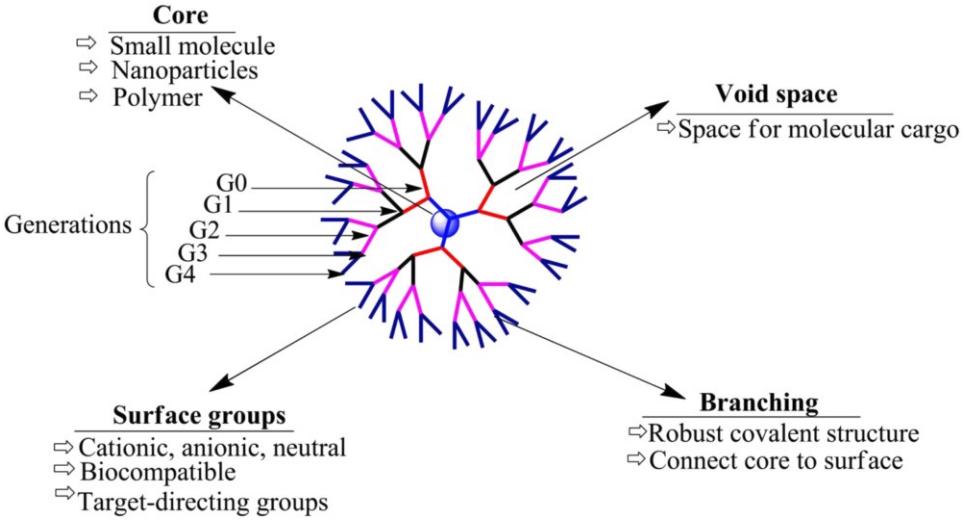

Scheme 1.4. General representation of the model structure of a dendrimer. Reprinted with permission from Reference 133.

1.4.1 Synthesis of Dendrimers

Dendrimers are synthesized via two general approaches: divergent and convergent. In a typical divergent approach, branches are growing from a multifunctional core molecule through stepwise reactions. Scheme 1.5a and 1.5b show the most common strategies. In Scheme 1.5a, new branches are formed after each reaction, and the resulting terminal groups participate in subsequent reactions, leading to formation of higher generations;[134] a well-known example of dendrimers being prepared by this approach is poly(amidoamine) (PAMAM) dendrimers.[157] In Scheme 1.5b, after each

coupling step, an activation step is used to activate the terminal groups before the next coupling reaction;[134] a famous example of dendrimers being prepared by this approach is poly(propyleneimine) (PPI) dendrimers.[158] In a convergent approach, summarized in Scheme 1.5c, the individual dendrimer branches, called dendrons, are prepared through stepwise reactions, then coupled to a multifunctional core molecule.[159] Both divergent and convergent methods have their own advantages that have been reported thoroughly.[134,159]

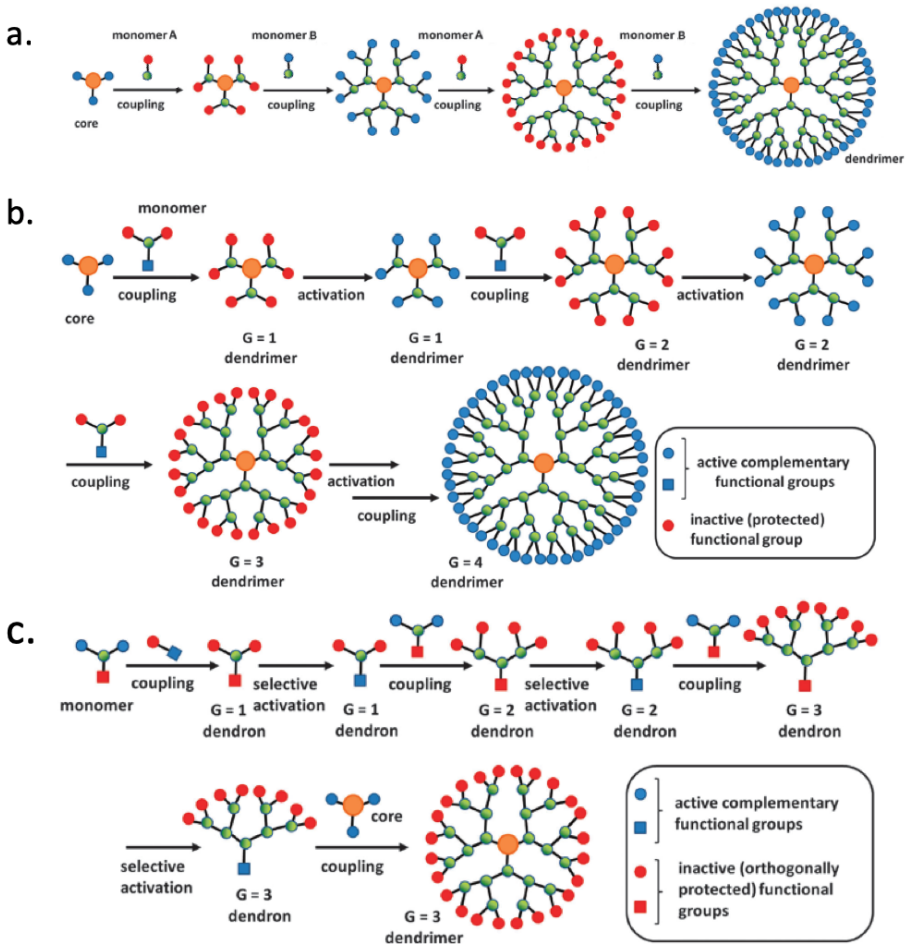

Scheme 1.5. (a) Synthesis of dendrimers by a divergent method (continuous coupling reactions). (b) Synthesis of dendrimers by a divergent method (coupling-activation process). (c) Synthesis of dendrimers by a convergent method. Reproduced from Ref. 134 with permission from the Royal Society of Chemistry.

1.4.2 PAMAM Dendrimers and PPI Dendrimers in Biomedical Applications

Among numerous types of dendrimers, poly(amidoamine) (PAMAM) and poly(propyleneimine) (PPI) dendrimers (Scheme 1.6[160]) are the ones most explored for biomedical applications;[158] they show good water solubility, can be transported in the circulatory system, and last a fairly long time in the body before being removed by the kidneys.[161] Drugs can be loaded into the interior space through complexation (driven by electrostatic interactions) or encapsulation (driven by hydrophobic forces), then released slowly in biological conditions (pH ≈ 7.4).[162–164] Even though some data suggest that the cytotoxicity of PAMAM and PPI dendrimers increases with each generation because of the increasing number of terminal amine groups, these dendrimers are considered biocompatible after appropriate modification.[165–167] Furthermore, the terminal amine groups can be used to conjugate with bio-imaging contrast agents, drugs, and specific protein/peptide binding groups through a covalent bond or combine with DNA/RNA by electrostatic interactions; therefore, achieving functions like bio-imaging,[151] drug delivery,[133] targeted therapies,[137] and gene delivery.[155] Clearly, dendrimers are excellent scaffolds, and researchers have been pursuing dendrimer-nanoparticle conjugated structures to extend the capabilities of dendrimers.[168,169]

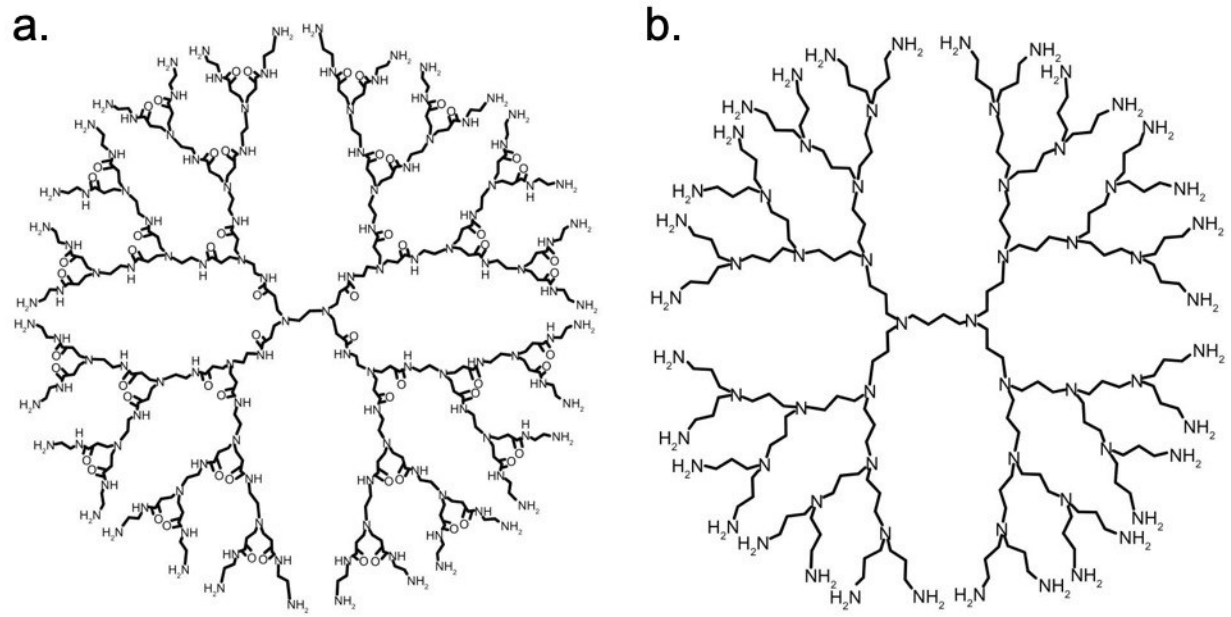

Scheme 1.6. A schematic representation of molecular structures of (a) PAMAM (G3) and (b) PPI (G4) dendrimers. Adapted with permission from Reference 160.

1.4.3 Dendrimer-Nanoparticle Conjugated Structures

As noted previously, capping ligands are crucial for tuning nanoparticle physico-chemical properties and achieving different functional applications.[170–172] Dendrimer structures are ideal choices of nanoparticle capping agents, allowing them to create multifunctional nano materials.[169] The conjugated structures have been prepared through different methods, such as denrimer-assembled nanoparticles (NPs) (Scheme 1.7a),[173–175] dendrimer-entrapped NPs (Scheme 1.7b),[176–178] stepwise divergent synthesis on NPs (Scheme 1.7c),[135,179,180] and dendron-grafted NPs (Scheme 1.7d).[181–183] The dendrimer capping not only increases the water solubility and stability of NPs, but also gives NPs loadable spaces and tunable functional groups, which enables the resulting conjugated structures to extend chemical modifications.[168,169]

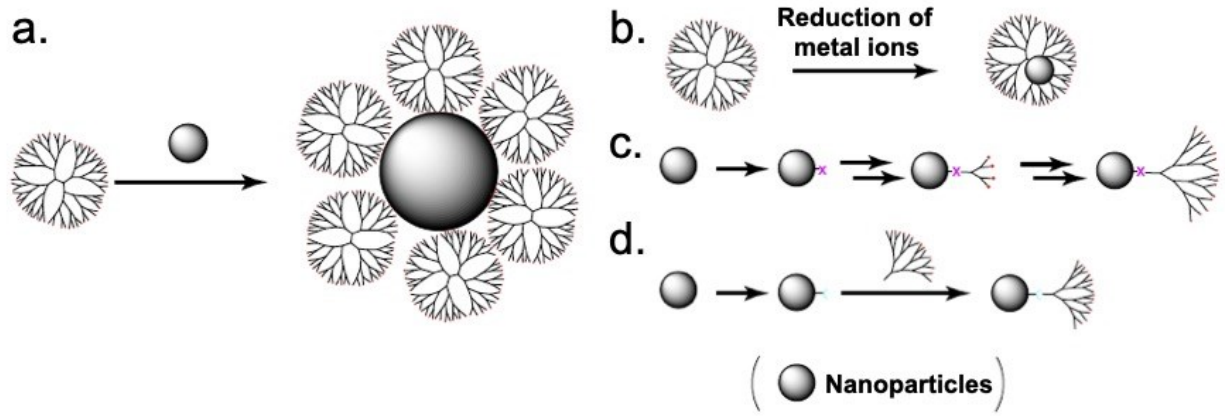

Scheme 1.7. Schematic illustration of the formation of dendrimer-based nanoparticles: a) dendrimer-assembled NPs, b) dendrimer-entrapped NPs, c) stepwise divergent synthesis on NPs, and d) dendron-grafted NPs. Adapted with permission from Reference 168.

1.5 Thesis Outline

SiNCs are promising nanomaterials for biomedical applications; however, their limited compatibility with water and biological media limits their use. The main purpose of the present thesis is to prepare SiNCs with high solubility without compromising their PL properties to extend their abilities for future use in biomedical applications. Chapter 2 focuses on building dendrimer structures on SiNCs to combine the complementary advantages of each material. Specifically, both divergent and convergent methods were used in trying to build dendrimer strucures on SiNCs. A series of stepwise reactions was performed on functionalized SiNCs successfully, providing a promising path to build dendrimer structures on SiNCs. Chapter 3 focuses on preparing amphiphilic SiNCs via mixed ligands. The stability of the resulting particles was studied under

simulated physiological conditions. Chapter 4 summarizes the main findings and proposes future directions.

1.6 References

(1) *Commission Recommendation of 18 October 2011 on the Definition of Nanomaterial Text with EEA Relevance*; 32011H0696; 2011.

(2) Buzea, C.; Pacheco, I. I.; Robbie, K. Nanomaterials and Nanoparticles: Sources and Toxicity. *Biointerphases* **2007**, *2* (4), MR17–MR71.

(3) Roduner, E. Size Matters: Why Nanomaterials Are Different. *Chem. Soc. Rev.* **2006**, *35* (7), 583–592.

(4) Isaeva, V. I.; Nefedov, O. M.; Kustov, L. M. Metal–Organic Frameworks-Based Catalysts for Biomass Processing. *Catalysts* **2018**, *8* (9), 368.

(5) Yang, Y.; Luo, M.; Zhang, W.; Sun, Y.; Chen, X.; Guo, S. Metal Surface and Interface Energy Electrocatalysis: Fundamentals, Performance Engineering, and Opportunities. *Chem* **2018**, *4* (9), 2054–2083.

(6) Saleem, A.; Imran, M.; Shahzadi, A.; Junaid, M.; Majeed, H.; Rafiq, A.; Shahzadi, I.; Ikram, M.; Naz, M.; Ali, S. Drastic Improvement in Catalytic, Optical and Visible-Light Photocatalytic Behavior of Cobalt and Nickel Doped TiO 2 Nanopowder. *Mater. Res. Express* **2019**, *6* (1), 015003.

(7) Wu, J.; Ran, P.; Zhu, S.; Mo, F.; Wang, C.; Fu, Y. A Highly Sensitive Electrochemiluminescence Sensor for the Detection of L-Cysteine Based on the Rhombus-Shaped Rubrene Microsheets and Platinum Nanoparticles. *Sens. Actuators B Chem.* **2019**, *278*, 97–102.

(8) Yang, Y.; Lu, L.; Tian, X.; Li, Y.; Yang, C.; Nie, Y.; Zhou, Z. Ratiometric Fluorescence Detection of Mercuric Ions by Sole Intrinsic Dual-Emitting Gold Nanoclusters. *Sens. Actuators B Chem.* **2019**, *278*, 82–87.

(9) Mehrzad-Samarin, M.; Faridbod, F.; Ganjali, M. R. A Luminescence Nanosensor for Ornidazole Detection Using Graphene Quantum Dots Entrapped in Silica Molecular Imprinted Polymer. *Spectrochim. Acta. A. Mol. Biomol. Spectrosc.* **2019**, *206*, 430–436.

(10) Wang, Y.; Zhou, X.; Yang, Z.; Wang, F.; Han, N.; Chen, Y.; Ho, J. C. GaAs Nanowires Grown by Catalyst Epitaxy for High Performance Photovoltaics. *Crystals* **2018**, *8* (9), 347.

(11) Xu, J.; Wang, H.; Yang, S.; Ni, G.; Zou, B. High-Sensitivity Broadband Colloidal Quantum Dot Heterojunction Photodetector for Night-Sky Radiation. *J. Alloys Compd.* **2018**, *764*, 446–451.

(12) Seoudi, R.; Althagafi, H. A. Dependence of Copper Phthalocyanine Photovoltaic Thin Film on the Sizes of Silver Nanoparticles. *Silicon* **2018**, *10* (5), 2165–2171.

(13) Huang, H.; Cui, Y.; Liu, M.; Chen, J.; Wan, Q.; Wen, Y.; Deng, F.; Zhou, N.; Zhang, X.; Wei, Y. A One-Step Ultrasonic Irradiation Assisted Strategy for the Preparation of Polymer-

Functionalized Carbon Quantum Dots and Their Biological Imaging. *J. Colloid Interface Sci.* **2018**, *532*, 767–773.
(14) Zhao, W.; Li, A.; Zhang, A.; Zheng, Y.; Liu, J. Recent Advances in Functional-Polymer-Decorated Transition-Metal Nanomaterials for Bioimaging and Cancer Therapy. *ChemMedChem* **2018**, *13* (20), 2134–2149.
(15) Luo, Y.; Li, Z.; Zhu, C.; Cai, X.; Qu, L.; Du, D.; Lin, Y. Graphene-like Metal-Free 2D Nanosheets for Cancer Imaging and Theranostics. *Trends Biotechnol.* **2018**, *36* (11), 1145–1156.
(16) Moreira, A. F.; Rodrigues, C. F.; Reis, C. A.; Costa, E. C.; Correia, I. J. Gold-Core Silica Shell Nanoparticles Application in Imaging and Therapy: A Review. *Microporous Mesoporous Mater.* **2018**, *270*, 168–179.
(17) ISO/TS 80004-2:2015(en), Nanotechnologies — Vocabulary — Part 2: Nano-objects
(18) Reed, M. A.; Randall, J. N.; Aggarwal, R. J.; Matyi, R. J.; Moore, T. M.; Wetsel, A. E. Observation of Discrete Electronic States in a Zero-Dimensional Semiconductor Nanostructure. *Phys. Rev. Lett.* **1988**, *60* (6), 535–537.
(19) Bentolila, L. A. 5 - Photoluminescent Quantum Dots in Imaging, Diagnostics and Therapy. In *Applications of Nanoscience in Photomedicine*; Hamblin, M. R., Avci, P., Eds.; Chandos Publishing: Oxford, 2015; pp 77–104.
(20) Éfros, A. L. Density of States and Interband Absorption of Light in Strongly Doped Semiconductors. *Sov. Phys. Uspekhi* **1974**, *16* (6), 789.
(21) Ekimov, A. I.; Efros, A. L.; Onushchenko, A. A. Quantum Size Effect in Semiconductor Microcrystals. *Solid State Commun.* **1985**, *56* (11), 921–924.
(22) Takagahara, T.; Takeda, K. Theory of the Quantum Confinement Effect on Excitons in Quantum Dots of Indirect-Gap Materials. *Phys. Rev. B* **1992**, *46* (23), 15578–15581.
(23) Brus, L. E. Electron–Electron and Electron-hole Interactions in Small Semiconductor Crystallites: The Size Dependence of the Lowest Excited Electronic State. *J. Chem. Phys.* **1984**, *80* (9), 4403–4409.
(24) Rogach, A. L.; Talapin, D. V.; Shevchenko, E. V.; Kornowski, A.; Haase, M.; Weller, H. Organization of Matter on Different Size Scales: Monodisperse Nanocrystals and Their Superstructures. *Adv. Funct. Mater.* **2002**, *12* (10), 653–664.
(25) Rossetti, R.; Nakahara, S.; Brus, L. E. Quantum Size Effects in the Redox Potentials, Resonance Raman Spectra, and Electronic Spectra of CdS Crystallites in Aqueous Solution. *J. Chem. Phys.* **1983**, *79* (2), 1086–1088.
(26) Murray, C. B.; Norris, D. J.; Bawendi, M. G. Synthesis and Characterization of Nearly Monodisperse CdE (E = Sulfur, Selenium, Tellurium) Semiconductor Nanocrystallites. *J. Am. Chem. Soc.* **1993**, *115* (19), 8706–8715.
(27) T, H.; H, S.; I, K. Mechanism of Formation of CdS and ZnS Ultrafine Particles in Reverse Micelles. *Ind. Eng. Chem. Res.* **1994**, *33* (12), 3262–3266.

(28) Micic, O. I.; Curtis, C. J.; Jones, K. M.; Sprague, J. R.; Nozik, A. J. Synthesis and Characterization of InP Quantum Dots. *J. Phys. Chem.* **1994**, *98* (19), 4966–4969.
(29) Olshavsky, M. A.; Goldstein, A. N.; Alivisatos, A. P. Organometallic Synthesis of Gallium-Arsenide Crystallites, Exhibiting Quantum Confinement. *J. Am. Chem. Soc.* **1990**, *112* (25), 9438–9439.
(30) Veinot, J. G. C. Synthesis, Surface Functionalization, and Properties of Freestanding Silicon Nanocrystals. *Chem. Commun.* **2006**, *0* (40), 4160–4168.
(31) Dashiell, M. W.; Denker, U.; Müller, C.; Costantini, G.; Manzano, C.; Kern, K.; Schmidt, O. G. Photoluminescence of Ultrasmall Ge Quantum Dots Grown by Molecular-Beam Epitaxy at Low Temperatures. *Appl. Phys. Lett.* **2002**, *80* (7), 1279–1281.
(32) Protesescu, L.; Yakunin, S.; Bodnarchuk, M. I.; Krieg, F.; Caputo, R.; Hendon, C. H.; Yang, R. X.; Walsh, A.; Kovalenko, M. V. Nanocrystals of Cesium Lead Halide Perovskites (CsPbX3, X = Cl, Br, and I): Novel Optoelectronic Materials Showing Bright Emission with Wide Color Gamut. *Nano Lett.* **2015**, *15* (6), 3692–3696.
(33) Hines, M. A.; Guyot-Sionnest, P. Synthesis and Characterization of Strongly Luminescing ZnS-Capped CdSe Nanocrystals. *J. Phys. Chem.* **1996**, *100* (2), 468–471.
(34) Yuan, R.; Ding, L.; Shao, G.; Zhang, Z.; Liu, J.; Xiang, W.; Liang, X. Suitable Medium for $CsPbBr_3$ Quantum Dots toward Light-Emitting-Diodes Fabrication. *Mater. Lett.* **2019**, *234*, 275–278.
(35) Medintz, I. L.; Uyeda, H. T.; Goldman, E. R.; Mattoussi, H. Quantum Dot Bioconjugates for Imaging, Labelling and Sensing. *Nat. Mater.* **2005**, *4* (6), 435–446.
(36) David Wegner, K.; Hildebrandt, N. Quantum Dots: Bright and Versatile in Vitro and in Vivo Fluorescence Imaging Biosensors. *Chem. Soc. Rev.* **2015**, *44* (14), 4792–4834.
(37) Houston, M. C. The Role of Mercury and Cadmium Heavy Metals in Vascular Disease, Hypertension, Coronary Heart Disease, and Myocardial Infarction. *Altern. Ther. Health Med.* **2007**, *13* (2), S128-133.
(38) Graeme, K. A.; Pollack, C. V. Heavy Metal Toxicity, Part I: Arsenic and Mercury. *J. Emerg. Med.* **1998**, *16* (1), 45–56.
(39) Gordon, R. B.; Bertram, M.; Graedel, T. E. Metal Stocks and Sustainability. *Proc. Natl. Acad. Sci.* **2006**, *103* (5), 1209–1214.
(40) Dasog, M.; Kehrle, J.; Rieger, B.; Veinot, J. G. C. Silicon Nanocrystals and Silicon-Polymer Hybrids: Synthesis, Surface Engineering, and Applications. *Angew. Chem. Int. Ed.* **2015**, *55* (7), 2322–2339.
(41) Silicon. *Wikipedia*; 2018.
(42) Canham, L. T. Silicon Quantum Wire Array Fabrication by Electrochemical and Chemical Dissolution of Wafers. *Appl. Phys. Lett.* **1990**, *57* (10), 1046–1048.
(43) Buriak, J. M. Organometallic Chemistry on Silicon and Germanium Surfaces. *Chem. Rev.* **2002**, *102* (5), 1271–1308.

(44) Dohnalová, K.; Gregorkiewicz, T.; Kůsová, K. Silicon Quantum Dots: Surface Matters. *J. Phys. Condens. Matter* **2014**, *26* (17), 173201.
(45) Bayliss, S. C.; Heald, R.; Fletcher, D. I.; Buckberry, L. D. The Culture of Mammalian Cells on Nanostructured Silicon. *Adv. Mater.* **1999**, *11* (4), 318–321.
(46) Stewart, M. P.; Buriak, J. M. Chemical and Biological Applications of Porous Silicon Technology. *Adv. Mater.* **2000**, *12* (12), 859–869.
(47) Erogbogbo, F.; Yong, K.-T.; Roy, I.; Xu, G.; Prasad, P. N.; Swihart, M. T. Biocompatible Luminescent Silicon Quantum Dots for Imaging of Cancer Cells. *ACS Nano* **2008**, *2* (5), 873–878.
(48) Cheng, K.-Y.; Anthony, R.; Kortshagen, U. R.; Holmes, R. J. High-Efficiency Silicon Nanocrystal Light-Emitting Devices. *Nano Lett.* **2011**, *11* (5), 1952–1956.
(49) Liu, C.-Y.; Holman, Z. C.; Kortshagen, U. R. Hybrid Solar Cells from P3HT and Silicon Nanocrystals. *Nano Lett.* **2009**, *9* (1), 449–452.
(50) Germanenko, I. N.; Li, S.; El-Shall, M. S. Decay Dynamics and Quenching of Photoluminescence from Silicon Nanocrystals by Aromatic Nitro Compounds. *J. Phys. Chem. B* **2001**, *105* (1), 59–66.
(51) Content, S.; Trogler, W. C.; Sailor, M. J. Detection of Nitrobenzene, DNT, and TNT Vapors by Quenching of Porous Silicon Photoluminescence. *Chem. – Eur. J.* **2000**, *6* (12), 2205–2213.
(52) Park, J.-H.; Gu, L.; von Maltzahn, G.; Ruoslahti, E.; Bhatia, S. N.; Sailor, M. J. Biodegradable Luminescent Porous Silicon Nanoparticles for *in Vivo* Applications. *Nat. Mater.* **2009**, *8* (4), 331–336.
(53) Erogbogbo, F.; Yong, K.-T.; Roy, I.; Hu, R.; Law, W.-C.; Zhao, W.; Ding, H.; Wu, F.; Kumar, R.; Swihart, M. T. In Vivo Targeted Cancer Imaging, Sentinel Lymph Node Mapping and Multi-Channel Imaging with Biocompatible Silicon Nanocrystals. *ACS Nano* **2010**, *5* (1), 413–423.
(54) Xu, Z.; Wang, D.; Guan, M.; Liu, X.; Yang, Y.; Wei, D.; Zhao, C.; Zhang, H. Photoluminescent Silicon Nanocrystal-Based Multifunctional Carrier for PH-Regulated Drug Delivery. *ACS Appl. Mater. Interfaces* **2012**, *4* (7), 3424–3431.
(55) Anglin, E. J.; Cheng, L.; Freeman, W. R.; Sailor, M. J. Porous Silicon in Drug Delivery Devices and Materials. *Adv. Drug Deliv. Rev.* **2008**, *60* (11), 1266–1277.
(56) Sato, K.; Tsuji, H.; Hirakuri, K.; Fukata, N.; Yamauchi, Y. Controlled Chemical Etching for Silicon Nanocrystals with Wavelength-Tunable Photoluminescence. *Chem. Commun.* **2009**, *0* (25), 3759–3761.
(57) Shirahata, N.; R. Linford, M.; Furumi, S.; Pei, L.; Sakka, Y.; J. Gates, R.; C. Asplund, M. Laser-Derived One-Pot Synthesis of Silicon Nanocrystals Terminated with Organic Monolayers. *Chem. Commun.* **2009**, *0* (31), 4684–4686.
(58) Heintz, A. S.; Fink, M. J.; Mitchell, B. S. Mechanochemical Synthesis of Blue Luminescent Alkyl/Alkenyl-Passivated Silicon Nanoparticles. *Adv. Mater.* **2007**, *19* (22), 3984–3988.

(59) Ehbrecht, M.; Ferkel, H.; Huisken, F.; Holz, L.; Polivanov, Y. N.; Smirnov, V. V.; Stelmakh, O. M.; Schmidt, R. Deposition and Analysis of Silicon Clusters Generated by Laser-induced Gas Phase Reaction. *J. Appl. Phys.* **1995**, *78* (9), 5302–5306.
(60) Tamir, S.; Berger, S. Laser Induced Deposition of Nanocrystalline Si with Preferred Crystallographic Orientation. *Appl. Surf. Sci.* **1995**, *86* (1), 514–520.
(61) Ehbrecht, M.; Huisken, F. Gas-Phase Characterization of Silicon Nanoclusters Produced by Laser Pyrolysis of Silane. *Phys. Rev. B* **1999**, *59* (4), 2975–2985.
(62) Li, X.; He, Y.; Swihart, M. T. Surface Functionalization of Silicon Nanoparticles Produced by Laser-Driven Pyrolysis of Silane Followed by HF−HNO3 Etching. *Langmuir* **2004**, *20* (11), 4720–4727.
(63) Mangolini, L.; Thimsen, E.; Kortshagen, U. High-Yield Plasma Synthesis of Luminescent Silicon Nanocrystals. *Nano Lett.* **2005**, *5* (4), 655–659.
(64) Pi, X. D.; Liptak, R. W.; Campbell, S. A.; Kortshagen, U. In-Flight Dry Etching of Plasma-Synthesized Silicon Nanocrystals. *Appl. Phys. Lett.* **2007**, *91* (8), 083112.
(65) Pi, X. D.; Liptak, R. W.; Nowak, J. D.; Wells, N. P.; Carter, C. B.; Campbell, S. A.; Kortshagen, U. Air-Stable Full-Visible-Spectrum Emission from Silicon Nanocrystals Synthesized by an All-Gas-Phase Plasma Approach. *Nanotechnology* **2008**, *19* (24), 245603.
(66) Littau, K. A.; Szajowski, P. J.; Muller, A. J.; Kortan, A. R.; Brus, L. E. A Luminescent Silicon Nanocrystal Colloid via a High-Temperature Aerosol Reaction. *J. Phys. Chem.* **1993**, *97* (6), 1224–1230.
(67) Fojtik, A.; Henglein, A. Luminescent Colloidal Silicon Particles. *Chem. Phys. Lett.* **1994**, *221* (5), 363–367.
(68) Holmes, J. D.; Ziegler, K. J.; Doty, R. C.; Pell, L. E.; Johnston, K. P.; Korgel, B. A. Highly Luminescent Silicon Nanocrystals with Discrete Optical Transitions. *J. Am. Chem. Soc.* **2001**, *123* (16), 3743–3748.
(69) Heath, J. R. A Liquid-Solution-Phase Synthesis of Crystalline Silicon. *Science* **1992**, *258* (5085), 1131–1133.
(70) Bley, R. A.; Kauzlarich, S. M. A Low-Temperature Solution Phase Route for the Synthesis of Silicon Nanoclusters. *J. Am. Chem. Soc.* **1996**, *118* (49), 12461–12462.
(71) Yang, C.-S.; Bley, R. A.; Kauzlarich, S. M.; Lee, H. W. H.; Delgado, G. R. Synthesis of Alkyl-Terminated Silicon Nanoclusters by a Solution Route. *J. Am. Chem. Soc.* **1999**, *121* (22), 5191–5195.
(72) Warner, J. H.; Hoshino, A.; Yamamoto, K.; Tilley, R. D. Water-Soluble Photoluminescent Silicon Quantum Dots. *Angew. Chem. Int. Ed.* **2005**, *44* (29), 4550–4554.
(73) Tilley, R. D.; Warner, J. H.; Yamamoto, K.; Matsui, I.; Fujimori, H. Micro-Emulsion Synthesis of Monodisperse Surface Stabilized Silicon Nanocrystals. *Chem. Commun.* **2005**, *0* (14), 1833–1835.

(74) Liu, S.; Sato, S.; Kimura, K. Synthesis of Luminescent Silicon Nanopowders Redispersible to Various Solvents. *Langmuir* **2005**, *21* (14), 6324–6329.
(75) Hessel, C. M.; Henderson, E. J.; Veinot, J. G. C. Hydrogen Silsesquioxane: A Molecular Precursor for Nanocrystalline Si−SiO2 Composites and Freestanding Hydride-Surface-Terminated Silicon Nanoparticles. *Chem. Mater.* **2006**, *18* (26), 6139–6146.
(76) Sun, W.; Qian, C.; Chen, K. K.; Ozin, G. A. Silicon Nanocrystals: It's Simply a Matter of Size. *ChemNanoMat* **2016**, *2* (9), 847–855.
(77) Sorarù, G. D.; Modena, S.; Bettotti, P.; Das, G.; Mariotto, G.; Pavesi, L. Si Nanocrystals Obtained through Polymer Pyrolysis. *Appl. Phys. Lett.* **2003**, *83* (4), 749–751.
(78) Pauthe, M.; Bernstein, E.; Dumas, J.; Saviot, L.; Pradel, A.; Ribes, M. Preparation and Characterisation of Si Nanocrystallites Embedded in a Silica Matrix. *J. Mater. Chem.* **1999**, *9* (1), 187–191.
(79) Hessel, C. M.; Reid, D.; Panthani, M. G.; Rasch, M. R.; Goodfellow, B. W.; Wei, J.; Fujii, H.; Akhavan, V.; Korgel, B. A. Synthesis of Ligand-Stabilized Silicon Nanocrystals with Size-Dependent Photoluminescence Spanning Visible to Near-Infrared Wavelengths. *Chem. Mater.* **2012**, *24* (2), 393–401.
(80) Yang, Z.; Dobbie, A. R.; Cui, K.; Veinot, J. G. C. A Convenient Method for Preparing Alkyl-Functionalized Silicon Nanocubes. *J. Am. Chem. Soc.* **2012**, *134* (34), 13958–13961.
(81) Yang, Z.; Dobbie, A. R.; Veinot, J. G. C. Shape Evolution of Faceted Silicon Nanocrystals upon Thermal Annealing in an Oxide Matrix. *MRS Online Proc. Libr. Arch.* **2013**, *1536*, 207–212.
(82) Pavesi, L.; Dal Negro, L.; Mazzoleni, C.; Franzò, G.; Priolo, F. Optical Gain in Silicon Nanocrystals. *Nature* **2000**, *408* (6811), 440–444.
(83) Yang, L.; Lua, Y.-Y.; Lee, M. V.; Linford, M. R. Chemomechanical Functionalization and Patterning of Silicon. *Acc. Chem. Res.* **2005**, *38* (12), 933–942.
(84) Kůsová, K.; Cibulka, O.; Dohnalová, K.; Pelant, I.; Valenta, J.; Fučíková, A.; Žídek, K.; Lang, J.; Englich, J.; Matějka, P.; et al. Brightly Luminescent Organically Capped Silicon Nanocrystals Fabricated at Room Temperature and Atmospheric Pressure. *ACS Nano* **2010**, *4* (8), 4495–4504.
(85) Godefroo, S.; Hayne, M.; Jivanescu, M.; Stesmans, A.; Zacharias, M.; Lebedev, O. I.; Van Tendeloo, G.; Moshchalkov, V. V. Classification and Control of the Origin of Photoluminescence from Si Nanocrystals. *Nat. Nanotechnol.* **2008**, *3* (3), 174–178.
(86) Dasog, M.; De los Reyes, G. B.; Titova, L. V.; Hegmann, F. A.; Veinot, J. G. Size vs Surface: Tuning the Photoluminescence of Freestanding Silicon Nanocrystals across the Visible Spectrum via Surface Groups. *ACS Nano* **2014**, *8* (9), 9636–9648.
(87) Robidillo, C. J. T.; Islam, M. A.; Aghajamali, M.; Faramus, A.; Sinelnikov, R.; Zhang, X.; Boekhoven, J.; Veinot, J. G. C. Functional Bioinorganic Hybrids from Enzymes and Luminescent Silicon-Based Nanoparticles. *Langmuir* **2018**, *34* (22), 6556–6569.

(88) Buriak, J. M. Illuminating Silicon Surface Hydrosilylation: An Unexpected Plurality of Mechanisms. *Chem. Mater.* **2014**, *26* (1), 763–772.
(89) Yang, Z.; Iqbal, M.; Dobbie, A. R.; Veinot, J. G. Surface-Induced Alkene Oligomerization: Does Thermal Hydrosilylation Really Lead to Monolayer Protected Silicon Nanocrystals? *J. Am. Chem. Soc.* **2013**, *135* (46), 17595–17601.
(90) Pujari, S. P.; Driss, H.; Bannani, F.; van Lagen, B.; Zuilhof, H. One-Pot Gram-Scale Synthesis of Hydrogen-Terminated Silicon Nanoparticles. *Chem. Mater.* **2018**, *30* (18), 6503–6512.
(91) Hua, F.; Swihart, M. T.; Ruckenstein, E. Efficient Surface Grafting of Luminescent Silicon Quantum Dots by Photoinitiated Hydrosilylation. *Langmuir* **2005**, *21* (13), 6054–6062.
(92) Purkait, T. K.; Iqbal, M.; Wahl, M. H.; Gottschling, K.; Gonzalez, C. M.; Islam, M. A.; Veinot, J. G. C. Borane-Catalyzed Room-Temperature Hydrosilylation of Alkenes/Alkynes on Silicon Nanocrystal Surfaces. *J. Am. Chem. Soc.* **2014**, *136* (52), 17914–17917.
(93) Yang, Z.; Gonzalez, C. M.; Purkait, T. K.; Iqbal, M.; Meldrum, A.; Veinot, J. G. C. Radical Initiated Hydrosilylation on Silicon Nanocrystal Surfaces: An Evaluation of Functional Group Tolerance and Mechanistic Study. *Langmuir* **2015**, *31* (38), 10540–10548.
(94) Pankove, J. I. *Optical Processes in Semiconductors*; Courier Corporation, 1975.
(95) Chelikowsky, J. R.; Cohen, M. L. Electronic Structure of Silicon. *Phys. Rev. B* **1974**, *10* (12), 5095.
(96) Delley, B.; Steigmeier, E. F. Quantum Confinement in Si Nanocrystals. *Phys. Rev. B* **1993**, *47* (3), 1397–1400.
(97) Hybertsen, M. S. Absorption and Emission of Light in Nanoscale Silicon Structures. *Phys. Rev. Lett.* **1994**, *72* (10), 1514–1517.
(98) Cullis, A. G.; Canham, L. T.; Calcott, P. D. J. The Structural and Luminescence Properties of Porous Silicon. *J. Appl. Phys.* **1997**, *82* (3), 909–965.
(99) Daldosso, N.; Pavesi, L. Nanosilicon Photonics. *Laser Photonics Rev.* **2009**, *3* (6), 508–534.
(100) Delerue, C.; Allan, G.; Lannoo, M. Theoretical Aspects of the Luminescence of Porous Silicon. *Phys. Rev. B* **1993**, *48* (15), 11024–11036.
(101) Kůsová, K.; Hapala, P.; Valenta, J.; Jelínek, P.; Cibulka, O.; Ondič, L.; Pelant, I. Direct Bandgap Silicon: Tensile-Strained Silicon Nanocrystals. *Adv. Mater. Interfaces* **2014**, *1* (2), 1300042.
(102) Kůsová, K.; Pelant, I.; Humpolíčková, J.; Hof, M. Comprehensive Description of Blinking-Dynamics Regimes in Single Direct-Band-Gap Silicon Nanocrystals. *Phys. Rev. B* **2016**, *93* (3), 035412.
(103) Lockwood, R.; McFarlane, S.; Rodríguez Núñez, J. R.; Wang, X. Y.; Veinot, J. G. C.; Meldrum, A. Photoactivation of Silicon Quantum Dots. *J. Lumin.* **2011**, *131* (7), 1530–1535.

(104) Goguenheim, D.; Lannoo, M. Theoretical Calculation of the Electron-Capture Cross Section Due to a Dangling Bond at the Si(111)-SiO_2 Interface. *Phys. Rev. B* **1991**, *44* (4), 1724–1733.
(105) Almeida, A. J.; Sahu, A.; Riedinger, A.; Norris, D. J.; Brandt, M. S.; Stutzmann, M.; Pereira, R. N. Charge Trapping Defects in CdSe Nanocrystal Quantum Dots. *J. Phys. Chem. C* **2016**, *120* (25), 13763–13770.
(106) Puzder, A.; Williamson, A. J.; Grossman, J. C.; Galli, G. Surface Chemistry of Silicon Nanoclusters. *Phys. Rev. Lett.* **2002**, *88* (9), 097401.
(107) Luppi, M.; Ossicini, S. Oxygen Role on the Structural and Optoelectronic Properties of Silicon Nanodots. *Phys. Status Solidi A* **2003**, *197* (1), 251–256.
(108) Luppi, M.; Ossicini, S. Ab Initio Study on Oxidized Silicon Clusters and Silicon Nanocrystals Embedded in SiO_2: Beyond the Quantum Confinement Effect. *Phys. Rev. B* **2005**, *71* (3), 035340.
(109) Wolkin, M. V.; Jorne, J.; Fauchet, P. M.; Allan, G.; Delerue, C. Electronic States and Luminescence in Porous Silicon Quantum Dots: The Role of Oxygen. *Phys. Rev. Lett.* **1999**, *82* (1), 197–200.
(110) Biteen, J. S.; Lewis, N. S.; Atwater, H. A.; Polman, A. Size-Dependent Oxygen-Related Electronic States in Silicon Nanocrystals. *Appl. Phys. Lett.* **2004**, *84* (26), 5389–5391.
(111) Kang, Z.; Liu, Y.; Tsang, C. H. A.; Ma, D. D. D.; Fan, X.; Wong, N.-B.; Lee, S.-T. Water-Soluble Silicon Quantum Dots with Wavelength-Tunable Photoluminescence. *Adv. Mater.* **2009**, *21* (6), 661–664.
(112) Sinelnikov, R.; Dasog, M.; Beamish, J.; Meldrum, A.; Veinot, J. G. C. Revisiting an Ongoing Debate: What Role Do Surface Groups Play in Silicon Nanocrystal Photoluminescence? *ACS Photonics* **2017**, *4* (8), 1920–1929.
(113) Chen, S.; Yang, K.; Tuguntaev, R. G.; Mozhi, A.; Zhang, J.; Wang, P. C.; Liang, X.-J. Targeting Tumor Microenvironment with PEG-Based Amphiphilic Nanoparticles to Overcome Chemoresistance. *Nanomedicine Nanotechnol. Biol. Med.* **2016**, *12* (2), 269–286.
(114) Weissleder, R. A Clearer Vision for *in Vivo* Imaging. *Nat. Biotechnol.* **2001**, *19*, 316–317.
(115) Berezin, M. Y.; Achilefu, S. Fluorescence Lifetime Measurements and Biological Imaging. *Chem. Rev.* **2010**, *110* (5), 2641–2684.
(116) Cheng, X.; B. Lowe, S.; J. Reece, P.; Justin Gooding, J. Colloidal Silicon Quantum Dots: From Preparation to the Modification of Self-Assembled Monolayers (SAMs) for Bio-Applications. *Chem. Soc. Rev.* **2014**, *43* (8), 2680–2700.
(117) Barnes, T. J.; Prestidge, C. A. Recent Advances in Porous Silicon-Based Therapeutic Delivery. *Ther. Deliv.* **2015**, *6* (2), 97–100.
(118) Joo, J.; Liu, X.; Kotamraju, V. R.; Ruoslahti, E.; Nam, Y.; Sailor, M. J. Gated Luminescence Imaging of Silicon Nanoparticles. *ACS Nano* **2015**, *9* (6), 6233–6241.

(119) Mobarok, M. H.; Purkait, T. K.; Islam, M. A.; Miskolzie, M.; Veinot, J. G. Instantaneous Functionalization of Chemically Etched Silicon Nanocrystal Surfaces. *Angew. Chem. Int. Ed.* **2017**, *56* (22), 6073–6077.
(120) Atkins, T. M.; Cassidy, M. C.; Lee, M.; Ganguly, S.; Marcus, C. M.; Kauzlarich, S. M. Synthesis of Long T1 Silicon Nanoparticles for Hyperpolarized 29Si Magnetic Resonance Imaging. *ACS Nano* **2013**, *7* (2), 1609–1617.
(121) Thompson, K.; Booske, J.; Gianchandani, Y.; Cooper, R. RF and Microwave Rapid Magnetic Induction Heating of Silicon Wafers. In *Advances in Microwave and Radio Frequency Processing*; Willert-Porada, M., Ed.; Springer Berlin Heidelberg, 2006; pp 673–680.
(122) Thompson, K.; Gianchandani, Y. B.; Booske, J.; Cooper, R. F. Direct Silicon-Silicon Bonding by Electromagnetic Induction Heating. *J. Microelectromechanical Syst.* **2002**, *11* (4), 285–292.
(123) Chinnathambi, S.; Chen, S.; Ganesan, S.; Hanagata, N. Silicon Quantum Dots for Biological Applications. *Adv. Healthc. Mater.* **2014**, *3* (1), 10–29.
(124) Peng, F.; Su, Y.; Zhong, Y.; Fan, C.; Lee, S.-T.; He, Y. Silicon Nanomaterials Platform for Bioimaging, Biosensing, and Cancer Therapy. *Acc. Chem. Res.* **2014**, *47* (2), 612–623.
(125) McVey, B. F. P.; Tilley, R. D. Solution Synthesis, Optical Properties, and Bioimaging Applications of Silicon Nanocrystals. *Acc. Chem. Res.* **2014**, *47* (10), 3045–3051.
(126) Clark, R. J.; Dang, M. K. M.; Veinot, J. G. C. Exploration of Organic Acid Chain Length on Water-Soluble Silicon Quantum Dot Surfaces. *Langmuir* **2010**, *26* (19), 15657–15664.
(127) Shiohara, A.; Hanada, S.; Prabakar, S.; Fujioka, K.; Lim, T. H.; Yamamoto, K.; Northcote, P. T.; Tilley, R. D. Chemical Reactions on Surface Molecules Attached to Silicon Quantum Dots. *J. Am. Chem. Soc.* **2010**, *132* (1), 248–253.
(128) Zhai, Y.; Dasog, M.; B. Snitynsky, R.; K. Purkait, T.; Aghajamali, M.; H. Hahn, A.; B. Sturdy, C.; L. Lowary, T.; C. Veinot, J. G. Water-Soluble Photoluminescent d -Mannose and l -Alanine Functionalized Silicon Nanocrystals and Their Application to Cancer Cell Imaging. *J. Mater. Chem. B* **2014**, *2* (47), 8427–8433.
(129) Nakahara, Y.; Machiya, K.; Sato, T.; Nwe, N. T.; Furuike, T.; Tamura, H.; Kimura, K. Synthesis of Silicon Quantum Dots Functionalized Chemically with Monosaccharides and Their Use in Biological Fluorescence Imaging. *Chem. Lett.* **2013**, *42* (5), 498–500.
(130) Hessel, C. M.; Rasch, M. R.; Hueso, J. L.; Goodfellow, B. W.; Akhavan, V. A.; Puvanakrishnan, P.; Tunnel, J. W.; Korgel, B. A. Alkyl Passivation and Amphiphilic Polymer Coating of Silicon Nanocrystals for Diagnostic Imaging. *Small* **2010**, *6* (18), 2026–2034.
(131) Henderson, E. J.; Shuhendler, A. J.; Prasad, P.; Baumann, V.; Maier-Flaig, F.; Faulkner, D. O.; Lemmer, U.; Wu, X. Y.; Ozin, G. A. Colloidally Stable Silicon Nanocrystals with Near-Infrared Photoluminescence for Biological Fluorescence Imaging. *Small* **2011**, *7* (17), 2507–2516.

(132) Xu, Z.; Li, Y.; Zhang, B.; Purkait, T.; Alb, A.; Mitchell, B. S.; Grayson, S. M.; Fink, M. J. Water-Soluble PEGylated Silicon Nanoparticles and Their Assembly into Swellable Nanoparticle Aggregates. *J. Nanoparticle Res.* **2015**, *17* (1), 56.
(133) Choudhary, S.; Gupta, L.; Rani, S.; Dave, K.; Gupta, U. Impact of Dendrimers on Solubility of Hydrophobic Drug Molecules. *Front. Pharmacol.* **2017**, *8*.
(134) Sowinska, M.; Urbanczyk-Lipkowska, Z. Advances in the Chemistry of Dendrimers. *New J. Chem.* **2014**, *38* (6), 2168–2203.
(135) Khodadust, R.; Unsoy, G.; Yalcın, S.; Gunduz, G.; Gunduz, U. PAMAM Dendrimer-Coated Iron Oxide Nanoparticles: Synthesis and Characterization of Different Generations. *J. Nanoparticle Res.* **2013**, *15* (3), 1488.
(136) Zhang, A.; Shu, L.; Bo, Z.; Schlüter, A. D. Dendronized Polymers: Recent Progress in Synthesis. *Macromol. Chem. Phys.* **2003**, *204* (2), 328–339.
(137) Li, J.; Liang, H.; Liu, J.; Wang, Z. Poly (Amidoamine) (PAMAM) Dendrimer Mediated Delivery of Drug and PDNA/SiRNA for Cancer Therapy. *Int. J. Pharm.* **2018**, *546* (1), 215–225.
(138) Kojima, C.; Tsumura, S.; Harada, A.; Kono, K. A Collagen-Mimic Dendrimer Capable of Controlled Release. *J. Am. Chem. Soc.* **2009**, *131* (17), 6052–6053.
(139) Chung, Y.-M.; Rhee, H.-K. Pt-Pd Bimetallic Nanoparticles Encapsulated in Dendrimer Nanoreactor. *Catal. Lett.* **2003**, *85* (3), 159–164.
(140) Crooks, R. M.; Zhao, M.; Sun, L.; Chechik, V.; Yeung, L. K. Dendrimer-Encapsulated Metal Nanoparticles: Synthesis, Characterization, and Applications to Catalysis. *Acc. Chem. Res.* **2001**, *34* (3), 181–190.
(141) Zhou, Z.; Wang, Y.; Yan, Y.; Zhang, Q.; Cheng, Y. Dendrimer-Templated Ultrasmall and Multifunctional Photothermal Agents for Efficient Tumor Ablation. *ACS Nano* **2016**, *10* (4), 4863–4872.
(142) Lesniak, W. G.; Oskolkov, N.; Song, X.; Lal, B.; Yang, X.; Pomper, M.; Laterra, J.; Nimmagadda, S.; McMahon, M. T. Salicylic Acid Conjugated Dendrimers Are a Tunable, High Performance CEST MRI NanoPlatform. *Nano Lett.* **2016**, *16* (4), 2248–2253.
(143) Chang, H.; Lv, J.; Gao, X.; Wang, X.; Wang, H.; Chen, H.; He, X.; Li, L.; Cheng, Y. Rational Design of a Polymer with Robust Efficacy for Intracellular Protein and Peptide Delivery. *Nano Lett.* **2017**, *17* (3), 1678–1684.
(144) Li, P.; Zhang, M.; Sun, X.; Guan, S.; Zhang, G.; Baumgarten, M.; Müllen, K. A Dendrimer-Based Highly Sensitive and Selective Fluorescence-Quenching Sensor for Fe^{3+} Both in Solution and as Film. *Biosens. Bioelectron.* **2016**, *85*, 785–791.
(145) Wang, S. H.; Shen, C. Y.; Lin, Y. M.; Du, J. C. Piezoelectric Sensor for Sensitive Determination of Metal Ions Based on the Phosphate-Modified Dendrimer. *Smart Mater. Struct.* **2016**, *25* (8), 085018.

(146) Ye, R.; Zhukhovitskiy, A. V.; Deraedt, C. V.; Toste, F. D.; Somorjai, G. A. Supported Dendrimer-Encapsulated Metal Clusters: Toward Heterogenizing Homogeneous Catalysts. *Acc. Chem. Res.* **2017**, *50* (8), 1894–1901.
(147) Caminade, A.-M.; Ouali, A.; Laurent, R.; Turrin, C.-O.; Majoral, J.-P. Coordination Chemistry with Phosphorus Dendrimers. Applications as Catalysts, for Materials, and in Biology. *Coord. Chem. Rev.* **2016**, *308*, 478–497.
(148) Zhang, J.; Ling, L.; Wang, C.-F.; Chen, S.; Chen, L.; Y. Son, D. Versatile Dendrimer-Derived Nanocrystal Microreactors towards Fluorescence Colloidal Photonic Crystals. *J. Mater. Chem. C* **2014**, *2* (18), 3610–3616.
(149) Chen, M.; Tian, Y.; Zhang, J.; Hong, R.; Chen, L.; Chen, S.; Y. Son, D. Fabrication of Crack-Free Photonic Crystal Films via Coordination of Microsphere Terminated Dendrimers and Their Performance in Invisible Patterned Photonic Displays. *J. Mater. Chem. C* **2016**, *4* (37), 8765–8771.
(150) Vunain, E.; Mishra, A.; Mamba, B. Dendrimers, Mesoporous Silicas and Chitosan-Based Nanosorbents for the Removal of Heavy-Metal Ions: A Review. *Int. J. Biol. Macromol.* **2016**, *86*, 570–586.
(151) Lakew Mekuria, S.; Ayane Debele, T.; Tsai, H.-C. PAMAM Dendrimer Based Targeted Nano-Carrier for Bio-Imaging and Therapeutic Agents. *RSC Adv.* **2016**, *6* (68), 63761–63772.
(152) Janaszewska, A.; Studzian, M.; Petersen, J. F.; Ficker, M.; Paolucci, V.; Christensen, J. B.; Tomalia, D. A.; Klajnert-Maculewicz, B. Modified PAMAM Dendrimer with 4-Carbomethoxypyrrolidone Surface Groups-Its Uptake, Efflux, and Location in a Cell. *Colloids Surf. B Biointerfaces* **2017**, *159*, 211–216.
(153) Kesharwani, P.; Jain, K.; Jain, N. K. Dendrimer as Nanocarrier for Drug Delivery. *Prog. Polym. Sci.* **2014**, *39* (2), 268–307.
(154) Wang, H.; Huang, Q.; Chang, H.; Xiao, J.; Cheng, Y. Stimuli-Responsive Dendrimers in Drug Delivery. *Biomater. Sci.* **2016**, *4* (3), 375–390.
(155) Yang, J.; Zhang, Q.; Chang, H.; Cheng, Y. Surface-Engineered Dendrimers in Gene Delivery. *Chem. Rev.* **2015**, *115* (11), 5274–5300.
(156) Kesharwani, P.; Iyer, A. K. Recent Advances in Dendrimer-Based Nanovectors for Tumor-Targeted Drug and Gene Delivery. *Drug Discov. Today* **2015**, *20* (5), 536–547.
(157) Tomalia, D. A.; Baker, H.; Dewald, J.; Hall, M.; Kallos, G.; Martin, S.; Roeck, J.; Ryder, J.; Smith, P. A New Class of Polymers: Starburst-Dendritic Macromolecules. *Polym. J.* **1985**, *17* (1), 117–132.
(158) Kaur, D.; Jain, K.; Mehra, N. K.; Kesharwani, P.; Jain, N. K. A Review on Comparative Study of PPI and PAMAM Dendrimers. *J. Nanoparticle Res.* **2016**, *18* (6), 146.
(159) Grayson, S. M.; Fréchet, J. M. J. Convergent Dendrons and Dendrimers: From Synthesis to Applications. *Chem. Rev.* **2001**, *101* (12), 3819–3868.

(160) Shao, N.; Su, Y.; Hu, J.; Zhang, J.; Zhang, H.; Cheng, Y. Comparison of Generation 3 Polyamidoamine Dendrimer and Generation 4 Polypropylenimine Dendrimer on Drug Loading, Complex Structure, Release Behavior, and Cytotoxicity. *Int. J. Nanomedicine* **2011**, *6*, 3361–3372.
(161) A. Mintzer, M.; W. Grinstaff, M. Biomedical Applications of Dendrimers: A Tutorial. *Chem. Soc. Rev.* **2011**, *40* (1), 173–190.
(162) Devarakonda, B.; Hill, R. A.; de Villiers, M. M. The Effect of PAMAM Dendrimer Generation Size and Surface Functional Group on the Aqueous Solubility of Nifedipine. *Int. J. Pharm.* **2004**, *284* (1), 133–140.
(163) Boas, U.; H. Heegaard, P. M. Dendrimers in Drug Research. *Chem. Soc. Rev.* **2004**, *33* (1), 43–63.
(164) Gupta, U.; Agashe, H. B.; Asthana, A.; Jain, N. K. Dendrimers: Novel Polymeric Nanoarchitectures for Solubility Enhancement. *Biomacromolecules* **2006**, *7* (3), 649–658.
(165) Jevprasesphant, R.; Penny, J.; Jalal, R.; Attwood, D.; McKeown, N. B.; D'Emanuele, A. The Influence of Surface Modification on the Cytotoxicity of PAMAM Dendrimers. *Int. J. Pharm.* **2003**, *252* (1), 263–266.
(166) Sadekar, S.; Ghandehari, H. Transepithelial Transport and Toxicity of PAMAM Dendrimers: Implications for Oral Drug Delivery. *Adv. Drug Deliv. Rev.* **2012**, *64* (6), 571–588.
(167) Albertazzi, L.; Gherardini, L.; Brondi, M.; Sulis Sato, S.; Bifone, A.; Pizzorusso, T.; Ratto, G. M.; Bardi, G. In Vivo Distribution and Toxicity of PAMAM Dendrimers in the Central Nervous System Depend on Their Surface Chemistry. *Mol. Pharm.* **2013**, *10* (1), 249–260.
(168) Sun, W.; Mignani, S.; Shen, M.; Shi, X. Dendrimer-Based Magnetic Iron Oxide Nanoparticles: Their Synthesis and Biomedical Applications. *Drug Discov. Today* **2016**, *21* (12), 1873–1885.
(169) Roy Barman, S.; Nain, A.; Jain, S.; Punjabi, N.; Mukherji, S.; Satija, J. Dendrimer as a Multifunctional Capping Agent for Metal Nanoparticles for Use in Bioimaging, Drug Delivery and Sensor Applications. *J. Mater. Chem. B* **2018**, *6* (16), 2368–2384.
(170) M. Rossi, L.; L. Fiorio, J.; S. Garcia, M. A.; P. Ferraz, C. The Role and Fate of Capping Ligands in Colloidally Prepared Metal Nanoparticle Catalysts. *Dalton Trans.* **2018**, *47* (17), 5889–5915.
(171) Pooja; Barman, P. B.; Hazra, S. K. Role of Capping Agent in Palladium Nanoparticle Based Hydrogen Sensor. *J. Clust. Sci.* **2018**, *29* (6), 1209–1216.
(172) Jhonsi, M. A.; Thulasi, S.; Kathiravan, A. Impact of Capping Agent on the Electron Transfer Dynamics of CdTe QDs with Methyl Viologen. *J. Lumin.* **2016**, *178*, 356–361.
(173) Liu, J.; Wang, F.; Han, Y.; Sun, M.; Li, H.; Hua, H.; Chen, C.; Lin, Y. Polyamidoamine Functionalized CdTeSe Quantum Dots for Sensitive Detection of Cry1Ab Protein in Vitro and in Vivo. *Sens. Actuators B Chem.* **2015**, *206*, 8–13.

(174) Ciganda, R.; Gu, H.; Hernandez, R.; Escobar, A.; Martínez, A.; Yates, L.; Moya, S.; Ruiz, J.; Astruc, D. Electrostatic Assembly of Functional and Macromolecular Ferricinium Chloride-Stabilized Gold Nanoparticles. *Inorg. Chem.* **2017**, *56* (5), 2784–2791.
(175) Luong, D.; Sau, S.; Kesharwani, P.; Iyer, A. K. Polyvalent Folate-Dendrimer-Coated Iron Oxide Theranostic Nanoparticles for Simultaneous Magnetic Resonance Imaging and Precise Cancer Cell Targeting. *Biomacromolecules* **2017**, *18* (4), 1197–1209.
(176) Deraedt, C.; Melaet, G.; Ralston, W. T.; Ye, R.; Somorjai, G. A. Platinum and Other Transition Metal Nanoclusters (Pd, Rh) Stabilized by PAMAM Dendrimer as Excellent Heterogeneous Catalysts: Application to the Methylcyclopentane (MCP) Hydrogenative Isomerization. *Nano Lett.* **2017**, *17* (3), 1853–1862.
(177) Mekuria, S. L.; Debele, T. A.; Tsai, H.-C. Encapsulation of Gadolinium Oxide Nanoparticle (Gd_2O_3) Contrasting Agents in PAMAM Dendrimer Templates for Enhanced Magnetic Resonance Imaging in Vivo. *ACS Appl. Mater. Interfaces* **2017**, *9* (8), 6782–6795.
(178) Divsar, F.; Ju, H. Electrochemiluminescence Detection of near Single DNA Molecules by Using Quantum Dots–Dendrimer Nanocomposites for Signal Amplification. *Chem. Commun.* **2011**, *47* (35), 9879–9881.
(179) Yen, C.-H.; Lien, H.-L.; Chung, J.-S.; Yeh, H.-D. Adsorption of Precious Metals in Water by Dendrimer Modified Magnetic Nanoparticles. *J. Hazard. Mater.* **2017**, *322*, 215–222.
(180) Wang, T.; Yang, W.-L.; Hong, Y.; Hou, Y.-L. Magnetic Nanoparticles Grafted with Amino-Riched Dendrimer as Magnetic Flocculant for Efficient Harvesting of Oleaginous Microalgae. *Chem. Eng. J.* **2016**, *297*, 304–314.
(181) J. Daou, T.; Pourroy, G.; M. Greneche, J.; Bertin, A.; Felder-Flesch, D.; Begin-Colin, S. Water Soluble Dendronized Iron Oxide Nanoparticles. *Dalton Trans.* **2009**, *0* (23), 4442–4449.
(182) Lamanna, G.; Kueny-Stotz, M.; Mamlouk-Chaouachi, H.; Ghobril, C.; Basly, B.; Bertin, A.; Miladi, I.; Billotey, C.; Pourroy, G.; Begin-Colin, S.; et al. Dendronized Iron Oxide Nanoparticles for Multimodal Imaging. *Biomaterials* **2011**, *32* (33), 8562–8573.
(183) Rosario-Amorin, D.; Gaboyard, M.; Clérac, R.; Vellutini, L.; Nlate, S.; Heuzé, K. Metallodendritic Grafted Core–Shell γ-Fe_2O_3 Nanoparticles Used as Recoverable Catalysts in Suzuki C-C Coupling Reactions. *Chem. – Eur. J.* **2012**, *18* (11), 3305–3315.

Chapter 2

Building Dendrimer Structures on SiNCs

2.1 Introduction

Dendrimers are synthetic highly branched polymers with tunable sizes that are prepared by stepwise growth in nanoscale.[1] This unique synthesis approach gives dendrimers exceptional properties, such as uniform size, sphere shape,[2] loadable void space, and tunable surface chemistry.[3] Many dendrimers, such as those based upon poly(amidoamine) (PAMAM) and poly(propyleneimine) (PPI), are believed to be delivery systems in chemotherapy because of their good biocompatibilities and drug loading/releasing abilities.[4]

Silicon nanocrystals (SiNCs) are another class of nanomaterials that have drawn attention because of their potential in biomedical applications, such as deep tissue imaging[5] and target tumor imaging.[6] SiNCs are particularly attractive due to better biocompatibility,[7] abundance,[8] and tunable photoluminescence.[9,10] In recent years, the preparation[11] and functionalization[12–15] of SiNCs have been studied well, however, the limited compatibility of these materials with water has restricted their deployment in this sector.

The goal of the work described herein has been to prepare dendrimer-coated SiNCs. In doing so, we would combine the complementary advantages of each material, e.g., imparting SiNCs with water solubility, drug loading/releasing ability, and rendering dendrimers traceable via the SiNC luminescent properties.

2.2 Experimental

2.2.1 Reagents and Materials

All reagents were used as received, unless otherwise indicated. Electronic grade hydrofluoric acid (HF, 49% aqueous solution) was purchased from J. T. Baker. Toluene (reagent grade), ethanol (reagent grade), hexane (reagent grade), dimethyl sulfoxide (DMSO, reagent grade), anhydrous methanol (99.8%), 11-bromo-1-undecene (95%), ethylenediamine (99%), trichlorosilane (99%), methyl 10-undecenoate (96%), fuming sulfuric acid (reagent grade, 20% free SO_3 bases), N-hydroxysulfosuccinimide sodium salt (Sulfo-NHS, 98%), N-(3-dimethylaminopropyl)-N′-ethylcarbodiimide (EDC, 97%), potassium bis(trimethylsilyl)amide (95%), polyester-32-hydroxyl-1-acetylene bis-MPA dendron, generation 5 (dendron-G5-acetylene-OH, 97%), polyester-32-hydroxyl-1-carboxyl bis-MPA dendron, generation 5 (dendron-G5-carboxyl-OH, 97%), glass beads (diam. ~5 mm), and 4 Å molecular sieves (beads, 4–8 mesh) were purchased from Millipore Sigma. Sulfuric acid (reagent grade, 95–98%), hydrochloric acid (HCl, 37%, ~12 mol/L), and magnesium sulfate (reagent grade) were obtained from Caledon Laboratory Chemicals. Calcium carbonate (certified ACS grade) and PTFE centrifuge tube (50-mL) were purchased from Thermo Fisher Scientific. PTFE syringe filter (0.45-μm) was purchased from Biomed Scientific. Dry toluene was obtained from a Grubbs-type solvent purification system (Innovative Technologies, Inc.) prior to use.

2.2.2 Divergent Synthesis of SiNC@PAMAM Using Ester Terminated SiNCs (SiNC-ester) as Core Material

The general approach for forming PAMAM dendrimers on the surfaces of SiNCs is summarized in Scheme 2.1. Briefly, hydride-terminated SiNCs (H-SiNCs) were reacted with methyl 10-undecenoate to form ester terminated SiNCs. Ester terminated SiNCs were reacted with ethylenediamine, followed by methyl acrylate; this was repeated several times to get higher generation dendrimer structures.

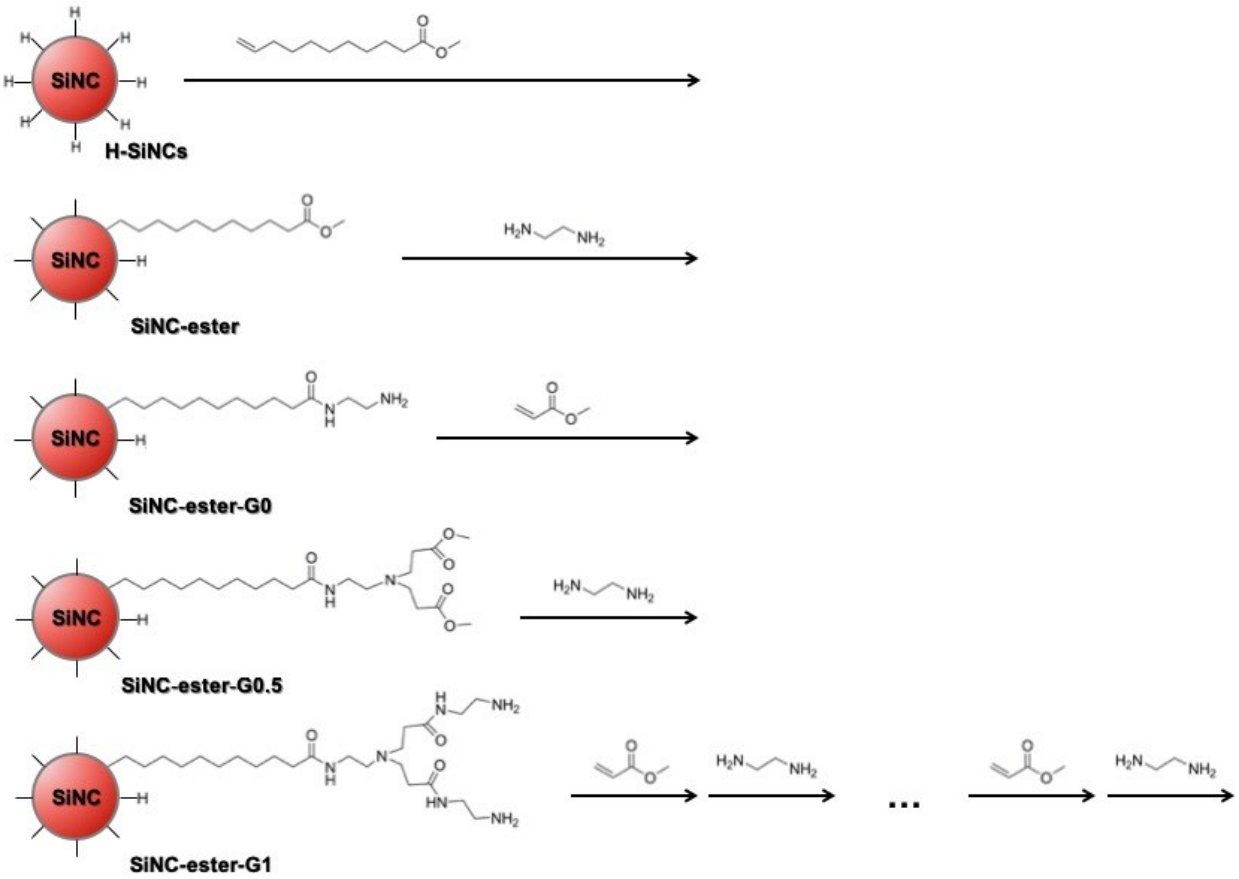

Scheme 2.1. A schematic representation of the synthesis of SiNC@PAMAM using ester terminated SiNCs (SiNC-ester) as the core material.

2.2.2.1 Synthesis of Hydride-Terminated SiNCs (H-SiNCs)

Preparation of Hydrogen Silsesquioxane (HSQ): A three-neck round bottom flask containing a magnetic stir bar was equipped with an addition funnel and two connecting tubes with stopcocks, as shown in Figure 2.1. The reaction flask was evacuated for 5 min and backfilled with Ar. This procedure was repeated three times, after which the reaction chamber was filled with Ar. Then, dry toluene (210 mL) was transferred into the addition funnel using a cannula. Under an Ar purge, concentrated sulfuric acid (70 mL) and fuming sulfuric acid (32.5 mL) were added to the round bottom flask, and dry toluene was added dropwise from the addition funnel to the acid mixture while stirring. (The mixture was viscous.) Subsequently, dry toluene (510 mL) and trichlorosilane (75 mL) were introduced to the addition funnel using a cannula, and a water trap (for absorbing the HCl formed during the reaction) was affixed to the Tygon® tubing attached to one of the outlets from the round bottom flask. Ar was purged slowly into the apparatus until constant bubbles (2 bubbles per sec) were observed in the water trap. Next, the toluene and trichlorosilane mixture was added dropwise (1 gtt/sec) to the flask while stirring, and the mixture was stirred for another 30 min. All the liquid was transferred into a 2 L separation funnel, followed by careful addition of a 33% aqueous sulfuric acid solution (600 mL) into the funnel and mixing. (This mixing step released heat; shaking and releasing the pressure should be done several times during this step.) A white precipitate formed during the mixing. After sitting for about 5 min, the white precipitate, along with the bottom layer (aqueous layer), was drained out. The organic layer was washed with

a 33% aqueous sulfuric acid solution (600 mL) two more times. The resulting organic layer containing the target product was transferred to an Erlenmeyer flask and dried over a mixture of calcium carbonate (~5 g) and magnesium sulfate (~5 g) for 12–16 h. The dried reaction mixture was isolated via suction filtration, and the product was obtained by removal of toluene using rotary evaporation, followed by drying in vacuo. The white solid product (yield: 28 g, 98%) was stored under vacuum until further use and was characterized by FTIR, and NMR (in toluene-D_8).

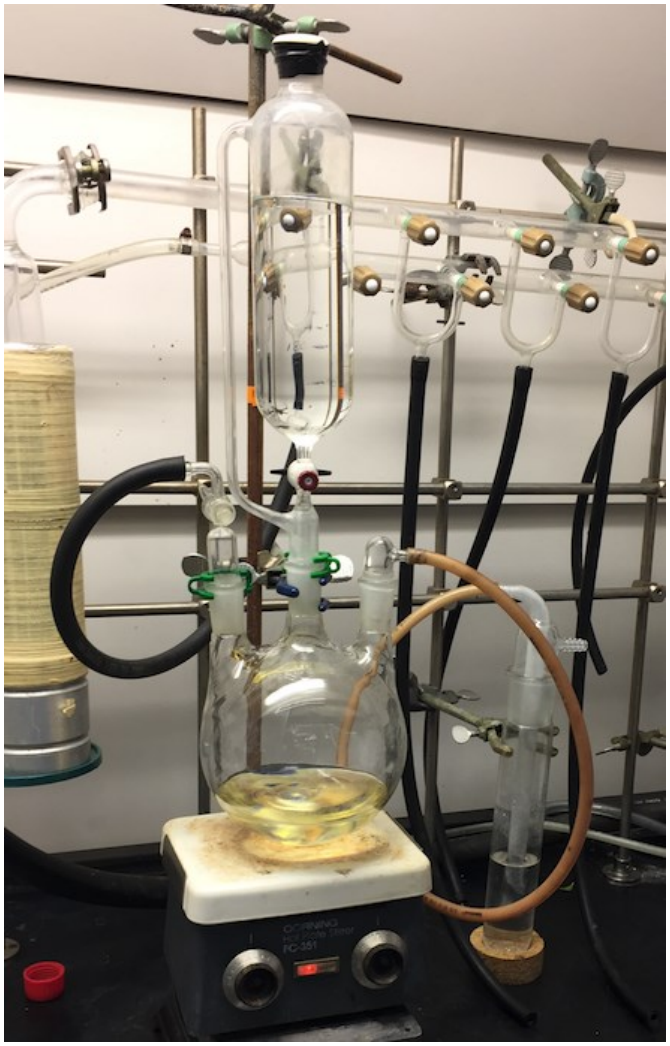

Figure 2.1. The apparatus for synthesizing HSQ.

Preparation of SiNC/SiO_2 Composite: SiNCs imbedded in an SiO_2-like matrix were prepared by thermal decomposition of HSQ following procedures developed by the Veinot group.[11] Thermal processing of HSQ (3.5 g) was performed in a Lindberg/Blue furnace at 1100 ℃ for 1 h under a slightly reducing atmosphere (5% H_2/95% Ar). (Heating profile: first, the temperature was set to increase from 25 to 1100 ℃ with a ramp rate of 18 ℃/min; next, the temperature was held at 1100 ℃ for 1 h; finally, the temperature was decreased from 1100 to 25 ℃ by natural cooling.) The resulting amber/black solid was transferred to an agate mortar, about 2 mL of ethanol were added, and the mixture was ground to a fine dark brown slurry. (During the grinding, more ethanol was added to keep the solid wet.) The slurry was transferred into a thick-walled flask containing glass beads and shaken for 8 h using a wrist action shaker. The solid was recovered via vacuum filtration using Durapore® Membrane 0.1 μm VVPP filter paper. The SiNCs/SiO_2 composite (yield: 3.3 g, 94%) was stored under ambient conditions until further use.

Preparation of Hydride-Terminated SiNCs (H-SiNCs): H-SiNCs were liberated from the SiNC/SiO_2 composite by alcoholic hydrofluoric acid etching.[11] In a typical etching procedure, SiNC/SiO_2 (600 mg) was weighed in a 50-mL PTFE beaker equipped with a magnetic stir bar, and 9 mL of ethanol were added. The turbid liquid was sonicated for 5 min to disperse the composite. Then, 9 mL of deionized water were added into the beaker, and the beaker was transferred to the fume hood in the HF lab to perform the etching step. (Caution: HF is extremely dangerous and

must be handled with great care.*) In the HF-lab fume hood, the beaker was fixed on a stir plate and the solution was stirred for 1 min. After decreasing the stir speed, 9 mL of 49% HF aqueous solution, measured in a PTFE measuring cylinder, were added into the beaker. The stir speed was changed back to normal, and the mixture was stirred for 40 min until its colour changed from brown to light yellow. At this stage of the etching procedure, toluene (~2.5 mL) was added to the solution to extract hydrophobic H-SiNCs, and the stirring was continued for another 30 s. The stirring was stopped to let the solution separate into two layers, and the top layer was transferred into a test tube with a pipette. This extraction step was repeated three more times until the aqueous layer became colourless. The H-SiNCs were isolated by centrifugation using a test tube centrifuge at 3000 rpm for 5 min, followed by two cycles of washing with dry toluene (~10 mL) and centrifugation at 3000 rpm for 5 min. After discarding the clear colourless supernatant, the H-SiNCs were used for the following reactions as soon as possible. H-SiNCs were characterized by FTIR and, in light of the air sensitivity of the H-SiNCs, no additional characterization was performed.

* Safety actions: besides the regular PPE, another pair of PTFE gloves (waterproof) were worn on top of nitrile gloves. Anyone who works with HF should be familiar with the HF SOP and emergency procedures.

2.2.2.2 Synthesis of Ester Terminated SiNCs (SiNC-ester)

Ester terminated SiNCs were prepared using a variation of the thermal hydrosilylation conditions reported elsewhere.[12] H-SiNCs prepared from etching SiNC/SiO_2 (600 mg) were dispersed with methyl 10-undecenoate (10 mL; 43 mmol), and the suspension was transferred into an Ar charged Schlenk flask equipped with a magnetic stir bar. The mixture was exposed to three freeze/pump/thaw cycles with an Ar charged Schlenk line. After the last thaw, the Schlenk flask was refilled with Ar and heated to 180 °C with stirring under static Ar. The yellow, cloudy solution became an orange, transparent solution in 1 h, and the reaction was kept heating for 24 h in total. The reaction mixture was transferred into a 50-mL PTFE centrifuge tube after the reaction cooled down. An antisolvent (hexane; 30 mL) was added to the resulting solution, and the precipitate was collected by centrifuging at 12000 rpm for 20 min. After discarding the clear, colourless supernatant, the yellow precipitate was dissolved in a minimum amount of toluene (~5 mL). Subsequently, hexane (30 mL) was added, and the particles were isolated by centrifugation (12000 rpm, 20 min). This dissolution/precipitation/centrifugation procedure was repeated twice. After the final cycle, the resulting yellow precipitate was dispersed in methanol (10 mL) to yield a turbid yellow suspension. The turbid suspension was filtered through a 0.45-μm PTFE syringe filter to yield a suspension that was transparent under ambient light. A 1 mL solution of SiNC-ester methanol was used for characterization, and the rest of the SiNC-ester methanol solution was stored under ambient conditions until further use. The 1 mL solution of SiNC-ester methanol was

dried in vacuo. Part of the resulting solid was sent for FTIR (~1 mg), TGA (~3 mg), and XPS measurements, and the rest of the solid (~3 mg) was dissolved in 600 μL toluene-D_8 and characterized by NMR.

2.2.2.3 Synthesis of PAMAM G0 Terminated SiNCs (SiNC-ester-G0)

The preparation of SiNC-ester-G0 followed the reported method of synthesizing the PAMAM dendrimer with some adaptation.[16–18] Ethylenediamine (10 mL; 149 mmol) and anhydrous methanol (10 mL) were transferred into a Schlenk flask equipped with a magnetic stir bar and stirred for 30 min in an ice/water bath. An ice-cold methanol suspension of SiNC-ester (8 mL) obtained from the procedure outlined in Section 2.2.2.2 was transferred into an addition funnel that sat on top of the Schlenk flask. Ar was purged into the apparatus for 5 min with the addition funnel uncapped as the gas outlet. After the purging process, the addition funnel was capped, and the system was kept under static Ar. The entire reaction system was wrapped in aluminum foil to minimize exposure to light, and the SiNC-ester methanol suspension was added dropwise to the ethylenediamine solution. After the addition, the ice bath was removed, the mixture was warmed to room temperature with stirring, and the reaction was left to settle for 48 h. The residual ethylenediamine and solvent were evaporated under reduced pressure until the volume of liquid was approximately 2 mL. This residue was transferred into a 50-mL PTFE centrifuge tube, followed by addition of toluene (10 mL) and hexane (30 mL). Subsequently, the mixture was centrifuged at 12000 rpm for 20 min to yield a yellow precipitate. The precipitate was purified

further via three dispersion/precipitation/centrifugation cycles using a toluene (10 mL)/hexane (30 mL) solvent/antisolvent mixture and centrifugation at 12000 rpm for 20 min. The resulting precipitate was air dried for 2 min and dispersed in methanol (10 mL) to yield a turbid yellow suspension. The suspension was clarified by passing it through a 0.45-μm PTFE syringe filter. A 2-mL portion of the resulting solution (SiNC-ester-G0 methanol solution) was used for characterization, and the rest was stored under ambient conditions until further use. The 2 mL of SiNC-ester-G0 methanol solution were dried in vacuo. The resulting solid was characterized by FTIR, TGA, and XPS.

2.2.2.4 Synthesis of PAMAM G0.5 Terminated SiNCs (SiNC-ester-G0.5)

PAMAM G0.5 terminated SiNCs were prepared by reacting SiNC-ester-G0 with methyl acrylate through a Michael addition. An 8-mL solution of SiNC-ester-G0 methanol obtained from the previous step was transferred into a Schlenk flask and stirred with a magnetic stir bar for 30 min in an ice bath. Then, a mixture of anhydrous methanol (10 mL) and methyl acrylate (10 mL, 113 mmol) was cooled in an ice bath and transferred into an additional funnel that sat on top of the Schlenk flask. Ar was purged into the apparatus for 5 min with the addition funnel uncapped as the gas outlet. After the purging process, the addition funnel was capped, and the system was kept under static Ar. The entire reaction system was wrapped in aluminum foil to minimize exposure to light, and the methanol/methyl acrylate mixture was added dropwise to the SiNC-ester-G0 methanol solution. After the addition, the ice bath was removed, and the mixture was kept stirring

for 48 h at room temperature. The residual methyl acrylate and solvent were evaporated under reduced pressure until the volume of liquid was around 2 mL. The residue was transferred into a 50-mL PTFE centrifuge tube, followed by addition of toluene (10 mL) and hexane (30 mL). The mixture was centrifuged at 12000 rpm for 20 min to get the precipitate. The precipitate was purified further via three dispersion/precipitation/centrifugation cycles using a toluene (10 mL)/hexane (30 mL) solvent/antisolvent mixture and centrifugation at 12000 rpm for 20 min. The resulting precipitate was air dried for 2 min and dispersed in methanol (10 mL) to yield a turbid yellow suspension. The suspension was clarified by passing it through a 0.45-μm PTFE syringe filter. A 2-mL portion of the resulting solution (SiNC-ester-G0.5 methanol solution) was used for characterization, and the rest was stored under ambient conditions until further use. The 2 mL of SiNC-ester-G0.5 methanol solution were dried in vacuo, and the resulting solid was characterized by FTIR, TGA and XPS.

2.2.2.5 Synthesis of PAMAM G1 Terminated SiNCs (SiNC-ester-G1) and PAMAM G1.5 Terminated SiNCs (SiNC-ester-G1.5)

The synthesis of SiNC-ester-G1was similar to that of SiNC-ester-G0 (procedure in Section 2.2.2.3), and the synthesis of SiNC-ester-G1.5 was similar to that of SiNC-ester-G0.5 (procedure in Section 2.2.2.4).

2.2.3 Divergent Synthesis of SiNC@PAMAM Using Organic Ammonium Ion Terminated SiNCs (SiNC-ammonium) as the Core Material.

Another strategy for building the PAMAM dendrimer on the surface of SiNCs is shown in Scheme 2.2. Organic ammonium ion terminated SiNCs (SiNC-ammonium) were synthesized first. Then, they were reacted with methyl acrylate, followed by ethylenediamine repetitively to get higher generation of dendrimer structures.

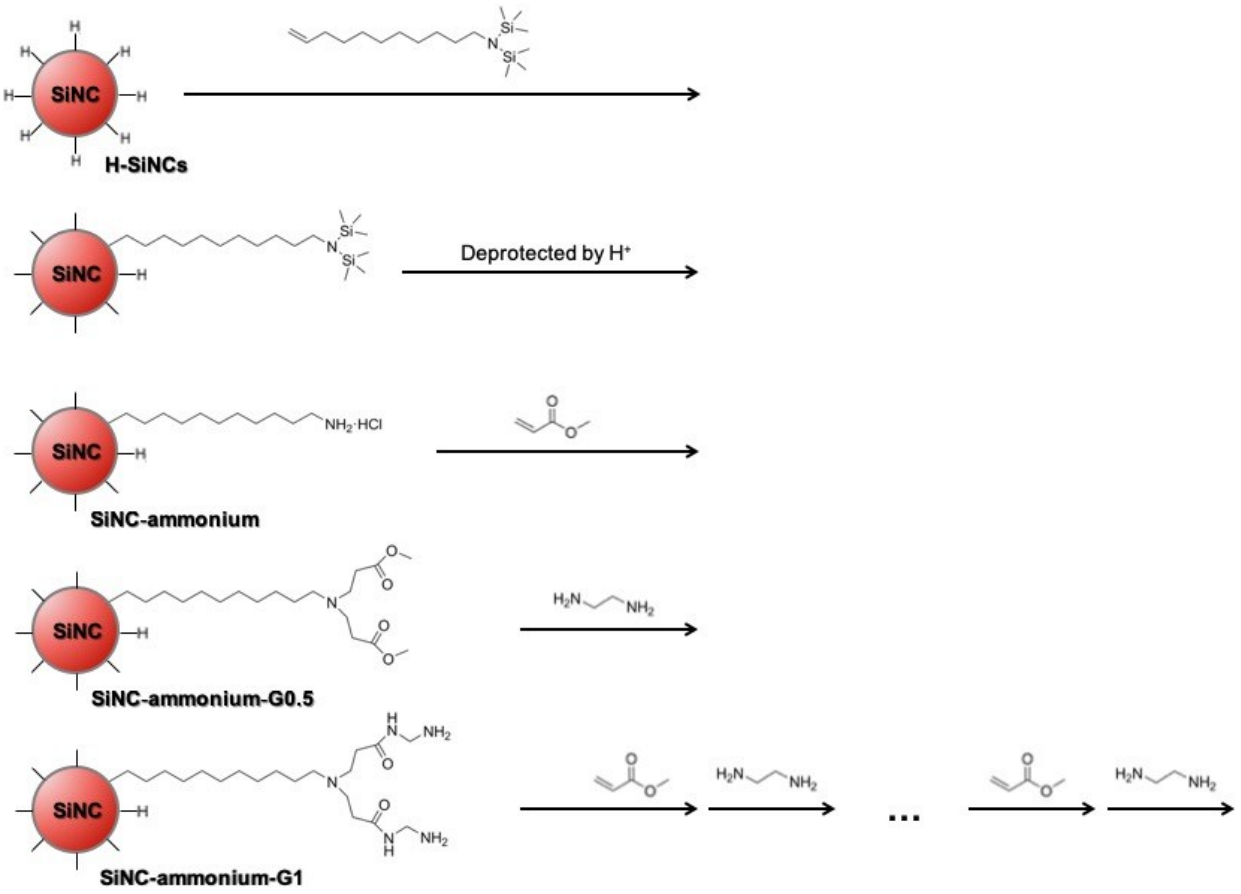

Scheme 2.2. A schematic representation of the synthesis of SiNC@PAMAM using organic ammonium ion terminated SiNCs (SiNC-ammonium) as the core material.

2.2.3.1 Synthesis of N, N-Bis(trimethylsilyl)-10-Undecen-1-Amine

N,N-bis(trimethylsilyl)-10-undecen-1-amine was synthesized by reacting 11-bromo-1-undecene with potassium bis(trimethylsilyl)amide.[19,20] (Note: potassium bis(trimethylsilyl)amide and N,N-bis(trimethylsilyl)-10-undecen-1-amine are moisture sensitive. Care must be exercised to minimize exposure to water. All the glassware used in this Section is oven dried at 125 ℃.) In a nitrogen filled glove box, a minimum amount of dry toluene (~40 mL) was used to dissolve potassium bis(trimethylsilyl)amide (10.5 g; 50 mmol). The resulting solution was transferred into a Schlenk bomb (a round bottom and heavy walled tube, with only one opening accessed by a Teflon plug valve, used as a closed system for conducting reactions at elevated pressures and temperatures), followed by adding 11-bromo-1-undecene (12 g; 49 mmol) into the flask. The flask was sealed, removed from the glovebox, and heated at 102 ℃ with stirring. Throughout the heating process, the initial dark red solution became cloudy and brown. After 36 h the brown suspension was transferred via cannula to a zeolite (activated in the oven for 48 h) loaded Schlenk frit and filtered into an oven dried Schlenk flask. The redundant solvent was removed under reduced pressure until the volume of liquid was approximately 20 mL. Then, the residue was transferred via cannula to a 50-mL oven dried Schlenk flask (round bottom, short neck), and the Schlenk flask was connected to a vacuum distillation set up under Ar purge. The crude product mixture was purified via vacuum (~4 mTorr) distillation, and pure N,N-bis(trimethylsilyl)-10-undecen-1-amine was collected at 100 ℃ with a Schlenk tube as a clear colourless liquid. After the collection, the

Schlenk tube was kept in a nitrogen filled glovebox until further use. The resulting N,N-bis(trimethylsilyl)-10-undecen-1-amine (yield: 11 g, 72%) was characterized by NMR in toluene-D_8.

2.2.3.2 Synthesis of Organic Ammonium Ion-Terminated SiNCs (SiNC-ammonium)

H-SiNCs obtained using the procedure described in Section 2.2.2.1 were dispersed in N,N-bis(trimethylsilyl)-10-undecen-1-amine (10 g; 32 mmol), and the cloudy mixture was transferred to an oven dried Schlenk flask equipped with a magnetic stir bar. The mixture was exposed to three freeze/pump/thaw cycles, after which the mixture was placed under an Ar atmosphere, and the Schlenk flask was heated to 160 °C under static Ar. After 24 h, a dark red solution containing the crude product was obtained. An orange-red solid was obtained upon addition of toluene (15 mL) and acetonitrile (15 mL), followed by centrifugation at 12000 rpm for 20 min. After discarding the colourless supernatant, the orange precipitate was dissolved in toluene (20 mL), and the mixture was transferred into an Erlenmeyer flask equipped with a magnetic stir bar. A hydrochloric acid ethanoic solution (1 mL, 1 mol/mL) was added dropwise with stirring to yield an orange precipitate. The mixture was transferred to two test tubes, and the precipitate was collected by centrifugation (3000 rpm, 10 min). Three cycles of dissolution/precipitation/centrifugation (10 mL of methanol/30 mL of toluene/3000 rpm, 10 min) were performed to purify the product. The resulting precipitate was dissolved in methanol (10 mL), yielding an orange solution. A 2-ml portion of the orange solution was dried in vacuo, and the resulting solid was characterized by FTIR, NMR (in

DMSO-D_6), and XPS; the rest of the solution was stored under ambient conditions until further use.

2.2.3.3 Synthesis of PAMAM G0.5 Terminated SiNCs (SiNC-ammonium-G0.5)

The synthesis of SiNC-ammonium-G0.5 was similar to that of SiNC-ester-G0.5 (procedure in Section 2.2.2.4). Specifically, the starting material, SiNC-ester-G0 in methanol, was changed to SiNC-ammonium in methanol obtained from the previous step. All other conditions (material usage amount, reactions conditions, and purification steps) were kept the same. The resulting product was dissolved in methanol (10 mL), then the solution was filtered through a 0.45-μm PTFE syringe filter. The product was characterized by FTIR and XPS; the rest of the solution was stored under ambient conditions until further use.

2.2.3.4 Synthesis of PAMAM G1 Terminated SiNCs (SiNC-ammonium-G1)

The synthesis of SiNC-ammonium-G1 was similar to that of SiNC-ester-G0 (procedure in Section 2.2.2.3). Specifically, the reagent, SiNC-ester methanol solution, was changed to SiNC-ammonium-G0.5 methanol solution obtained from the previous step. All other conditions (material usage amount, reactions conditions, and purification steps) were kept the same. The resulting product was dispersed in methanol (10 mL), then the solution was filtered through a 0.45-μm PTFE syringe filter. The product was characterized by FTIR and XPS; the rest of the solution was stored under ambient conditions until further use.

2.2.4 The Attempt of Using a Convergent Method to Prepare a SiNC@dendrimer Structure

2.2.4.1 H-SiNCs Coupled with Polyester-32-Hydroxyl-1-Acetylene Bis-MPA Dendron, Generation 5 (dendron-G5-acetylene-OH)

The coupled product was prepared using thermal hydrosilylation between H-SiNCs and dendron-G5-acetylene-OH (Scheme 2.3).[21] A 5-mL sample of dry DMSO (dried by 4 Å molecular sieves) was used to disperse H-SiNCs (by etching 50 mg Si/SiO_2; procedure in Section 2.2.2.1), and the mixture was transferred into a Schlenk flask equipped with a magnetic stir bar. Another 5 mL of dry DMSO was used to dissolve 25 mg of dendron-G5-acetylene-OH (7 μmol), and this solution was added into the Schlenk flask. Three freeze/pump/thaw cycles were applied to the mixture with an Ar charged Schlenk line. After the last thaw, the Schlenk flask was heated to 170 °C for 24 h under static Ar. The brown slurry did not show any notable change during the heating. The reaction mixture was transferred into a 50-mL PTFE centrifuge tube, followed by adding 30 mL of toluene to precipitate the potential product and the unreacted reagent, dendron-G5-acetylene-OH. The precipitate was obtained by centrifuging at 12000 rpm for 20 min. After decanting the supernatant, the precipitate was dispersed with 40 mL of toluene and centrifuged at 12000 rpm for 20 min two more times. The resulting precipitate was air dried for 5 min, then dispersed in ethanol by sonicating for 20 min. The mixture was transferred into Fisherbrand™ dialysis tubing (12000 to 14000 d) and dialyzed with DI-water, changing the water every 2 h five times. After dialysis, the

resulting mixture was separated by centrifugation at 3000 rpm for 20 min. The supernatant was clear and did not show notable PL under UV light; the precipitate showed faint pink PL under UV light. The precipitate was characterized by FTIR.

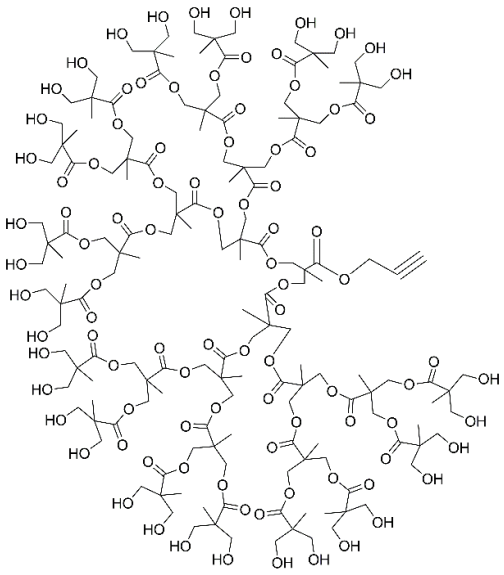

Scheme 2.3. A schematic representation of the structure of dendron-G5-acetylene-OH.

2.2.4.2 SiNC-ammonium Coupled with Polyester-32-Hydroxyl-1-Carboxyl Bis-MPA Dendron, Generation 5 (dendron-G5-carboxyl-OH)

The coupled product was prepared using an EDC/NHS coupling reaction between SiNC-ammonium and dendron-G5-carboxyl-OH (Scheme 2.4).[21] A 13-mg sample of dendron-G5-carboxyl-OH (3.5 μmol) was dissolved with 1.5 mL of DMSO in a standard vial equipped with a magnetic stir bar. Sulfo-NHS (5 mg; 23 μmol) and EDC (30 mg; 193 μmol) were added into the vial, and the mixture was stirred for 30 min to active the carboxylic group in the dendron. A 0.5-

mL solution of 5 mg SiNC-ammonium in DMSO was added into the vial, and the mixture was left stirring at room temperature for 10 h. On completion of the reaction, the solution remained clear and yellow in colour. The solution was transferred into a 50-mL PTFE centrifuge tube, followed by addition of toluene (30 mL). A precipitate was formed and collected by centrifugation at 12000 rpm for 20 min. After decanting the colorless supernatant, the precipitate was dissolved in methanol (5 mL), followed by addition of 30 mL of toluene as an antisolvent. The precipitate was collected and purified further via another two cycles of dispersion/precipitation/centrifugation using a toluene (10 mL)/hexane (30 mL) solvent/antisolvent mixture and 12000 rpm for 20 min centrifugation. The resulting product was air dried for 5 min, and a small amount of product (~4 mg) was characterized by FTIR. The rest of the product was dissolved in 5 mL of methanol and stored in a standard vial under ambient conditions.

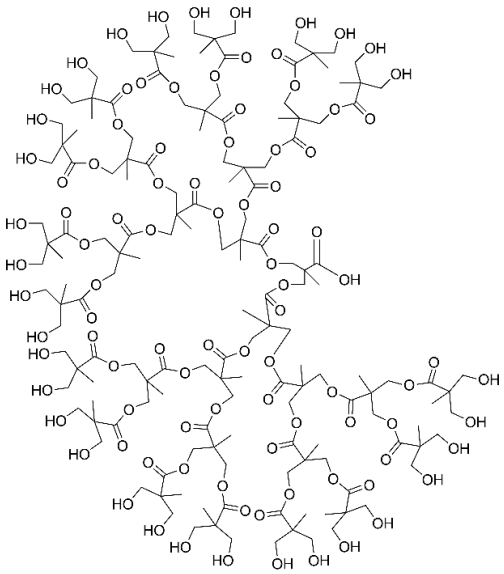

Scheme 2.4. A schematic representation of the structure of dendron-G5-carboxyl-OH.

2.2.5 Material Characterization and Instrumentation

Fourier-transform infrared (FTIR) spectra were acquired using a Nicolet Magna 750 IR spectrophotometer. ^{1}H Nuclear Magnetic Resonance Spectroscopy (NMR) was performed using an Agilent VNMRS four-channel, dual receiver 700 MHz spectrometer. Thermal gravimetric analysis (TGA) data were obtained with a Mettler Toledo TGA/DSC 1 Star System under an Ar atmosphere (25–800 ℃, 10 ℃/min).

X-ray Photoelectron Spectroscopy (XPS) was performed on a Kratos Axis Ultra instrument operating in energy spectrum mode at 140 W. Samples were prepared by depositing SiNC solutions onto a copper foil substrate and drying at room temperature to obtain a thin film coating. The base and operating chamber pressure were maintained at 10^{-7} Pa. A monochromatic Al Kα source (λ = 8.34 Å) was used to irradiate the samples, and the spectra were obtained with an electron take-off angle of 90°. CasaXPS software (VAMAS) was used to interpret high-resolution spectra. All spectra were internally calibrated to the C 1s emission (284.8 eV). The following is an example that uses a high-resolution Si 2p region to show the fitting process: first, a background-subtracted spectrum was obtained by subtracting the background from the original spectrum; then, the background-subtracted spectrum was processed to deconvolute the Si $2p_{1/2}$ peak from the spin-orbit doublet. To perform the spin-orbit stripping procedure, the energy difference between the Si $2p_{3/2}$ and Si $2p_{1/2}$ peaks was fixed at 0.6 eV, and the Si $2p_{1/2}$ to Si $2p_{3/2}$ peak area ratio was fixed at

0.5. The full widths at half-maximum (FWHM) of all peaks were fixed to be the same, except for the Si (0) $2p_{3/2}$ and Si (0) $2p_{1/2}$ components.[22]

2.3 Results and Discussion

In the present study, a convergent method and a divergent method were explored to build dendrimer structures on SiNCs. In divergent methods, ester terminated SiNCs (SiNC-ester) or ammonium terminated SiNCs (SiNC-ammonium) were prepared first as the core material, then repetitively reacted with ethylenediamine/methyl acrylate or methyl acrylate/ethylenediamine, respectively, to get a higher generation of dendrimers. In convergent methods, H-SiNCs or ammonium terminated SiNCs were coupled with commercialized dendrons to obtain the desired products.

2.3.1 Characterizations of H-SiNCs, SiNC-ammonium, and SiNC-ester

H-SiNCs: Hydride-terminated SiNCs (H-SiNCs) were prepared following procedures developed in the Veinot laboratory. First, hydrogen silsesquioxane (HSQ) was synthesized and characterized by FTIR. In the FTIR spectrum (Figure 2.2), a characteristic absorption peak at 2251 cm^{-1} was assigned to Si-H stretching. The peak between 1300 and 800 cm^{-1} was assigned to internal vibrations of the Si-O-Si cage framework. These peaks indicated the successful preparation of HSQ.[11]

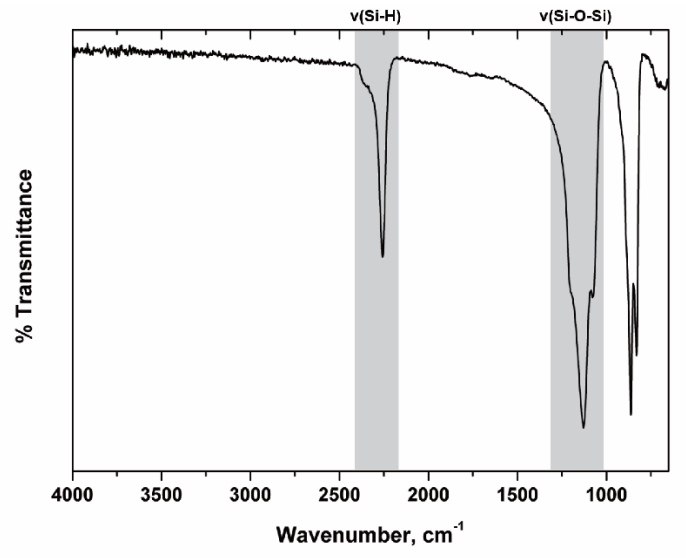

Figure 2.2. FTIR spectrum of synthesized HSQ.

The successful preparation of HSQ also was confirmed by NMR in toluene-D_8 (Figure 2.3). In the NMR spectrum, a characteristic broad peak at 4–5 ppm could be found and assigned to Si-H hanging around the Si-O-Si cage framework, which indicates the successful preparation of HSQ (despite several sharp peaks at ~4.3 ppm, which are assigned to Si-H from low polymerized HSQ; this will be discussed more in Chapter 4).

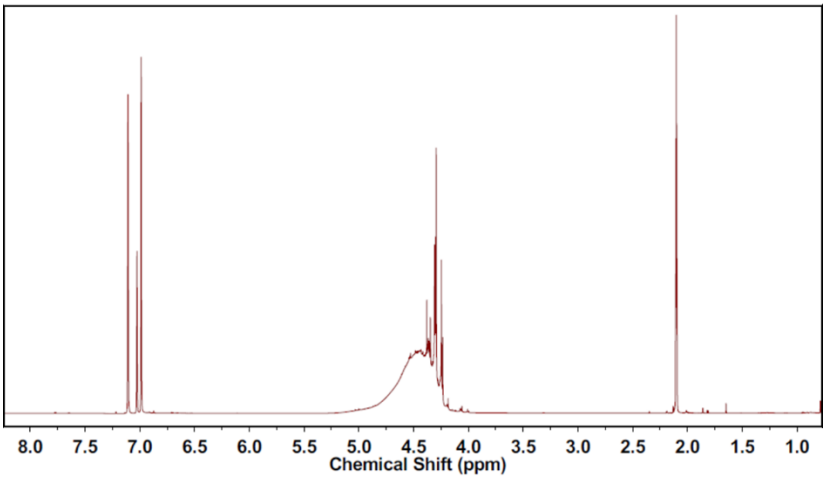

Figure 2.3. ^{1}H NMR spectrum of HSQ in toluene-D_8.

By annealing hydrogen silsequioxane (HSQ) at 1100 °C under a slightly reducing atmosphere, SiNCs/SiO_2 composite was formed. The SiNCs were liberated from the composite by etching in alcoholic hydrofluoric acid and became H-SiNCs. In the FTIR spectrum (Figure 2.4), the peaks at 2100–2000 cm^{-1} and 1100–1000 cm^{-1} correspond to residual Si-H and Si-O-Si, respectively, indicating the successful preparation of H-SiNCs. However, the H-SiNCs tended to be oxidized by O_2 and had limited solubility in solvents. Their surfaces needed to be passivated with ligands to get higher stability and solubility.

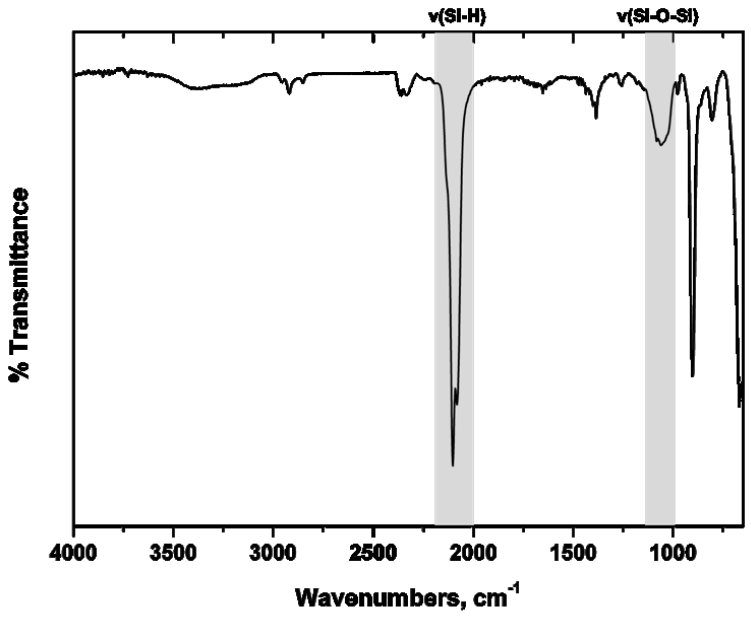

Figure 2.4. FTIR spectrum of H-SiNCs.

In the present work, SiNCs that are soluble in polar solvents (methanol) were needed to adapt the reaction conditions of a Michael addition and amination reaction, therefore, methyl 10-

undecenoate or N,N-bis(trimethylsilyl)-10-undecen-1-amine was used to prepare ester or ammonium terminated SiNCs, respectively.

SiNC-ammonium: First, the capping agent, N,N-bis(trimethylsilyl)-10-undecen-1-amine, was synthesized. The successful preparation of N,N-bis(trimethylsilyl)-10-undecen-1-amine was confirmed by NMR (Figure 2.5). ^{1}H NMR (500 MHz, Toluene-D_8) δ (ppm) = 5.80 (m, 1 H, H_2C=C$\underline{H}$CH_2), 4.99 (m, 2 H, $\underline{H_2}$C=CHCH_2), 2.65 (m, 2 H, -$\underline{H_2}$C-N), 2.05 (m, 2 H, =CH-C$\underline{H_2}$-), 1.35 (m, 14 H, -(C$\underline{H_2}$)$_7$-), 0.05 (s, 18 H, -[Si(C$\underline{H_3}$)$_3$]$_2$).

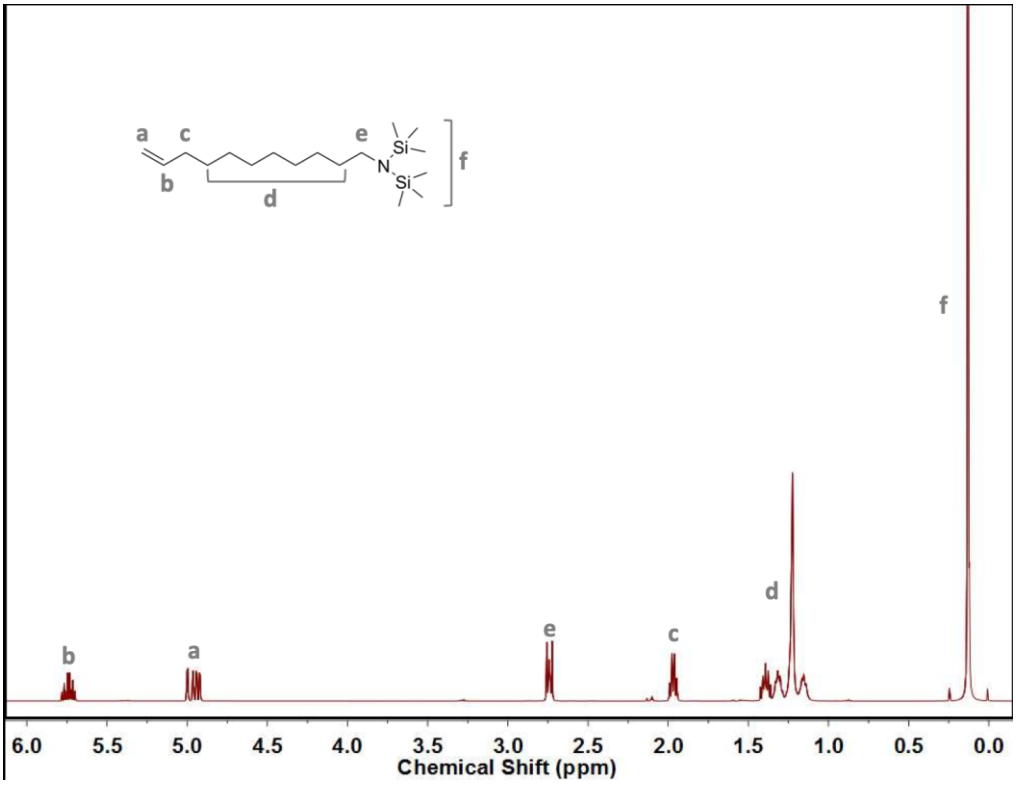

Figure 2.5. ^{1}H NMR spectrum of N,N-bis(trimethylsilyl)-10-undecen-1-amine in toluene-D_8.

After the thermal hydrosilylation reaction of H-SiNCs and N,N-bis(trimethylsilyl)-10-undecen-1-amine, followed by a hydrolysis reaction to remove trimethylsilyl groups, the resulting product, SiNC-ammonium, exhibited good solubility in methanol; this methanol solution showed red photoluminescence under UV light (~350 nm). The successful functionalization and deprotection were confirmed by NMR and FTIR. The ^{1}H NMR spectrum of SiNC-ammonium in DMSO-D_6 (Figure 2.6) indicated the presence of undecylammonium groups on the surface of SiNCs. In addition to the solvent peaks (DMSO-D_6, δ (ppm)= 2.5 and HDO, δ (ppm)= 3.3), there were three other broad peaks that agreed with the signals from ligands attached to SiNCs.[24] The broadened peaks were possibly due to the extended relaxation time because of the slow tumbling of particles in solution.[25] The peak at 2.9–2.7 ppm was attributed to the -C$\underline{H}_2$- that was connected directly to the amine group, the peaks at 1.8–1.1 ppm were attributed to other -C$\underline{H}_2$- groups in the alkyl chain, and the peak at 8.5–8.0 ppm was attributed to the organic ammonium ion.

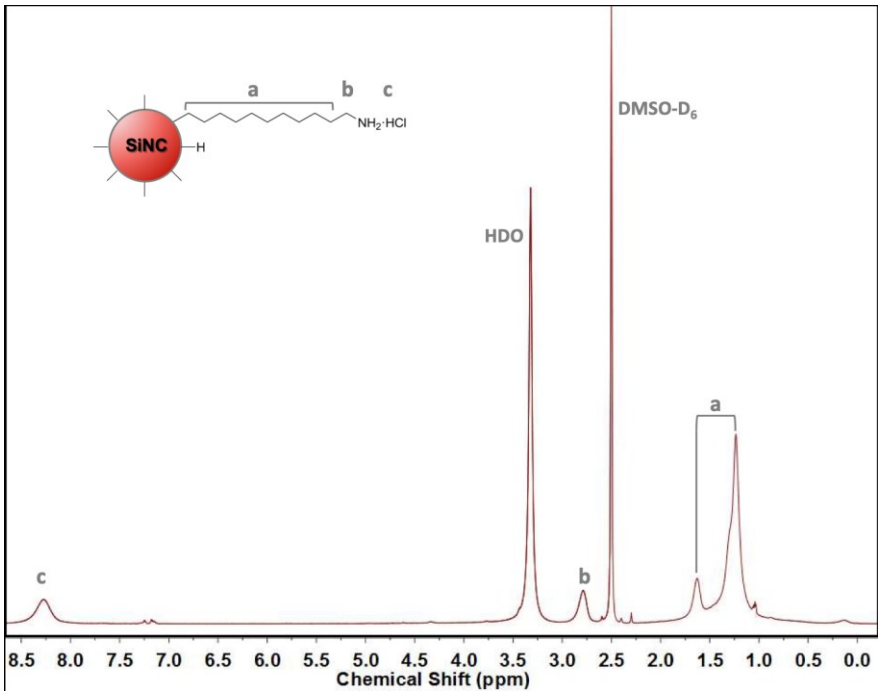

Figure 2.6. ^{1}H NMR spectrum of SiNC-ammonium in DMSO-D_6.

The successful preparation of SiNCs with the desired surface groups was confirmed by FTIR spectroscopy (Figure 2.7). The peaks between 2200 and 2000 cm^{-1} and between 1200 and 950 cm^{-1} corresponded to residual Si-H and Si-O-Si, respectively.[12] The presence of alkyl chain groups was indicated by the two sharp peaks at 3000–2800 cm^{-1} (C-H_x stretching) and the low intensity peak at 1380–1470 cm^{-1} (C-H_x bending). The stretching frequencies of N-H stretching from organic ammonium ion ($–NH_3^+$) overlapped with signals from alkyl chain stretching, therefore, the whole peak was broadened. The presence of the N-H stretching (3450–3250 cm^{-1}) and bending (1650–1500 cm^{-1}) was another proof of the existence of an ammonium group (amine group) in the product.[26]

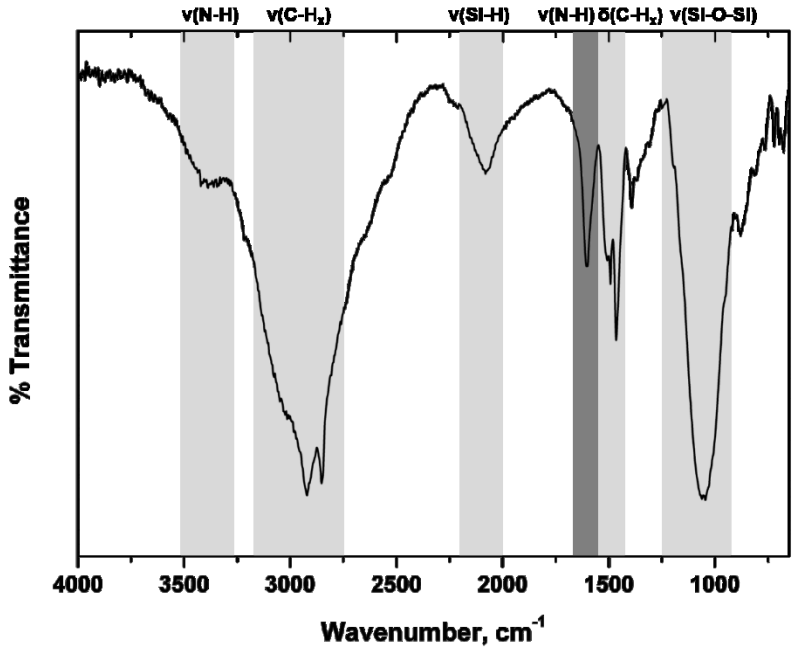

Figure 2.7. FTIR spectrum of SiNC-ammonium.

Survey X-ray photoelectron spectroscopy (XPS) confirms that the resulting SiNCs contain Si, C, N, and Cl (Figure 2.8a). This indicates that the terminal groups of SiNCs are alkylammonium chloride groups. High-resolution XP (HRXP) spectra of the Si 2p region, the C 1s region, and the N 1s region reveal more information on the surfaces of SiNC-ammonium. In the Si 2p region (Figure 2.8b), a characteristic peak at 99.3 eV indicates that the sample contains a Si (0) core. Additional peaks, Si (I) at 100.3 eV, Si (III) at 102.3 eV, and Si (IV) at 103.5 eV, result from surface ligands and suboxides, which agrees with the FTIR data. In the N 1s region (Figure 2.8d), two peaks at 399.8 eV and 401.6 eV assigned to the alkylamine group ($-CH_2-NH_2$) and alkylammonium group ($-CH_2-NH_3^+$),[27] respectively, confirm the successful preparation of alkylammonium terminated SiNCs and also explain the source of the Cl component in the XPS

survey data, the alkylammonium chloride groups. In the C 1s region (Figure 2.8c), the strong peak at 284.8 eV corresponds to C-C in alkyl chains. A peak with higher binding energy at 286.0 eV corresponding to C-N provides another proof of the formation of SiNC-ammonium.

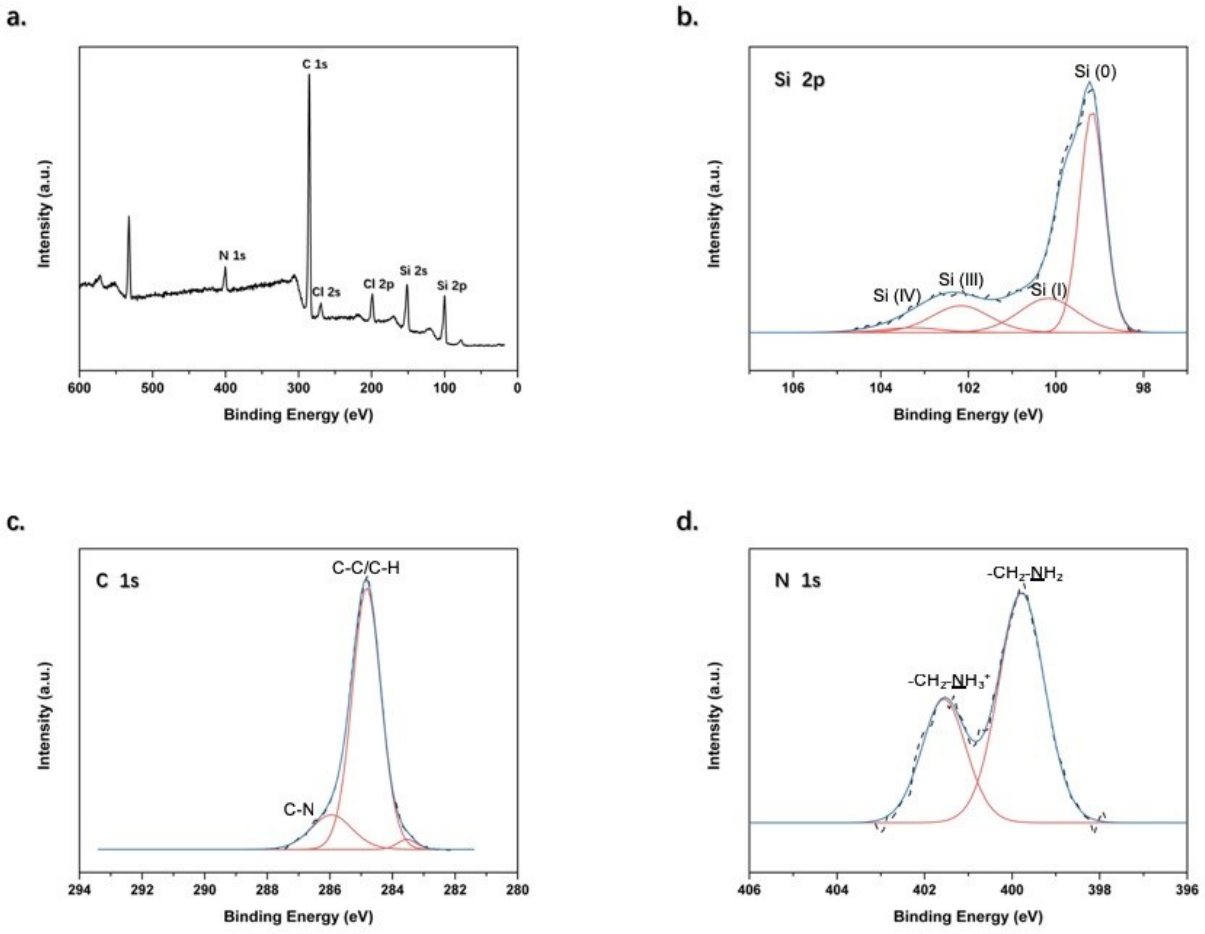

Figure 2.8. (a) Survey scan of SiNC-ammonium. (b) HRXP spectra of the Si 2p region of SiNC-ammonium. Please note, only $2p_{3/2}$ components are shown; $2p_{1/2}$ components are omitted for clarity. (c) HRXP spectra of the C 1s region of SiNC-ammonium. (d) HRXP spectra of the N 1s region of SiNC-ammonium. In (b), (c), and (d), the dashed black lines are the experimental data and the blue lines are the fitting data.

SiNC-ester: the ester terminated SiNCs (SiNC-ester) were obtained through the thermal hydrosilylation reaction of H-SiNCs and methyl 10-undecenoate. After the functionalization, the resulting product was partially soluble in methanol. The filtrate of the methanol solution showed a dark orange colour and red photoluminescence under UV light (~350 nm). The successful functionalization was confirmed by NMR and FTIR. In the NMR spectrum of SiNC-ester (Figure 2.9), the broad peaks at 3.70–3.40 ppm, 2.60–2.15 ppm, and 2.05–0.8 ppm were attributed to –O–C<u>H</u>$_3$, –C<u>H</u>$_2$–COO–, and other –C<u>H</u>$_2$– groups on the alkyl chain, respectively.

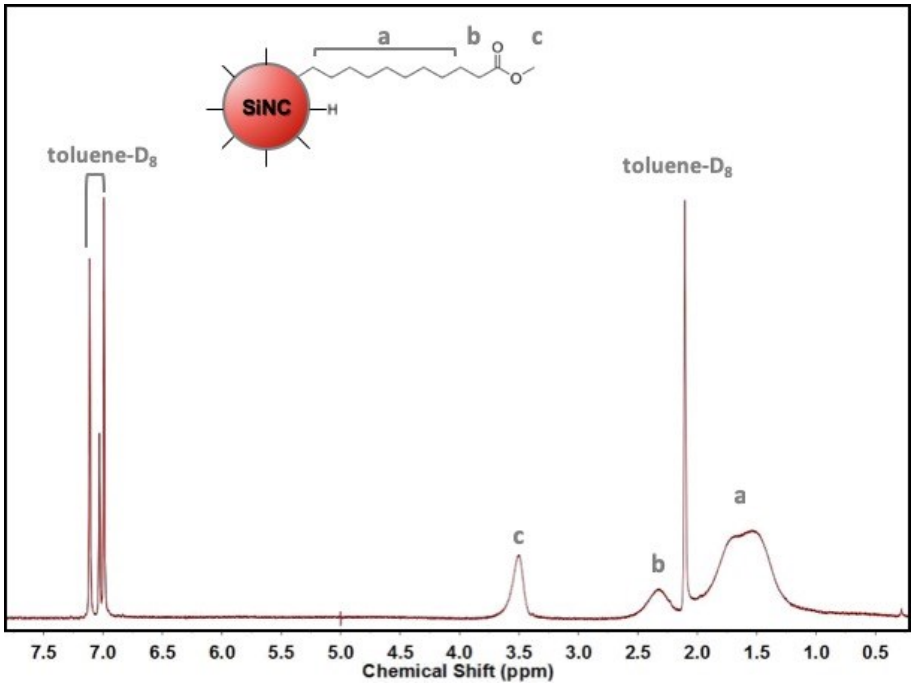

Figure 2.9. ^{1}H NMR spectrum of SiNC-ester in toluene-D$_8$.

In the FTIR spectrum of SiNC-ester (Figure 2.10), the peak between 2100 and 2000 cm^{-1} and the peak between 1100 and 1000 cm^{-1} corresponded to Si-H and Si-O-Si, respectively. The presence of alkyl chain groups was indicated by the two sharp peaks at 3000–2800 cm^{-1} (C-H$_x$

stretching) and the low intensity peak at 1380–1470 cm^{-1} (C-H_x bending). The peak at 1850–1650 cm^{-1} corresponding to the C=O stretching and the peak around 1200 cm^{-1} corresponding to the C–O stretching indicated the existence of an ester group in the product.

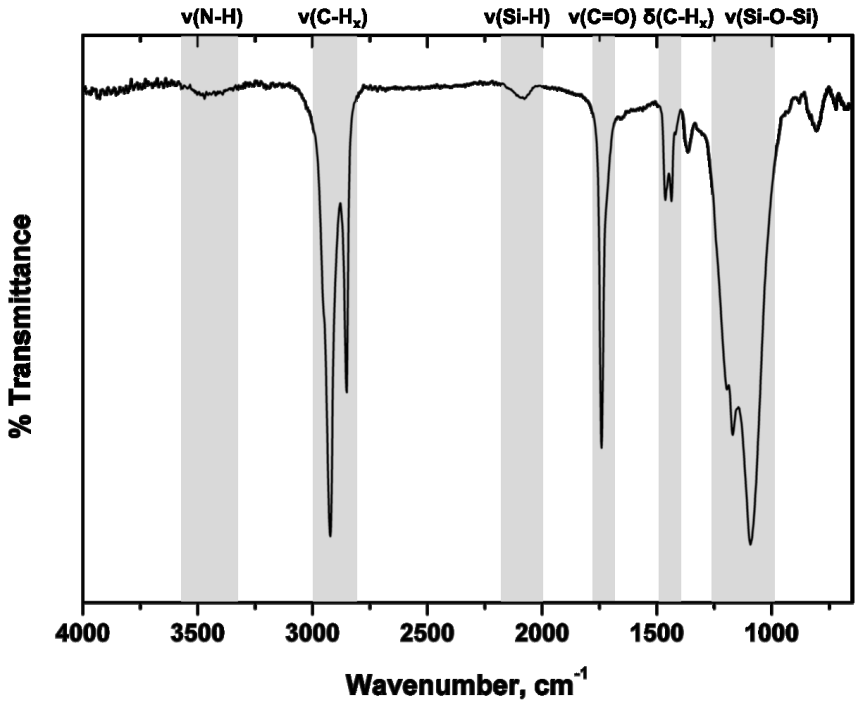

Figure 2.10. FTIR spectrum of SiNC-ester.

Further exploration of the ester terminated SiNCs was performed using XPS. Survey X-ray photoelectron spectroscopy (XPS) confirms that the resulting SiNCs contain Si, C, and O. In HRXP spectra of the Si 2p region (Figure 2.11a), a characteristic peak at 99.3 eV indicates that the sample contains a Si (0) core. Additional peaks, Si (I) at 100.3 eV, Si (III) at 102.3 eV, and Si (IV) at 103.5 eV, result from surface ligands and suboxides, which agrees with the FTIR data. In the C 1s region (Figure 2.11b), the strong peak at 284.8 eV corresponds to C-C in alkyl chains. The other

two peaks, at 286.5 eV and 289.0 eV, correspond to -(C=O)-O-CH_3 and -(C=O)-O, respectively, (and no C=C could be found), which indicate the successful preparation of SiNC-ester.

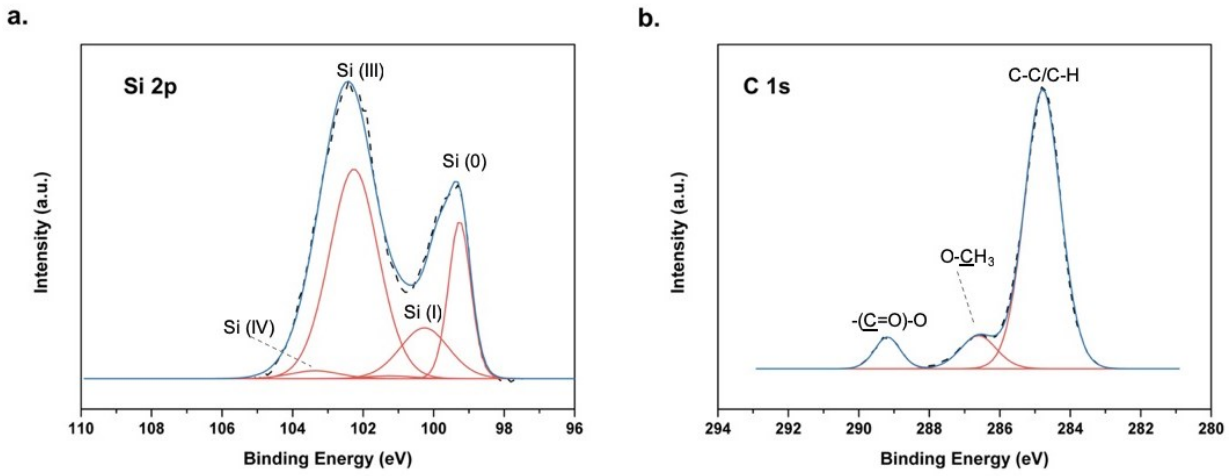

Figure 2.11. (a) HRXP spectra of the Si 2p region of SiNC-ester. Please note, only $2p_{3/2}$ components are shown; $2p_{1/2}$ components are omitted for clarity. (b) HRXP spectra of the C 1s region of SiNC-ester. In (a) and (b), the dashed black lines are the experimental data and the blue lines are the fitting data.

2.3.2 Divergent Method to Synthesize SiNC@PAMAM

After getting the two core materials, SiNC-ester and SiNC-ammonium, a Michael addition and amination reaction were applied repetitively to get a higher generation of dendrimers. The progress of the reactions was confirmed by FTIR (Figure 2.12). Taking SiNC-ester-PAMAM as an example, in Figure 2.12a, peaks, such as C-H (sp^3) stretching (3000–2840 cm^{-1}), -CH_2- bending (1500–1300 cm^{-1}), and Si-O-Si stretching (1200–950 cm^{-1}), indicated the presence of an alkyl chain structure and SiNCs in the conjugates. As the reactions progressed, signals from N-H stretching around 3500–3200 cm^{-1} and N-H bending (from -CONH- group) around 1600–1500 cm^{-1} started showing

up after SiNC-ester-G0, which indicated the existence of NH or NH_2 groups in the conjugates. From SiNC-ester to SiNC-ester-G0, the signal of C=O stretching from the -$COOCH_3$ group (1800–1700 cm^{-1}) disappeared, while the signal of C=O stretching from the -CONH- group (1700–1600 cm^{-1}) showed up, which indicated the occurrence of the amination reaction. From SiNC-ester-G0 to SiNC-ester-G0.5, the signal of C=O stretching from the -$COOCH_3$ group (1800–1700 cm^{-1}) and the signal of C=O stretching from the -CONH- group (1700–1600 cm^{-1}) appeared, indicating the occurrence of the Michael addition. The conclusion is that the repetitive reactions of the amination reaction and the Michael addition worked well on the surface of SiNCs and could be confirmed by comparing the signal of C=O from different groups through SiNC-ester to SiNC-ester-G1.5. A similar trend could be found in the FTIR data (Figure 2.12b) of SiNC-ammonium to SiNC-ammonium-G1, which indicated that the Michael addition worked well in the case of using SiNC-ammonium as the core material.

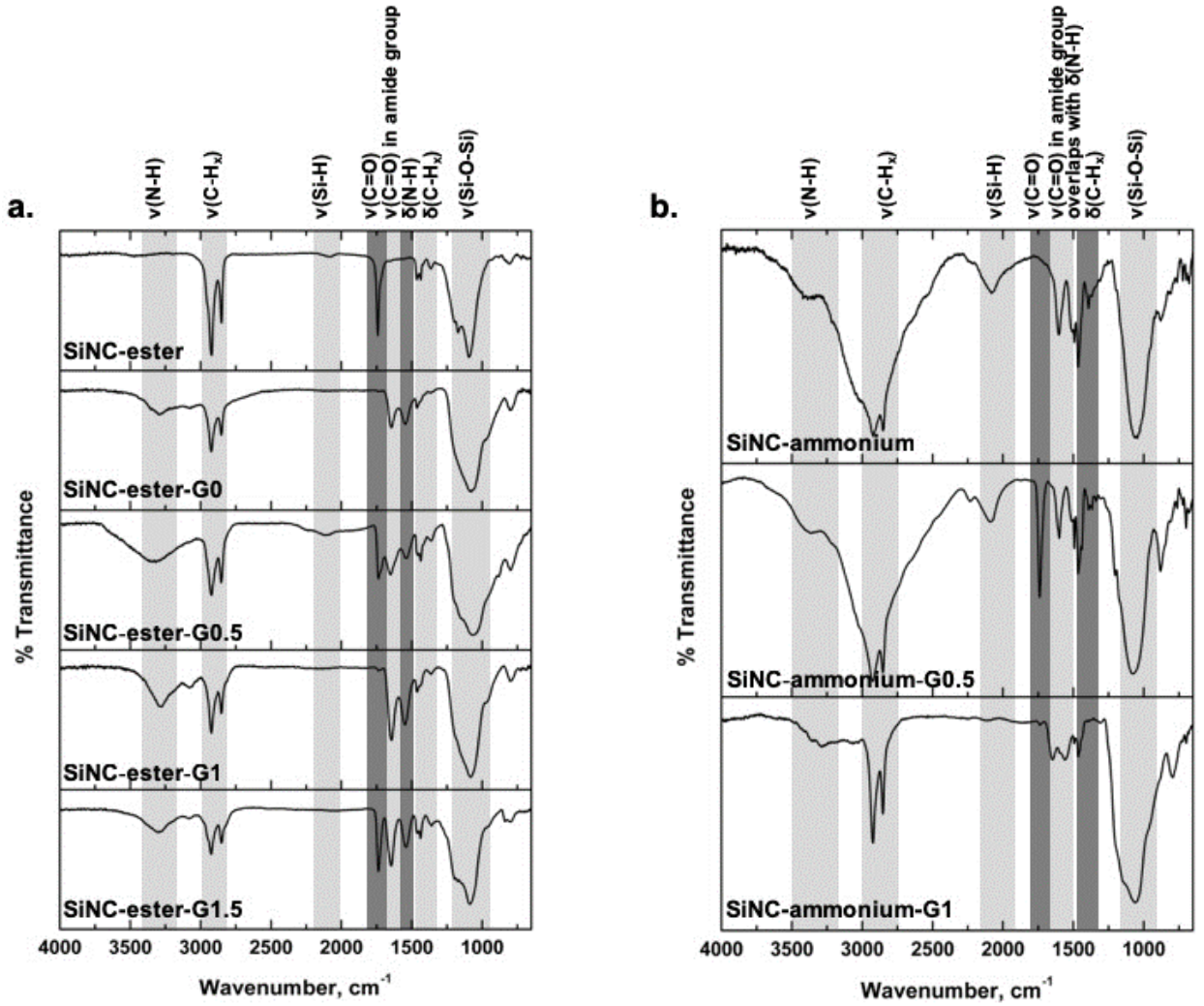

Figure 2.12. (a) FTIR of different generations of SiNC-ester-PAMAM. (b) FTIR of different generations of SiNC-ammonium-PAMAM.

Thermal gravimetric analysis (TGA) of SiNC-ester-PAMAM was performed to test whether the ligands are stepwise functionalized on SiNCs after each reaction or not, and the data is shown in Figure 2.13. The weight loss released the amount of ligands being functionalized on SiNCs. As the reaction progressed, the total weight loss increased from SiNC-ester-G0 (43.9%), SiNC-ester-G0.5 (50.56%), to SiNC-ester-G1.5 (61.81%), which indicated that ligands are

"growing" on SiNCs with the reaction. There were two steps in each graph, Step 1 from 25 ℃ to 300 ℃ and Step 2 from 300 ℃ to 800 ℃. By analyzing the structure of SiNC@PAMAM, there were mainly two kinds of bonds in the structure, C—C and C—N. The bond energy of C—C (346 kJ/mol) was higher than that of C—N (305 kJ/mol).[28] A reasonable hypothesis could be made that Step 1 is attributed to the terminal functional group at the end of the long alkyl chain and Step 2 is attributed to the long alkyl chain. This hypothesis was confirmed by analyzing the ratio of weight loss in Step 2 to the weight remaining after Step 1, which is 0.37:1 in SiNC-ester-G0, 0.38:1 in SiNC-ester-G0.5, and 0.40:1 in SiNC-ester-G1.5. These ratios are quite close, which indicates that the new ligands reacted on the terminal groups on the SiNCs instead of the surfaces of SiNCs. This result reveals that the stepwise reactions based on the Michael addition and amination reaction worked well.

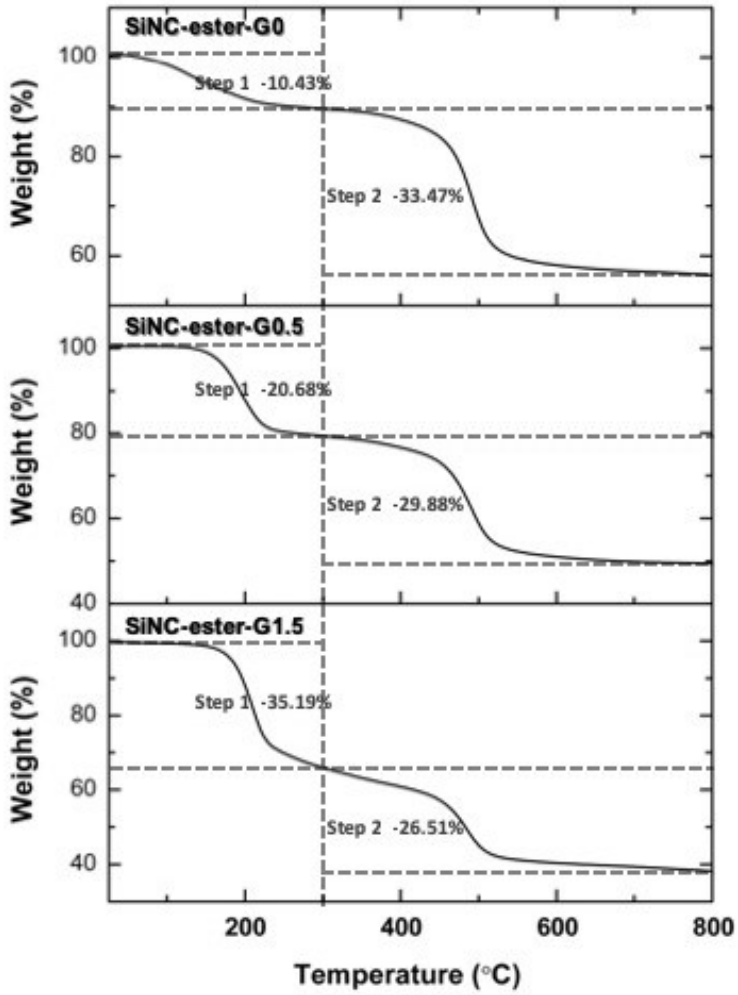

Figure 2.13. TGA data of SiNC-ester-G0, SiNC-ester-G0.5, and SiNC-ester-G1.5.

Further exploration of the progress of the Michael addition and the amination reaction on SiNCs was performed using XPS. A comparison of the HRXP spectra of the Si 2p region (Figure 2.14b) with the progress of the reactions shows that the intensity of the Si (0) component at 99.4 eV (and Si (I) at 100.4 eV) was decreasing while that of Si (III/IV) component (oxidized Si) at 102~104 eV was increasing, which means that the oxidation of silicon or some side reaction (e.g. ethylenediamine reacted with SiNCs) occurred during the reactions; this agrees with the PL blue

shifting from SiNC-ester to SiNC-ester-G1.5. In the HRXP spectra of the C 1s region (Figure 2.14a), signals from C-C/C-H can be found in all the spectra at 284.8 eV. From SiNC-ester to SiNC-ester-G0, the signals from -(C=O)-O-CH_3 (at 289.0 eV) and -(C=O)-O-CH_3 (at 286.5 eV) decreased/disappeared, while the peaks at 286.0 eV and 288.2 eV showed up, which correspond to C-N and -(C=O)-NH-, respectively, indicating that the amination reaction between -(C=O)-O-CH_3 and ethylenediamine took place, and an amide group formed. From SiNC-ester-G0 to SiNC-ester-G0.5, the signal from C-N (at 286.0 eV) decreased while signals from -(C=O)-O-CH_3 (at 289.0 eV) and -(C=O)-O-CH_3 (at 286.5 eV) increased/appeared, indicating that the Michael addition between the terminal group amine (from SiNC-ester-G0) and methyl acrylate took place, and an amide group formed. Similar analysis can be applied to the other three graphs, with more amine groups formed after each reaction, which indicates that the stepwise reactions are successful.

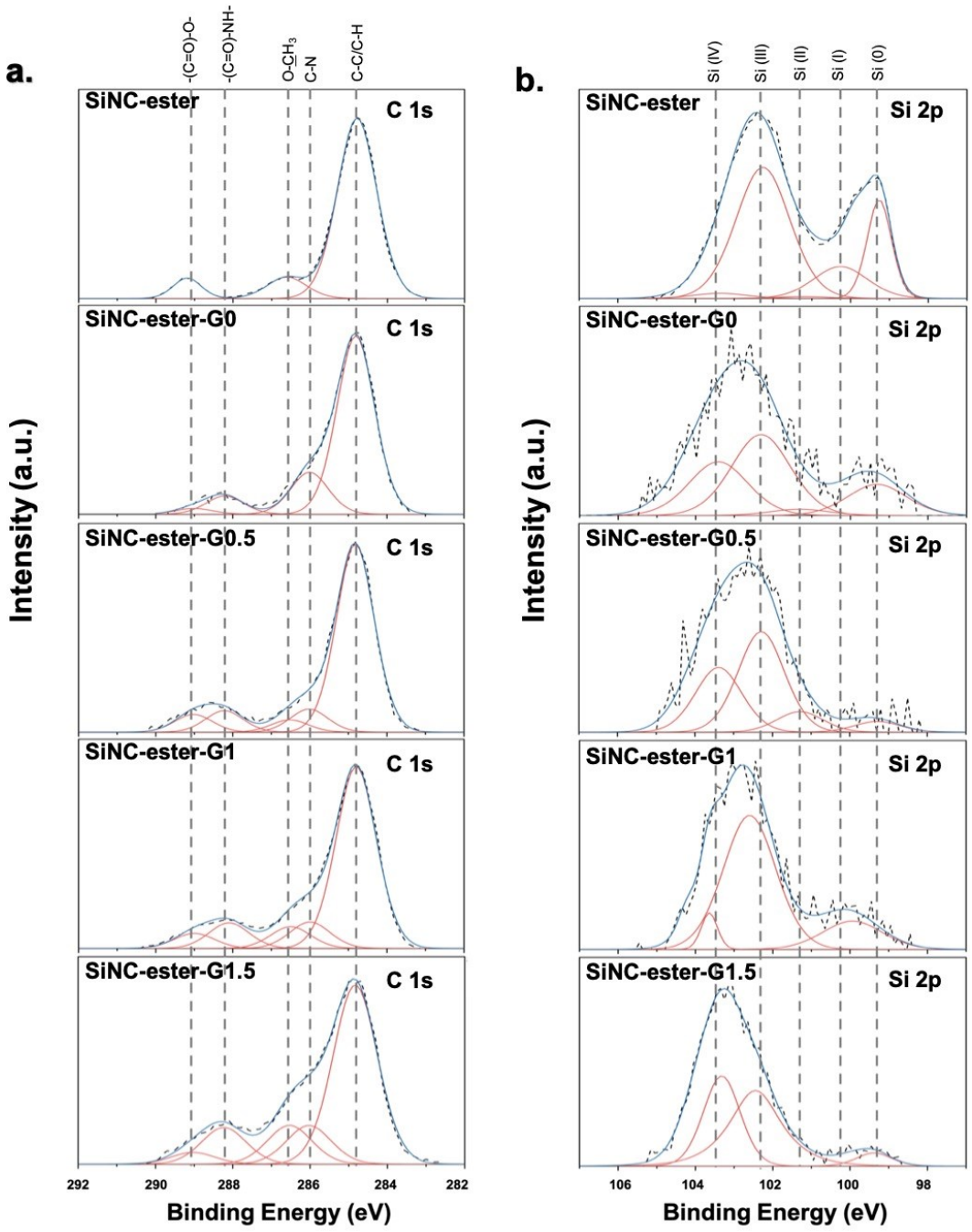

Figure 2.14. (a) HRXP spectra of the C 1s region of SiNC-ester to SiNC-ester-G1.5. (b) HRXP spectra of the Si 2p region of SiNC-ester to SiNC-ester-G1.5. Please note, only $2p_{3/2}$ components are shown; $2p_{1/2}$ components are omitted for clarity. In (a) and (b), the dashed black lines are the experimental data and the blue lines are the fitting data.

By analyzing the HRXP spectra from SiNC-ammonium to SiNC-ammonium-G1, similar trends could be found. In the Si 2p region (Figure 2.15c), with the progressing of reactions, Si cores tend to be oxidized (or react with ammine group). In the C 1s region (Figure 2.15a), signals from C-C/C-H (at 284.8 eV) could be found in all the three spectra, while the signal from C-N (at 286 eV) decreases from SiNC-ammonium to SiNC-ammonium-G0.5, then increases from SiNC-ammonium-G0.5 to SiNC-ammonium-G1. Meanwhile, signals from -(C=O)-NH- (at 288.2 eV) and -(C=O)-O-CH_3 (at 289.0 eV) increase during the process. These facts indicate that the stepwise reactions are successful. It is worth noting that the intensity of the C-N peak (at 286.0 eV) shows a large increase from SiNC-ammonium-G0.5 to SiNC-ammonium-G1, which may be caused by the reaction between ethylenediamine and SiNCs (a side reaction we would not expect; a reason for the blue shifting of the photoluminescence of resulting SiNCs). This result agrees with the N-Si peak at 398.2 eV in the HRXP spectra of the N 1s region (Figure 2.15 b) of SiNC-ammonium-G1 and the Si-N peak at around 103 eV in the HRXP spectra of the Si 2p region of SiNC-ammonium-G1.[29] Although the Michael addition and the amination reaction on SiNCs can be performed, the reagent, ethylenediamine, causes serious crosslinking between SiNCs, and there is a severe side reaction of ethylenediamine and SiNCs (which caused the PL blue-shifting of SiNCs, and potentially quenched the PL).

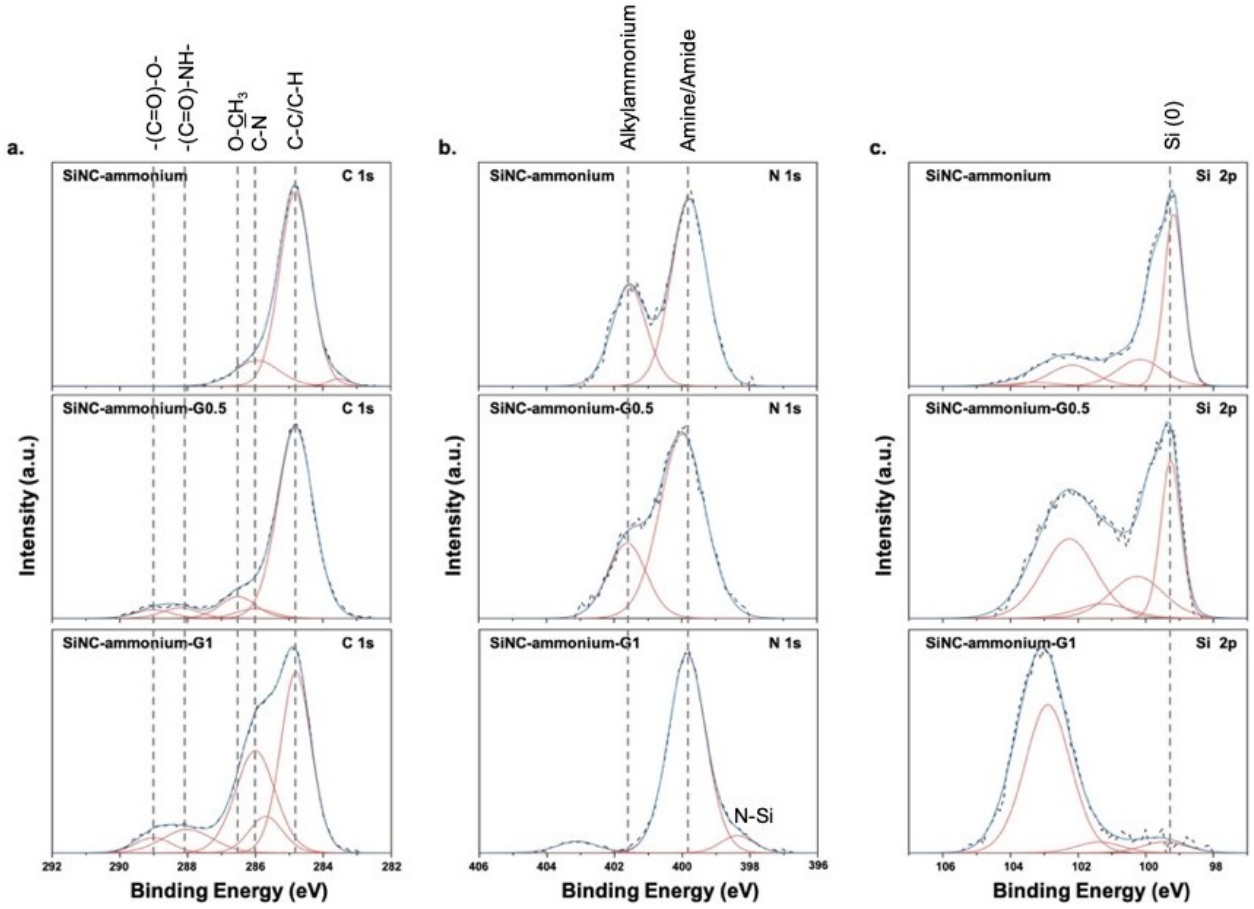

Figure 2.15. HRXP spectra of (a) the C 1s region, (b) the N 1s region, and (c) the Si 2p region of SiNC-ammonium to SiNC-ammonium-G1. Please note, in (c), only $2p_{3/2}$ components are shown; $2p_{1/2}$ components are omitted for clarity. In (a), (b), and (c), the dashed black lines are the experimental data and the blue lines are the fitting data.

Despite all these promising results, there was one fatal problem in the whole processes. The reagents, methyl 10-undecenoate and ethylenediamine, caused severe crosslinking of SiNCs since both sides of each reagent could react with the terminal group of SiNCs obtained from the last step. After each reaction, a large amount of SiNCs crosslinked and crashed out from the

solution. As the yield became very low, the reactions were hard to keep going until the crosslinking problem could be solved.

In order to overcome the crosslinking problem, a synthesis process without the use of the reagents that caused crosslinking will be discussed in Chapter 4.

2.3.3 Convergent Method to Synthesis SiNC@dendrimer

2.3.3.1 H-SiNCs Coupled with Dendron-G5-acetylene-OH

When the reaction of H-SiNCs and dendron-G5-acetylene-OH was stopped, the reaction mixture was still cloudy and showed light pink PL under UV light. After the dialysis purification and centrifugation, the precipitate was showing faint pink PL under UV light.

In the FTIR results of the supernatant and the precipitate (Figure 2.16), the expected peaks, 3600–3200 cm^{-1} (–OH), 3000–2840 cm^{-1} (C–H(sp3)), 2250–2125 cm^{-1} (Si–H), and 1690–1560 cm^{-1} (–COO–) can be found in the spectrum, which indicates the existence of dendron and SiNCs in the product. A strong signal of Si-O-Si between 1150 and 1000 cm^{-1} indicated the severe surface oxidation, which could be the reason for the disappearance of PL after dialysis. A plausible explanation for the unsuccessful reaction is that due to the bulky structure of dendrons, they could not approach the surfaces of SiNCs to complete the thermal hydrosilylation, therefore, the ligands failed to provide enough protection from oxidation. To overcome this problem, two strategies could be applied; this will be discussed in Chapter 4.

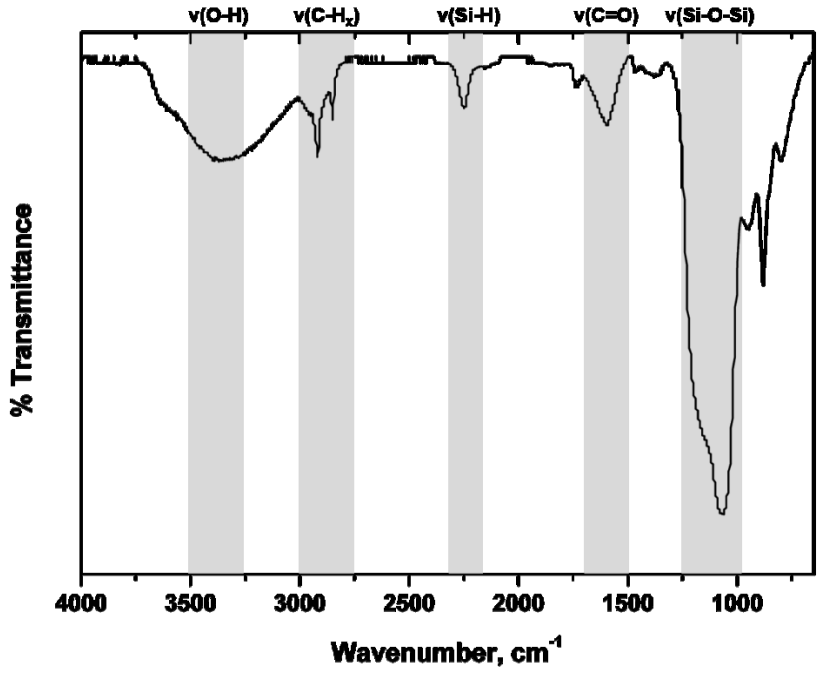

Figure 2.16. FTIR of the product of H-SiNCs and dendron-G5-acetylene-OH.

2.3.3.2 SiNC-Ammonium Coupled with Dendron-G5-Carboxyl-OH

In the case of the reaction between SiNC-ammonium and dendron-G5-carboxyl-OH, the product is partially soluble in water, methanol, or ethanol, and the resulting solutions showed light pink PL under UV light.

The product was characterized by FTIR (Figure 2.17). Peaks at 3600–3200 cm^{-1} (-OH), 3000–2840 cm^{-1} (C-H(sp3)), and 2250–2125 cm^{-1} (Si-H), could be found in the spectrum, as expected, indicating the existence of SiNCs and -OH groups in the product. The appearance of the C=O stretching signal from the -CONH- group (around 1700–1600 cm^{-1}) indicated the formation

of an amide bond. This result indicated that a reaction took place between the two reagents, with amide bonds forming during the reaction.

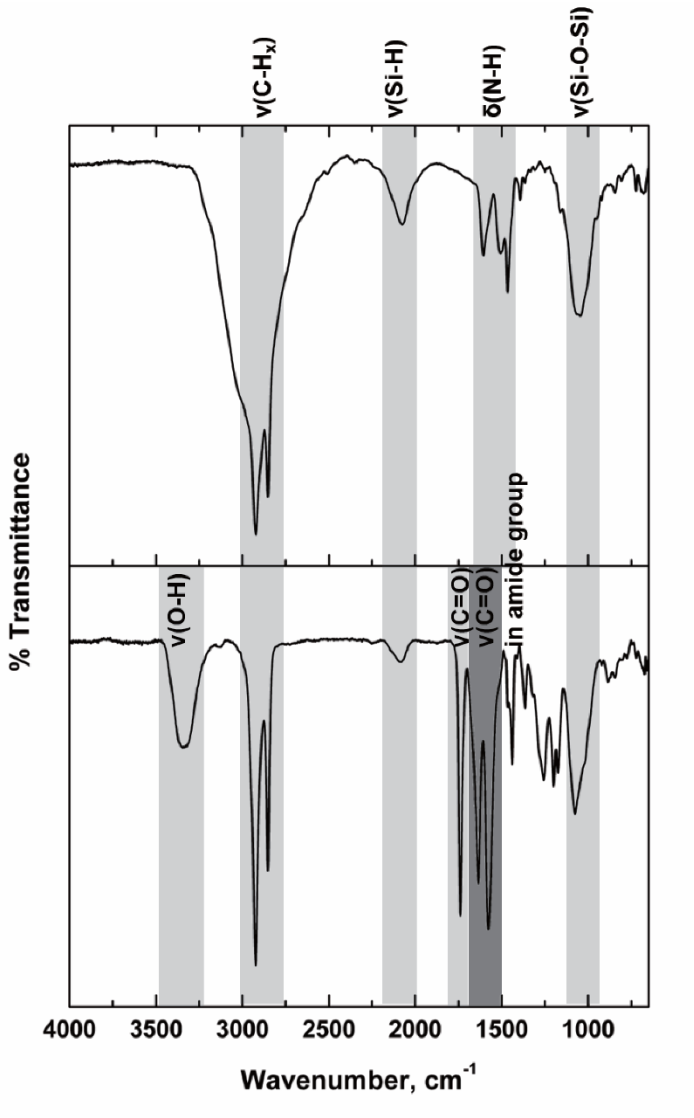

Figure 2.17. FTIR data of SiNC-ammonium (top line) and the product after it reacted with dendron-G5-carboxyl-OH (bottom line).

More work needs to be done to confirm the successful preparation of desire structure and determine the ratio of each component. Moreover, the reaction conditions need to be optimized.

2.4 Conclusions

In this chapter, two kinds of SiNCs, SiNC-ester and SiNC-ammonium, with good solubility in methanol were prepared. Four strategies were used in trying to build dendrimer structures on SiNCs. A series of stepwise reactions was performed on functionalized SiNCs. The possibility of using a Michael addition and amination reaction to build dendrimer structures on SiNCs and the limitations were discussed; they provide a promising path to build dendrimer structures on SiNCs. In the convergent methods, directly functionalizing SiNCs with a bulky dendron was performed, however, the poor coverage limited the solubility and PL property of the product. A more promising way, coupling the dendron with SiNCs functionalized with a long ligand, was attempted. However, the reaction conditions need to be optimized.

2.5 References

(1) Astruc, D.; Boisselier, E.; Ornelas, C. Dendrimers Designed for Functions: From Physical, Photophysical, and Supramolecular Properties to Applications in Sensing, Catalysis, Molecular Electronics, Photonics, and Nanomedicine. *Chem. Rev.* **2010**, *110* (4), 1857–1959.
(2) Li, X.; Kono, K. Functional Dendrimer–Gold Nanoparticle Hybrids for Biomedical Applications. *Polym. Int.* **2018**, *67* (7), 840–852.
(3) Boas, U.; Christensen, J. B.; Heegaard, P. M. Dendrimers: Design, Synthesis and Chemical Properties. *J. Mater. Chem.* **2006**, *16* (38), 3785–3798.
(4) Kaur, D.; Jain, K.; Mehra, N. K.; Kesharwani, P.; Jain, N. K. A Review on Comparative Study of PPI and PAMAM Dendrimers. *J. Nanoparticle Res.* **2016**, *18* (6), 146.
(5) Liu, J.; Erogbogbo, F.; Yong, K.-T.; Ye, L.; Liu, J.; Hu, R.; Chen, H.; Hu, Y.; Yang, Y.; Yang, J. Assessing Clinical Prospects of Silicon Quantum Dots: Studies in Mice and Monkeys. *ACS Nano* **2013**, *7* (8), 7303–7310.
(6) Erogbogbo, F.; Yong, K.-T.; Roy, I.; Hu, R.; Law, W.-C.; Zhao, W.; Ding, H.; Wu, F.; Kumar, R.; Swihart, M. T. In Vivo Targeted Cancer Imaging, Sentinel Lymph Node Mapping and

Multi-Channel Imaging with Biocompatible Silicon Nanocrystals. *ACS Nano* **2010**, *5* (1), 413–423.
(7) McVey, B. F.; Tilley, R. D. Solution Synthesis, Optical Properties, and Bioimaging Applications of Silicon Nanocrystals. *Acc. Chem. Res.* **2014**, *47* (10), 3045–3051.
(8) Buriak, J. M. Organometallic Chemistry on Silicon and Germanium Surfaces. *Chem. Rev.* **2002**, *102* (5), 1271–1308.
(9) Dasog, M.; De los Reyes, G. B.; Titova, L. V.; Hegmann, F. A.; Veinot, J. G. Size vs Surface: Tuning the Photoluminescence of Freestanding Silicon Nanocrystals across the Visible Spectrum via Surface Groups. *ACS Nano* **2014**, *8* (9), 9636–9648.
(10) Maier-Flaig, F.; Rinck, J.; Stephan, M.; Bocksrocker, T.; Bruns, M.; Kübel, C.; Powell, A. K.; Ozin, G. A.; Lemmer, U. Multicolor Silicon Light-Emitting Diodes (SiLEDs). *Nano Lett.* **2013**, *13* (2), 475–480.
(11) Hessel, C. M.; Henderson, E. J.; Veinot, J. G. C. Hydrogen Silsesquioxane: A Molecular Precursor for Nanocrystalline Si−SiO_2 Composites and Freestanding Hydride-Surface-Terminated Silicon Nanoparticles. *Chem. Mater.* **2006**, *18* (26), 6139–6146.
(12) Yang, Z.; Iqbal, M.; Dobbie, A. R.; Veinot, J. G. Surface-Induced Alkene Oligomerization: Does Thermal Hydrosilylation Really Lead to Monolayer Protected Silicon Nanocrystals? *J. Am. Chem. Soc.* **2013**, *135* (46), 17595–17601.
(13) Kelly, J. A.; Veinot, J. G. C. An Investigation into Near-UV Hydrosilylation of Freestanding Silicon Nanocrystals. *ACS Nano* **2010**, *4* (8), 4645–4656.
(14) Mobarok, M. H.; Purkait, T. K.; Islam, M. A.; Miskolzie, M.; Veinot, J. G. Instantaneous Functionalization of Chemically Etched Silicon Nanocrystal Surfaces. *Angew. Chem. Int. Ed.* **2017**, *56* (22), 6073–6077.
(15) Yang, Z.; Gonzalez, C. M.; Purkait, T. K.; Iqbal, M.; Meldrum, A.; Veinot, J. G. Radical Initiated Hydrosilylation on Silicon Nanocrystal Surfaces: An Evaluation of Functional Group Tolerance and Mechanistic Study. *Langmuir* **2015**, *31* (38), 10540–10548.
(16) Pan, B.; Cui, D.; Gao, F.; He, R. Growth of Multi-Amine Terminated Poly (Amidoamine) Dendrimers on the Surface of Carbon Nanotubes. *Nanotechnology* **2006**, *17* (10), 2483.
(17) Abu-Reziq, R.; Alper, H.; Wang, D.; Post, M. L. Metal Supported on Dendronized Magnetic Nanoparticles: Highly Selective Hydroformylation Catalysts. *J. Am. Chem. Soc.* **2006**, *128* (15), 5279–5282.
(18) Khodadust, R.; Unsoy, G.; Yalcın, S.; Gunduz, G.; Gunduz, U. PAMAM Dendrimer-Coated Iron Oxide Nanoparticles: Synthesis and Characterization of Different Generations. *J. Nanoparticle Res.* **2013**, *15* (3), 1488.
(19) Schneider, M. J.; Schäfer, R.; Mülhaupt, R. Aminofunctional Linear Low Density Polyethylene via Metallocene-Catalysed Ethene Copolymerization with N,N-Bis(Trimethylsilyl)-1-Amino-10-Undecene. *Polymer* **1997**, *38* (10), 2455–2459.

(20) Zhang, M.; Kim, H. K.; Chalkova, E.; Mark, F.; Lvov, S. N.; Chung, T. M. New Polyethylene Based Anion Exchange Membranes (PE–AEMs) with High Ionic Conductivity. *Macromolecules* **2011**, *44* (15), 5937–5946.
(21) Luong, D.; Sau, S.; Kesharwani, P.; Iyer, A. K. Polyvalent Folate-Dendrimer-Coated Iron Oxide Theranostic Nanoparticles for Simultaneous Magnetic Resonance Imaging and Precise Cancer Cell Targeting. *Biomacromolecules* **2017**, *18* (4), 1197–1209.
(22) Webb, L. J.; Nemanick, E. J.; Biteen, J. S.; Knapp, D. W.; Michalak, D. J.; Traub, M. C.; Chan, A. S. Y.; Brunschwig, B. S.; Lewis, N. S. High-Resolution X-Ray Photoelectron Spectroscopic Studies of Alkylated Silicon(111) Surfaces. *J. Phys. Chem. B* **2005**, *109* (9), 3930–3937.
(23) Yu, X.; Wang, X.; Zhang, Q.; Li, J.; Liu, J. Oxidation-Resistant, Solution-Processed Plasmonic Ni Nanochain-SiOx ($x < 2$) Selective Solar Thermal Absorbers. *J. Appl. Phys.* **2014**, *116* (7), 073508.
(24) Purkait, T. K.; Iqbal, M.; Islam, M. A.; Mobarok, M. H.; Gonzalez, C. M.; Hadidi, L.; Veinot, J. G. C. Alkoxy-Terminated Si Surfaces: A New Reactive Platform for the Functionalization and Derivatization of Silicon Quantum Dots. *J. Am. Chem. Soc.* **2016**, *138* (22), 7114–7120.
(25) Cheng, X.; Lowe, S. B.; Ciampi, S.; Magenau, A.; Gaus, K.; Reece, P. J.; Gooding, J. J. Versatile "Click Chemistry" Approach to Functionalizing Silicon Quantum Dots: Applications toward Fluorescent Cellular Imaging. *Langmuir* **2014**, *30* (18), 5209–5216.
(26) Robidillo, C. J. T.; Islam, M. A.; Aghajamali, M.; Faramus, A.; Sinelnikov, R.; Zhang, X.; Boekhoven, J.; Veinot, J. G. C. Functional Bioinorganic Hybrids from Enzymes and Luminescent Silicon-Based Nanoparticles. *Langmuir* **2018**, *34* (22), 6556–6569.
(27) Jansen, R. J. J.; Van Bekkum, H. XPS of Nitrogen-Containing Functional Groups on Activated Carbon. *Carbon* **1995**, *33* (8), 1021–1027.
(28) Johnson, S. G. National Standard Reference Data Series https://www.nist.gov/srd/national-standard-reference-data-series (accessed Sep 28, 2018).
(29) Dasog, M.; Yang, Z.; Regli, S.; Atkins, T. M.; Faramus, A.; Singh, M. P.; Muthuswamy, E.; Kauzlarich, S. M.; Tilley, R. D.; Veinot, J. G. C. Chemical Insight into the Origin of Red and Blue Photoluminescence Arising from Freestanding Silicon Nanocrystals. *ACS Nano* **2013**, *7* (3), 2676–2685.

Chapter 3

Preparation of Amphiphilic-SiNCs via Mixed-Surface Ligands

3.1 Introduction

Inorganic nanocrystals (e.g., magnetic, semiconductor, and metallic materials) have become cutting-edge tools in biomedicine, especially in the fields of diagnosis and therapy of diseases.[1] One of the primary issues in exploiting their biomedical applications is to enable these nanomaterials with water solubility or an amphiphilic property. After having grown rapidly in the last few decades, CdSe/ZnS quantum dots (QD),[2] iron oxide nanoparticles,[3] and gold nanoparticles[4] with amphiphilic property have been prepared successfully and used in cancer imaging and gene delivery. Compared to these nanostructures, silicon nanocrystals (SiNCs) have considerable merits; they are abundant, biocompatible, biodegradable, have a long photoluminescence lifetime and bright red/near-infrared PL.[5,6] However, SiNCs with amphiphilic properties have not been studied well.

The commonly used methods to prepare amphiphilic nanoparticle is to coat particles with amphiphilic polymers[1–3,7–10] or to functionalize them with mixed ligands[4,11] (one is hydrophilic, and the other one is hydrophobic). In the present work, we have prepared amphiphilic SiNCs (AP-SiNCs) successfully by thermal hydrosilylation of H-SiNCs with the mixed ligands (allyloxy

(polyethylene oxide) and methyl 10-undecenoate), and the stabilities of SiNCs in buffer solutions were studied to adapt the needs of various applications.

3.2 Experimental

3.2.1 Reagents and Materials

All reagents were used as received, unless otherwise indicated. Electronic grade hydrofluoric acid (HF, 49% aqueous solution) was purchased from J. T. Baker. Toluene (reagent grade), ethanol (reagent grade), hexane (reagent grade), chloroform (reagent grade), methyl 10-undecenoate (96%), Tris(hydroxymethyl)aminomethane hydrochloride (Tris-HCl, reagent grade), NaCl (reagent grade), $NaHCO_3$ (reagent grade), KCl (reagent grade), K_2HPO_4 (reagent grade), $MgCl_2$ (reagent grade), $CaCl_2$ (reagent grade), Na_2SO_4 (reagent grade), Na_2HPO_4 (reagent grade), KH_2PO_4 (reagent grade), glass beads (diam. ~5 mm), Durapore® Membrane 0.1 μm VVPP filter paper, 4 Å molecular sieves (beads, 4–8 mesh), and Amicon Ultra-15 centrifugal filter units were purchased from Millipore Sigma. Hydrochloric acid (HCl, 37%, ~12 mol/L) was obtained from Caledon Laboratory Chemicals, and diluted solutions (1 mol/L and 3 mol/L) were prepared by addition of Milli-Q water. PTFE (polytetrafluoroethylene) centrifuge tubes (50-mL) and 0.2-μm nylon syringe filters were purchased from Thermo Fisher Scientific. Dry toluene was obtained from a Grubbs-type solvent purification system (Innovative Technologies, Inc.) prior to use. Allyloxy (polyethylene oxide) (35–50 EO, 1500–2000 g/mol) was purchased from Gelest

Incorporation and dried by heating at 50 °C via vacuum (~0.2 mTorr) for 48 h. Milli-Q water obtained from a Milli-Q® Reference water purification system. Commercial hydrogen silsesquioxane (HSQ) was obtained as a methyl isobutyl ketone solution from Dow Corning; the solvent was removed under vacuum, and the resulting white solid was used without further purification.

3.2.2 Synthesis of Hydride-Terminated SiNCs (H-SiNCs)

3.2.2.1 Preparation of SiNC/SiO_2 Composite

SiNCs embedded in an SiO_2-like matrix were prepared by thermal decomposition of HSQ following procedures developed by the Veinot group.[12] Thermal processing of HSQ (3.5 g, obtained from Dow Corning) was performed in a Lindberg/Blue furnace at 1100 ℃ for 1 h and 10 min under a slightly reducing atmosphere (5% H_2/95% Ar). (Heating profile: first, the temperature was set to increase from 25 to 1100 ℃ with a ramp rate of 18 ℃/min. Next, the temperature was held at 1100 ℃ for 1 h and 10 min. Finally, the temperature was decreased from 1100 to 25 ℃ by natural cooling.) The resulting amber/black solid was ground in an agate mortar with hexane added to keep the solid wet. After the mixture was ground to a fine dark brown slurry, the grinding was continued without adding more hexane until all the hexane evaporated and the slurry became a fine powder. The brown powder was transferred into a thick-walled flask containing glass beads and shaken for 8 h using a wrist action shaker. Next, ethanol was added into the flask to make a

suspension of SiNC/SiO_2 composite. The suspension was filtered via vacuum filtration using Durapore® Membrane 0.1 μm VVPP filter paper. The SiNCs/SiO_2 composite (yield: 3.3 g, 94%) was stored under ambient conditions until further use.

3.2.2.2 Preparation of Hydride-Terminated SiNCs (H-SiNCs)

H-SiNCs were liberated from the SiNC/SiO_2 composite by alcoholic hydrofluoric acid etching.[12] A detailed procedure of H-SiNCs preparation is given in Section 2.2.2.1. Briefly, 300 mg of SiNC/SiO_2 composite were etched with 4.5 mL of a solution of ethanol:H_2O:49% HF (volume ratio 1:1:1). After 1-h etching, the H-SiNCs were extracted with toluene several times until the aqueous layer became colourless. The H-SiNCs were isolated by centrifugation (3000 rpm, 5 min), followed by washing with dry toluene (4 Å molecular sieves were used to adsorb residual water) two more times. The resulting H-SiNCs should be used for the next step as soon as possible to minimize the surface oxidation.

3.2.3 Synthesis of Amphiphilic SiNCs (AP-SiNCs)

3.2.3.1 Thermal Hydrosilylation

AP-SiNCs were prepared by thermal hydrosilylation of H-SiNCs with the mixed ligands,[13] allyloxy (polyethylene oxide) and methyl 10-undecenoate (Scheme 3.1). In a nitrogen filled glovebox, allyloxy (polyethylene oxide) (4 g, 2.3 mmol) was transferred into an oven dried Schlenk flask equipped with a magnetic stir bar. The flask was sealed, transferred out of the

glovebox, then connected to an Ar charged Schlenk line. Methyl 10-undecenoate (8 mL, 34 mmol) was used to disperse H-SiNCs obtained from Section 3.2.2. The suspension was transferred into the Schlenk flask under an Ar purge. Three freeze/pump/thaw cycles were applied to the mixture. After the last thaw, the flask was refilled with Ar and placed in a pre-heated silicon oil bath (180 °C) on a hot plate under static Ar. The reaction was kept stirring for 1 h, 12 h, or 24 h (at 180 °C) to get AP-SiNCs with different reaction times. The brown slurry turned into a yellow transparent solution in 1 h.

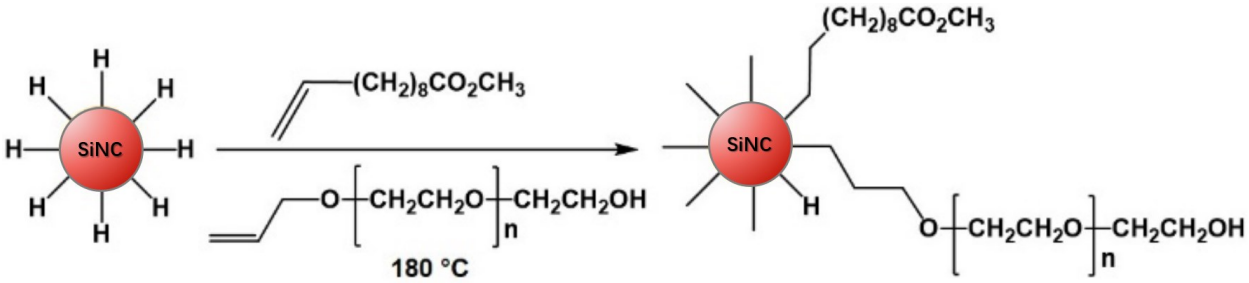

Scheme 3.1. A schematic representation of the preparation of amphiphilic SiNCs via a one-step, mixed ligand hydrosilylation.

3.2.3.2 Purification of the Reaction

After 24 h, the reaction mixture was cooled down naturally to about 50 °C, then transferred to a 50-mL Teflon centrifuge tube, followed by addition of hexane (~40 mL); a pale-yellow precipitate formed. After sitting for 5 min, all the precipitate settled at the bottom of the centrifuge tube, and the supernatant was removed with a Pasteur pipette. The precipitate was dispersed in 5 mL of chloroform, followed by addition of 20 mL of hexane as an anti-solvent. After mixing, the mixture was centrifuged at 5000 rpm for 10 min. The solution separated into 2 layers, an almost colourless

top layer not showing PL under UV light (~350 nm) and a dark orange oily bottom layer showing red PL under UV light (~350 nm). The top layer was removed, while the bottom layer was washed with 5 mL of chloroform and 20 mL of hexane, followed by centrifugation at 5000 rpm for 10 min; this procedure was repeated four more times. After each washing cycle, the volume of the bottom layer decreased because the free allyloxy (polyethylene oxide) ligands were removed from the mixture. After the fifth washing, the bottom layer was treated with 30 mL of hexane to precipitate the resulting AP-SiNCs. After another centrifugation (5000 rpm, 10 min), the supernatant was decanted, and the resulting brown precipitate was dissolved in 5 mL of ethanol (100%). Then, 10 mL of hexane were added to and mixed with the AP-SiNCs ethanol solution. Next, the mixture was centrifuged at 5000 rpm for 10 min. The solution separated into two layers, an almost colourless top layer not showing PL under UV light (~350 nm) and an orange oily bottom layer showing red PL under UV light (~350 nm). After the top layer was removed with a Pasteur pipette, the bottom layer was washed with 5 mL of ethanol (100%) and 10 mL of hexane, followed by centrifugation at 5000 rpm for 10 min; this procedure was repeated four more times. After the fifth washing, 30 mL of hexane were added to precipitate the AP-SiNCs. The final precipitate was isolated by centrifugation at 5000 rpm for 10 min. The resulting yellow solid can be dissolved in toluene or ethanol and stored as a toluene or ethanol solution in a freezer at -20 °C until further use.

3.2.3.3 Solvent Exchange from Ethanol to Water

The AP-SiNCs precipitate prepared from Section 3.2.3.2 was dispersed in 10 mL ethanol, followed by addition of 40 mL of Milli-Q water. The mixed solvent was evaporated under reduced pressure until the volume of liquid was reduced to ~15 mL to minimize the ethanol component. The resulting solution was filtered through a 0.2-μm nylon syringe filter. The filtrate was transferred into an Amicon Ultra-15 centrifugal filter unit (30 kDa), followed by centrifugation at 5000 rpm for 30 min, and the filtrate was discarded. Another 5 mL of Milli-Q water were added into the remaining solution, the mixture was centrifuged at 5000 rpm for 30 min, and the filtrate was discarded; this washing step was repeated four more times to get rid of residual ethanol. Then, the resulting solution (~3 mL) was transferred to a glass vial. A 0.2-mL portion of the solution was freeze dried, then sent for TGA measurement; the rest of the solution was kept in a freezer at -20 °C until further use. From the TGA results, the SiNC-core based concentration can be determined (10.4 mg/mL in the 1-h reaction, 14.0 mg/mL in the 12-h reaction, and 12.2 mg/mL in the 24-h reaction).

3.2.3 The Study of the Stabilities of AP-SiNCs in Buffer Solutions

3.2.3.1 Preparation of Phosphate-Buffered Saline (PBS)

The preparation of PBS followed the recipe from *Cold Spring Harb. Protoc. 2006*[14] with minor changes. The following chemicals, NaCl (4.0 g), KCl (0.1 g), Na_2HPO_4 (0.72 g), and KH_2PO_4

(0.12 g), were weighed in a 1000-mL beaker, followed by addition of 500 mL of Milli-Q water. The pH of the solution was adjusted to 7.4 by addition of an aqueous HCl solution (3.0 mol/L). The resulting solution was transferred into a glass bottle and stored in the fridge (4 ℃) until further use.

3.2.3.2 Preparation of Tris-Buffered Saline (TBS)

The preparation of TBS followed the recipe from *Cold Spring Harb. Protoc. 2014*[15] with minor changes. NaCl (4.4 g) and Tris(hydroxymethyl)aminomethane hydrochloride (Tris-HCl, 1.2 g) were weighed in a 1000-mL beaker, followed by addition of 500 mL of Milli-Q water. The pH of the solution was adjusted to 7.5 by addition of an aqueous HCl solution (3.0 mol/L). The resulting solution was transferred into a glass bottle and stored in the fridge (4 ℃) until further use.

3.2.3.3 Preparation of Simulated Body Fluid (SBF)

The preparation of SBF followed a reported method with minor changes.[16] 900 mL of Milli-Q water were put in a 1000-mL plastic beaker equipped with a magnetic stir bar, and a label was affixed at the 900-mL mark. The water was discarded, and 700 mL of Milli-Q water (preheated to ~37 ℃) were added to the beaker. The beaker was put in a water bath on a hotplate, and the temperature of the water was kept at 36.5 ± 1.5 ℃. The following chemicals were added in sequence: NaCl (8.035 g), $NaHCO_3$ (0.355 g), KCl (0.225 g), K_2HPO_4 (0.176 g), $MgCl_2$ (0.146 g), aqueous HCl solution (1.0 mol/L, 39 mL), $CaCl_2$ (0.292 g), and Na_2SO_4 (0.072 g). (Each chemical

should be dissolved completely before adding the next one.) Next, Milli-Q water was added into the beaker until the liquid level reached the 900-mL mark. Another two chemicals, Tris (6.118 g) and an aqueous HCl solution (1.0 mol/L, 5 mL), were measured and kept in standard vials. The temperature of the solution was maintained at 36.5 ± 0.5 ℃, and a pH meter was placed into the solution to monitor the pH change. Tris was added into the solution slowly until the pH increased from 2.15 to 7.45; at this point, the addition of Tris was stopped, and an aqueous HCl solution (1.0 mol/L) was added dropwise, lowering the pH to 7.41. Then, the addition of the aqueous HCl solution was stopped, and the rest of the Tris was added slowly until the pH reached 7.45. The above process was repeated until all the Tris (6.118 g) was added into the solution. After that, the pH of the final solution was adjusted to 7.40 by addition of an aqueous HCl solution (1 mol/L) at 36.5 ℃. The resulting solution was transferred into a 1000-mL volumetric flask and made up to the mark with Milli-Q water. After mixing, the solution was transferred into a plastic bottle and stored in the fridge (4 ℃) until further use.

3.2.3.4 Stability Test of SiNCs in Different Buffers

The stability of AP-SiNCs was studied by monitoring the changes in the size (by dynamic light scattering) and the photoluminescence (by photoluminescence spectrometer) of AP-SiNCs in the presence of a buffer solution. There were three batches of AP-SiNCs with different reaction times (a 1-h reaction, a 12-h reaction, and a 24-h reaction) and three commonly used buffer solutions (PBS, TBS, and SBF) prepared. Nine combinations of AP-SiNCs in buffer solution were studied

in this section. The process of monitoring the changes in the size and the photoluminescence of AP-SiNCs from a 24-h reaction in a PBS solution is used as an example here (all the other eight combinations follow the same process). The SiNC-core based concentration of concentrated AP-SiNCs aqueous solution (obtained from the 24-h reaction) was calculated from the TGA data (12.2 mg/mL). A 2-mL portion of the solution was transferred into a standard glass vial, followed by addition of 0.44 mL of Milli-Q water to adjust the concentration of the resulting solution to 10.0 mg/mL. PBS (40 mL) was transferred into a 50-mL medical grade polypropylene centrifuge tube and warmed up in an incubator (37 ℃) for 2 h, followed by addition of 0.6 mL of AP-SiNCs solution (10 mg/mL). After mixing, the mixture was filtered through a 0.2-μm nylon syringe filter, and the filtrate was collected with a new polypropylene centrifuge tube. A 0.7-mL portion of the resulting solution was transferred into a standard vial, and PL and DLS measurements were performed immediately; the rest of the solution in the polypropylene centrifuge tube was stored in the incubator (37 ℃). During the first three hours, a 0.7-mL portion of the solution was taken every half hour, and the rest of the solution was returned to the incubator. Between 3 h and 12 h, a 0.7-mL portion of the solution was taken every hour, and the rest of the solution was returned to the incubator. After this point, the same amount of sample was taken at 24 h, 48 h, 72 h, 96 h, and 120 h. Then, samples were taken weekly.

3.2.6 Material Characterization and Instrumentation

Fourier-transform infrared (FTIR) spectra were acquired using a Nicolet Magna 750 IR spectrophotometer. ^{1}H Nuclear Magnetic Resonance Spectroscopy (NMR) was performed using an Agilent VNMRS four-channel, dual receiver 700 MHz spectrometer. Thermal gravimetric analysis (TGA) data were obtained with a Mettler Toledo TGA/DSC 1 Star System under an Ar atmosphere (25–800 ℃, 10 ℃/min). Dynamic light scattering (DLS) data was obtained using a Malvern Zetasizer Nano S series dynamic light scattered with 633 nm laser. All the samples were equilibrated to 25 ℃ prior to data acquisition. Photoluminescence spectra of the samples were obtained using a Varian Cary Eclipse fluorescence spectrophotometer (λ_{ex} = 400 nm).

X-ray Photoelectron Spectroscopy (XPS) was performed on a Kratos Axis Ultra instrument operating in energy spectrum mode at 140 W. Samples were prepared by depositing SiNC solutions onto a copper foil substrate and drying at room temperature to obtain a thin film coating. The base and operating chamber pressure were maintained at 10^{-7} Pa. A monochromatic Al Kα source (λ = 8.34 Å) was used to irradiate the samples, and the spectra were obtained with an electron take-off angle of 90°. CasaXPS software (VAMAS) was used to interpret high-resolution spectra. All spectra were calibrated internally to the C 1s emission (284.8 eV). The following is an example that uses a high-resolution Si 2p region to show the fitting process: first, a background-subtracted spectrum was obtained by subtracting the background from the original spectrum; then, the background-subtracted spectrum was processed to deconvolute the Si $2p_{1/2}$ peak from the spin-

orbit doublet. To perform the spin-orbit stripping procedure, the energy difference between the Si $2p_{3/2}$ and Si $2p_{1/2}$ peaks was fixed at 0.6 eV, and the Si $2p_{1/2}$ to Si $2p_{3/2}$ peak area ratio was fixed at 0.5. The full widths at half-maximum (FWHM) of all peaks were fixed to be the same, except for the Si (0) $2p_{3/2}$ and Si (0) $2p_{1/2}$ components.[17]

3.3 Results and Discussion

In the present study, the thermal hydrosilylation of H-SiNCs with the mixed ligand, allyloxy poly(ethylene oxide) and methyl 10-undecenoate, was performed. The resulting AP-SiNCs showed amphiphilic property. In order to extend the possible applications in bio-systems, their stabilities in different buffer solutions, PBS, TBS, and SBF, were tested.

3.3.1 Characterizations of AP-SiNCs

Modifying polyethylene glycol (PEG) was a commonly used method to increase the water solubility and biocompatibility of materials. However, functionalizing H-SiNCs with PEG alone has limitations, such as blue PL and a limited solubility in water, based on former reports.[18] So, another functional group, methyl 10-undecenoate, was introduced to the reaction to overcome these drawbacks because methyl 10-undecenoate has been reported to work as both a functioning group and a catalyst in hydrosilylation reactions.[19] In the thermal hydrosilation, methyl 10-undecenoate (34 mmol) and allyloxy (polyethylene glycol) (2.3 mmol) were added into the H-SiNCs (obtained from etching 300 mg $SiNC/SiO_2$ composite), followed by heating at 180 ℃.

The successful functionalization of the SiNCs (from the 24-h reaction) was confirmed by FTIR (Figure 3.1) and NMR (Figure 3.2). In the FTIR spectrum, the peaks, at 2950–2850 and 1500–1250 cm^{-1}, which were assigned to C-H (sp^3) stretching and C-H (sp^3) bending, respectively, could be found in all three samples. A characteristic peak at 3480 cm^{-1} found in allyloxy (polyethylene glycol) and AP-SiNCs was assigned to O-H stretching. Likewise, another characteristic peak at 1740 cm^{-1} found in methyl 10-undecenoate and AP-SiNCs was assigned to C=O stretching. These features indicate that both ligands are present in the product.

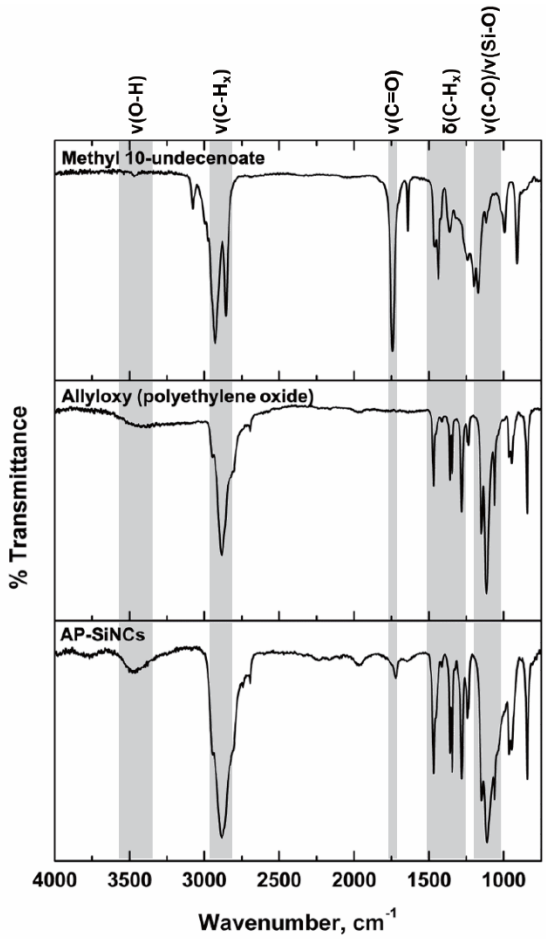

Figure 3.1. FTIR spectra of methyl 10-undecenoate, allyloxy (polyethylene oxide), and AP-SiNCs (from top to bottom).

From the NMR spectra of methyl 10-undecenoate, allyloxy (polyethylene glycol), and AP-SiNCs, it is seen that the protons from CH_2=CH- (6.0–4.75 ppm) (the terminal group of impurities, allyloxy (polyethylene glycol) and methyl 10-undecenoate) became negligible after the reaction. The peak (1.0–0.75 ppm) that showed up in the AP-SiNCs was attributed to Si-CH_2- formed during the reaction, indicating the successful functionalization of SiNCs. The sharp peaks in the reagents became broad peaks in the product, which agrees with the signals from ligands that attached to SiNCs.[20,21]

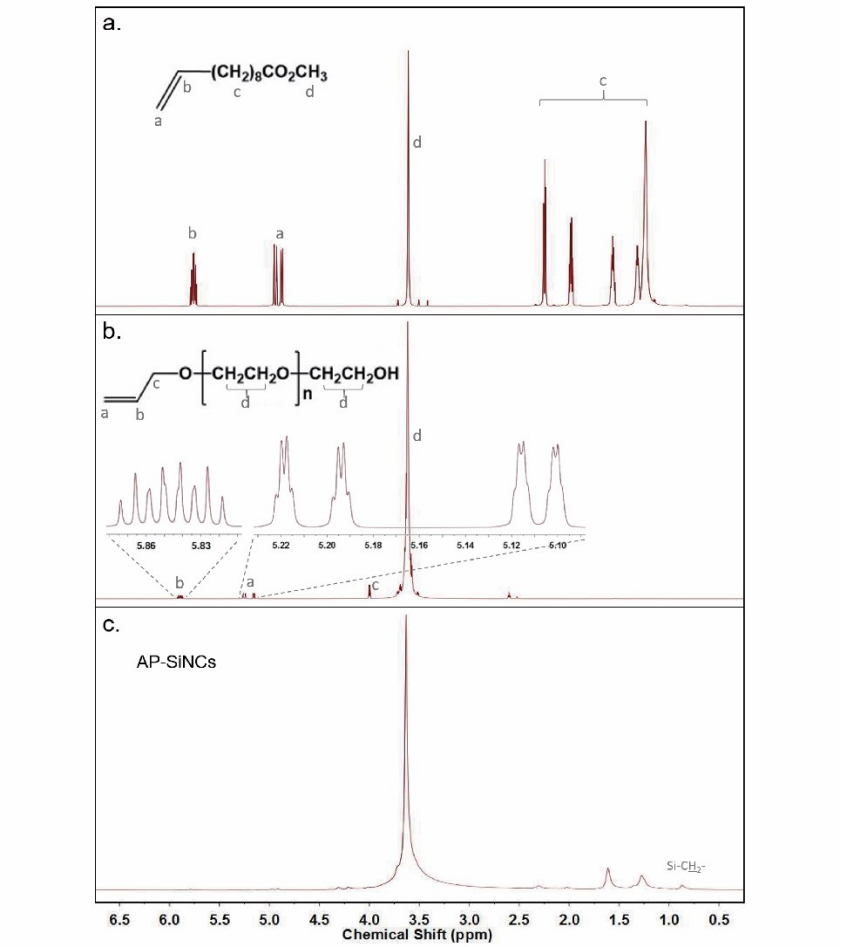

Figure 3.2. NMR spectra of (a) methyl 10-undecenoate, (b) allyloxy (polyethylene glycol), and (c) AP-SiNCs in chloroform-D.

Further exploration of the composition of AP-SiNCs (from the 24-h reaction) was performed using X-ray photoelectron spectroscopy (XPS). Survey XPS confirms that the resulting SiNCs contained Si, C, and O. In high-resolution XP (HRXP) spectra of the Si 2p region (Figure 3.3a), a characteristic peak at 99.3 eV indicates that the sample contains a Si (0) core. Additional peaks, Si (I) at 100.3 eV, Si (III) at 102.3 eV, and Si (IV) at 103.5 eV, result from surface ligands and suboxides, which agrees with the FTIR data. Although surface oxidation is evidenced, Si (0) is the dominant component in the resulting SiNCs; this indicated the AP-SiNCs were passivated well by the mixed ligands and showed relatively good stability. In HRXP spectra of the C 1s region (Figure 3.3b), the strong peak at 284.8 eV corresponds to C-C in alkyl chains. The other two peaks, at 286.5 eV and 288.2 eV, correspond to C-O and -(C=O)-O-,[22] respectively. The high intensity of the C-O peak indicates that both ligands are present in AP-SiNCs.

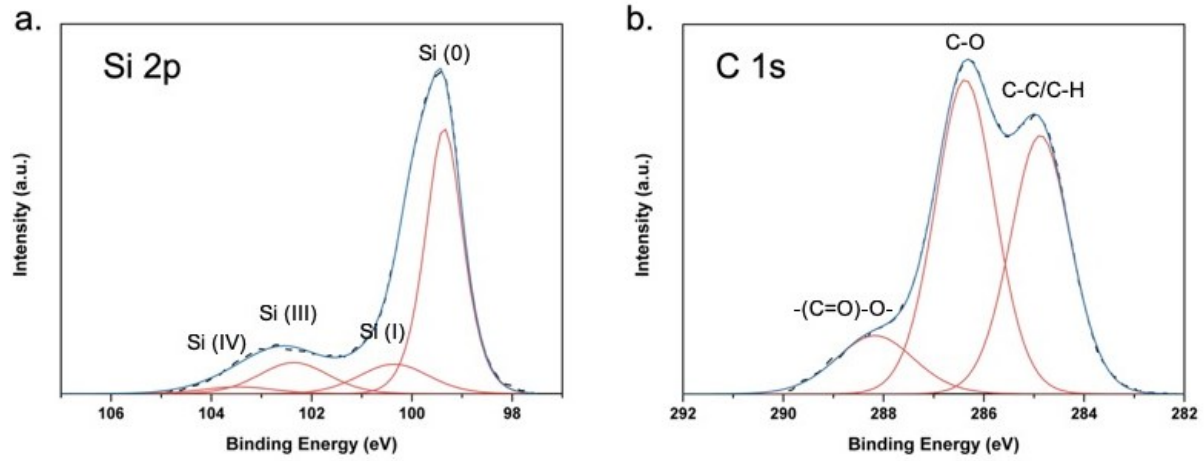

Figure 3.3. (a) HRXP spectra of the Si 2p region of AP-SiNCs. Please note, only $2p_{3/2}$ components are shown; $2p_{1/2}$ components are omitted for clarity. (b) HRXP spectra of the C 1s region of AP-SiNCs. In (a) and (b), the dashed black lines are the experimental data and the blue lines are the fitting data.

After analyzing the composition of the AP-SiNCs, DLS was used to determine the solvodynamic diameters of AP-SiNCs (from the 24-h reaction) in toluene and water (Figure 3.4). As expected, the solvodynamic diameters of SiNCs are larger in water (21.03 ± 3.6 nm) than in toluene (7.9 ± 1.0 nm) because the bonded hydrophilic PEG ligands (allyloxy (polyethylene oxide)) are extended on the surfaces of SiNCs in water and contracted/wrapped on the surfaces of SiNCs in toluene; this provides another proof that allyloxy (polyethylene oxide) was functionalized on SiNCs.

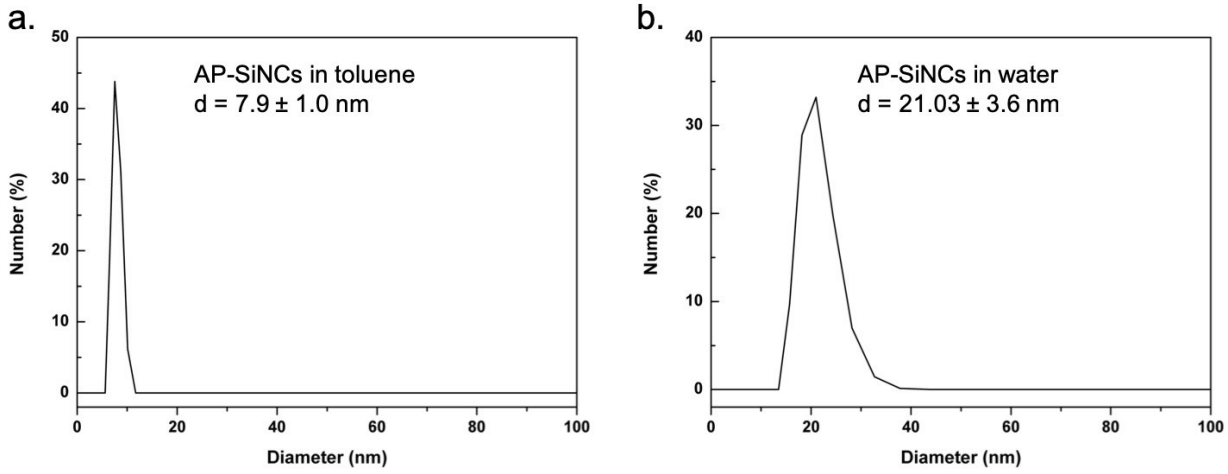

Figure 3.4. DLS analysis and solvodynamic diameters of the AP-SiNCs in (a) toluene and (b) water.

Thermal gravimetric analysis (TGA) of AP-SiNCs was performed to compare the surface conditions of the three batches of AP-SiNCs (from a 1-h reaction, a 12-h reaction, and a 24-h reaction) and to determine the SiNC-core based concentrations of these AP-SiNCs. By comparing the TGA data of pure PEG ligands and AP-SiNCs (Figure 3.5), the graphs of AP-SiNCs show 2

steps (first step: 25–450 ℃; second step: 450–800 ℃) instead of one step in the graph of PEG. This indicates that there is another kind of ligand other than PEG ligands functionalized on the surfaces of SiNCs and that there are SiNC-cores left after heated up to 800 ℃. This helps in sketching an image of AP-SiNCs: ligands, PEG and methyl 10-undecenoate, functionalized on SiNC-cores. In the TGA results of AP-SiNCs, the first step is assigned to the decomposition of PEG ligands, and the second step is assigned to the cleavage between methyl 10-undecenoate and SiNC-cores, which agrees with the TGA results of SiNC-ester-PAMAM (results in Figure 2.13, Section 2.3.2). However, the expected trend that the weight remaining after 800 ℃ (SiNC-core) from the 1-h reaction, the 12-h reaction, to 24-h reaction increases cannot be found. A plausible explanation is that even after the tedious purification process, there is still an uncertain amount of free PEG ligands remaining in the three products, and the decomposition of those free allyloxy (polyethylene oxide) ligands and the decomposition of the allyloxy (polyethylene oxide) ligands functionalized on SiNCs overlap. By comparing step 2 of the TGA results of AP-SiNCs, the ratios of the weight loss in step 2 (from methyl 10-undecenoate ligands) to the weight remaining after 800 ℃ (from SiNC-cores) are 0.342 in the 1-h reaction, 0.409 in the 12-h reaction, and 0.503 in the 24-h reaction; this increasing trend indicates that more methyl 10-undecenoate ligands were functionalized on the surfaces of SiNCs with increasing reacting time. This can be explained by the oligomers of methyl 10-undecenoate formed during the reaction and by a longer time needed for methyl 10-undecenoate to approach the surfaces of SiNCs in order to passivate the SiNCs well

because of the bulky structure of allyloxy (polyethylene oxide) ligands. Moreover, because more hydrophobic ligands (methyl 10-undecenoate) were functionalized on SiNCs, the AP-SiNCs obtained from a longer reacting time are expected to have higher stability in aqueous solutions.

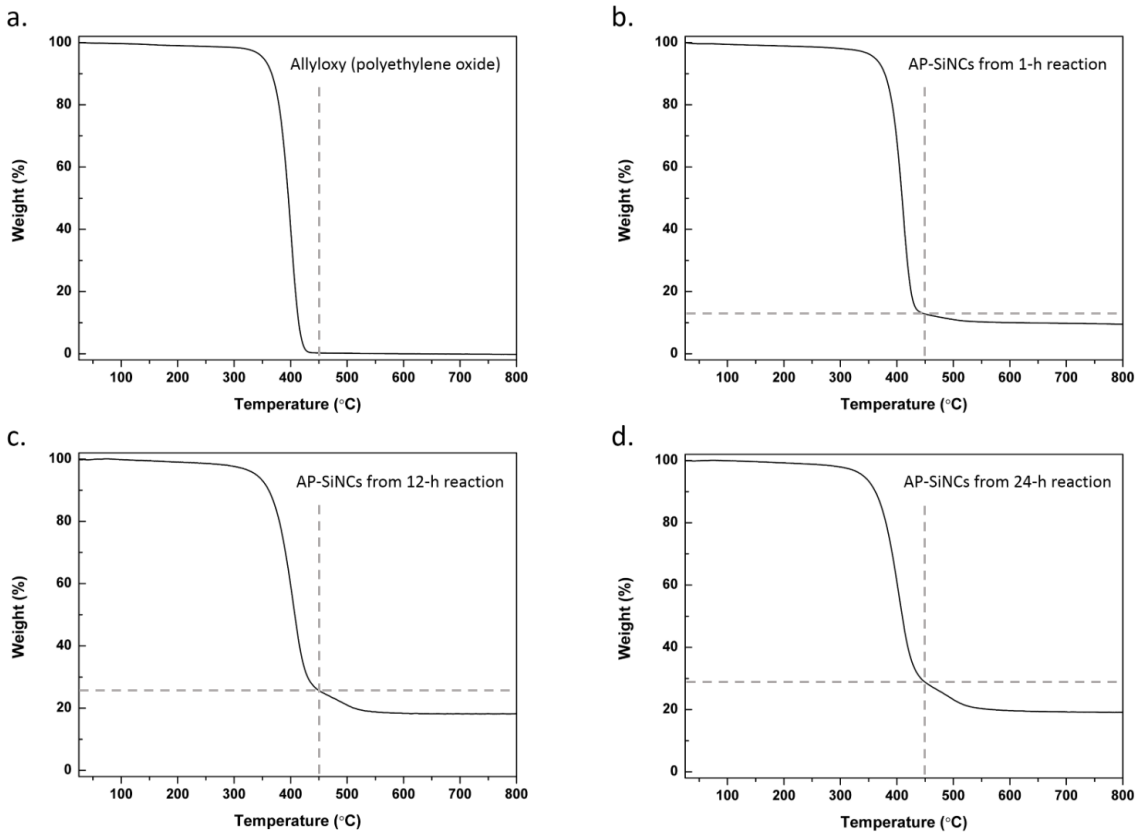

Figure 3.5. TGA data of (a) allyloxy (polyethylene oxide), (b) AP-SiNCs from the 1-h reaction, (c) AP-SiNCs from the 12-h reaction, and (d) AP-SiNCs from the 24-h reaction.

3.3.2 The Stability Test of AP-SiNCs

The stability test of AP-SiNCs was performed by keeping the three batches of AP-SiNCs (obtained from a 1-h reaction, a 12-h reaction, and a 24-h reaction) in three kinds of buffer solutions (PBS,

TBS, SBF) that are widely used in biology labs to mimic bio-systems. The nine combinations were studied by monitoring the changes in the size and the photoluminescence with dynamic light scattering (DLS) and photoluminescence spectroscopy, respectively, at different time periods.

Based on former reports, the ligand oligomerization can be induced in a thermal hydrosilylation.[13] In the present work, a similar result is expected as the reaction time becomes longer. More ligands oligomers (especially for methyl 10-undencenoate) are formed on SiNCs to form a hydrophobic shell, therefore, the stability of AP-SiNCs becomes higher from the 1-h reaction, to the 12-h reaction, to the 24-h reaction. In the DLS data of AP-SiNCs in SBF (Figure 3.6a), the sizes of AP-SiNCs from the 12-h reaction and the 24-h reaction remained around 20 nm, despite some fluctuations, while the sizes of AP-SiNCs from the 1-h reaction showed a clear increasing trend after the first few hours of fluctuation (The initial sizes of AP-SiNCs are not shown in the figure because of the way the data is plotted.). A plausible explanation is that in the 1-h reaction, the functionalization was not completed; only a few PEG ligands, which were not enough to cover the whole surface area of SiNC, were functionalized on the surfaces of SiNCs. Under this condition, the resulting AP-SiNCs from the 1-h reaction behaved as a surfactant, with a hydrophilic tail (PEG ligands) and a hydrophobic head (SiNCs functionalized with methyl 10-undecenoate), in an aqueous solution. This structure tends to self-assemble to form a larger structure driven by the hydrophobic effect in an aqueous solution in a certain concentration range. However, in the 12-h reaction and the 24-h reaction, the surfaces of AP-SiNCs were well

passivated by the two ligands, therefore, the sizes did not change with the time. Similar trends could be found in the cases of AP-SiNCs in PBS and AP-SiNCs in TBS, which could be explained with the same theory and mutually verified.

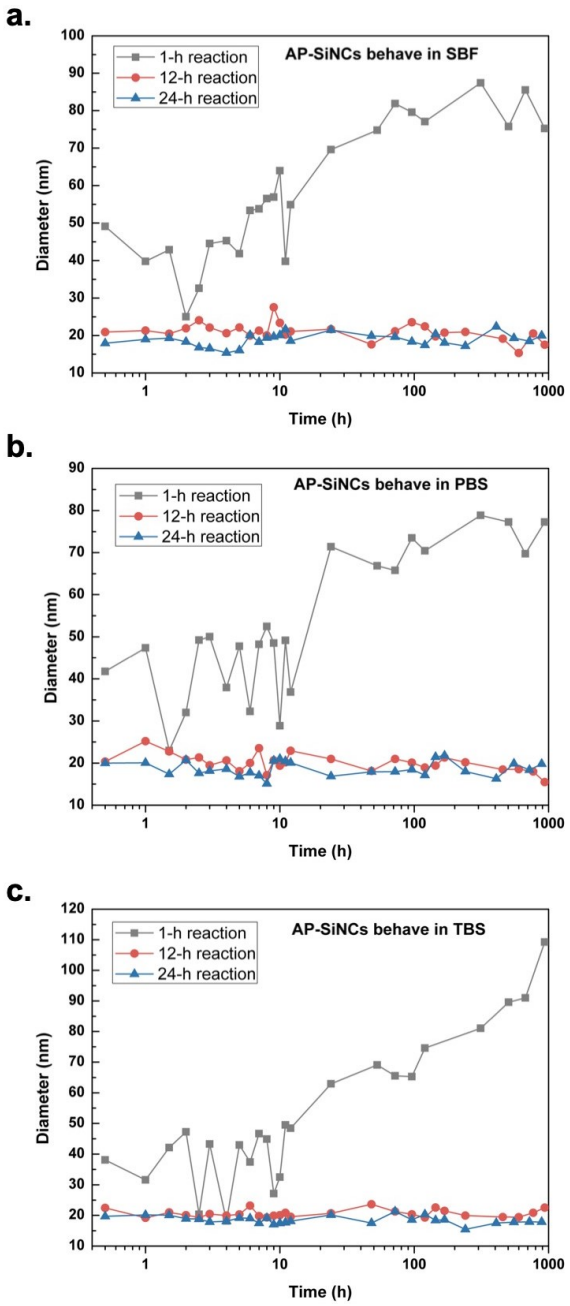

Figure 3.6. The solvodynamic diameter changes of AP-SiNCs in buffer solutions, (a) SBF, (b) PBS, and (c) TBS by DLS measurement.

The stability test of AP-SiNCs also was investigated by monitoring the PL changes of AP-SiNCs in buffer solutions. In Figure 3.7a, the emission peaks of SiNCs show a gradual blue shifting from ~650 nm to ~625 nm during the whole testing range, most likely due to the increase in surface oxidation of SiNCs. In the first 24 h, the PL intensity increased by ~9% of the initial value, which likely is caused by the decreasing amount of surface trap states due to the removal of the remaining Si-Hs on the surfaces of SiNCs upon oxidation.[23] From 24 h to 120 h, the PL intensity gradually decreased, which could be caused by both surface oxidation and the degradation of SiNCs under weak base conditions.[24] When comparing the behavior of AP-SiNCs from the 12-h reaction in SBF (Figure 3.7b) with that of AP-SiNCs from the 1-h reaction, a similar gradual trend in PL blue shifting could be found, but the shift distance (~641 nm to ~626 nm) is smaller than that of AP-SiNCs from the 1-h reaction. Moreover, the increasing duration of the PL of AP-SiNCs from the 12-h reaction was longer than that of AP-SiNCs from the 1-h reaction, which indicates a slower oxidation process; the reason could be that more hydrophobic ligand (methyl 10-undecenoate) oligomers were formed with a longer reaction time, and the oligomers provided a better protection for SiNCs from water molecules. The PL intensity did not show an obvious decrease in trend until the last 24 h. In the case of AP-SiNCs from the 24-h reaction, the SiNCs showed the best stability among the three batches of SiNCs, as expected. In the whole measuring period, only an ~15 nm blue shifting occurred, and the PL intensity did not show a clear decreasing trend, which indicates that more ligand oligomers formed after reacting for 12 h.

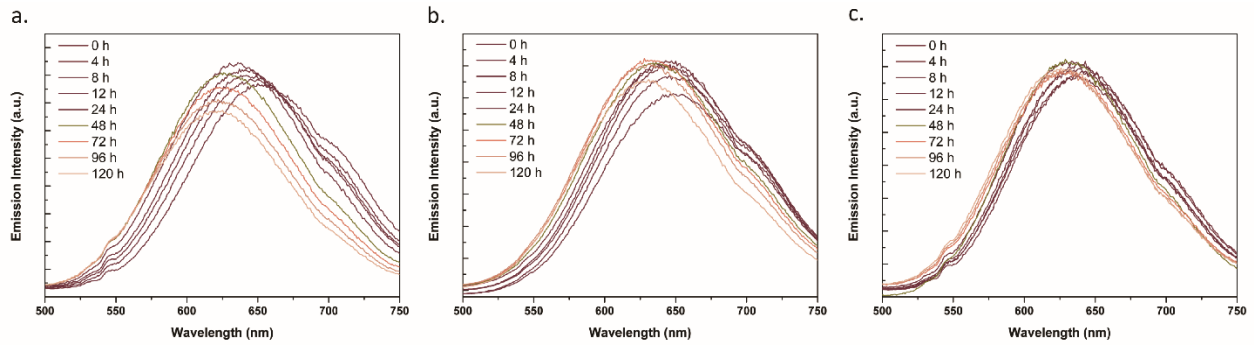

Figure 3.7. PL spectra as a function of exposure time (0–120 h) to SBF. The PL changes of (a) SiNCs from the 1-h reaction, (b) SiNCs from the 12-h reaction, and (c) SiNCs from the 24-h reaction.

Similar results were obtained in the case of AP-SiNCs in PBS or TBS, and the PL spectra are shown in Figure 3.8.

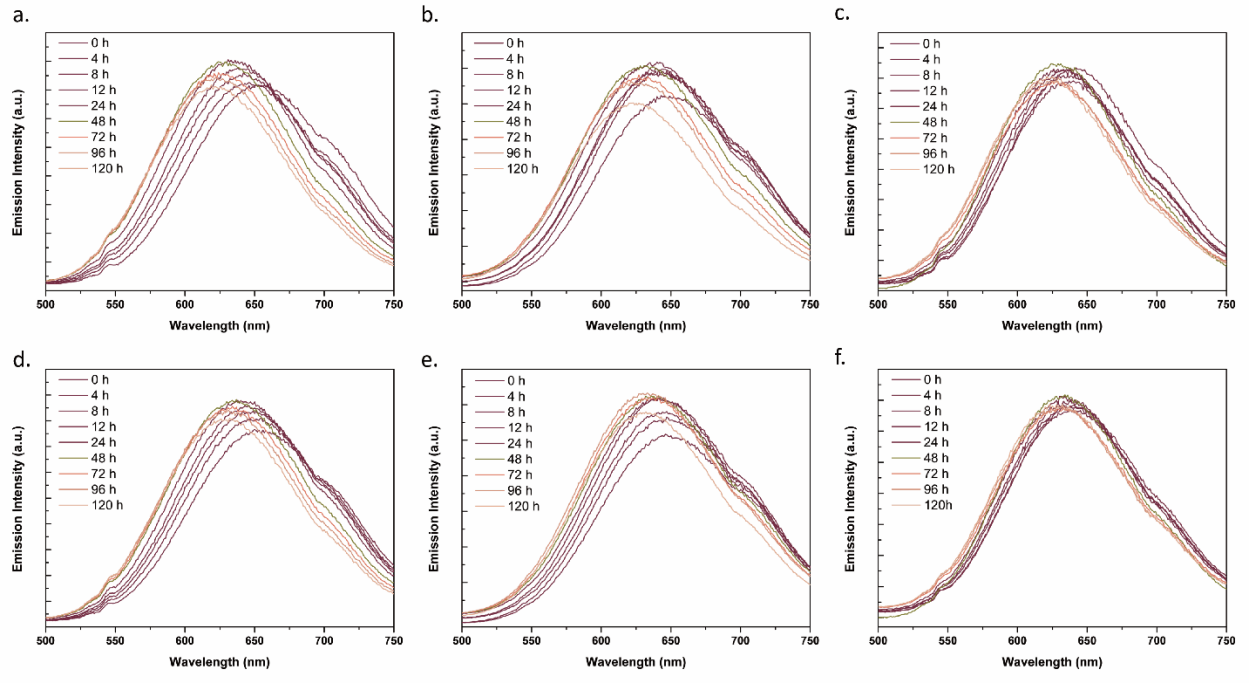

Figure 3.8. PL spectra as a function of exposure time (0–120 h) to PBS (a–c) or TBS (d–f). (a) and (d) show the PL changes of SiNCs from the 1-h reaction, (b) and (e) show the PL changes of SiNCs from the 12-h reaction, (c) and (f) show the PL changes of SiNCs from the 24-h reaction.

Five-week extension experiments were performed to probe the long-term stability of AP-SiNCs in buffer solutions. The AP-SiNCs in SBF was used as an example to show the long-term changes. The PL spectra of SiNCs from the 1-h reaction (Figure 3.9a), show a significant decreasing trend in the PL intensity of SiNCs, along with a slight blue shifting. The PL intensity dropped by ~50% in two weeks, which could be caused mainly by the degradation of SiNCs under weak base conditions. In the PL spectra of SiNCs from the 12-h reaction (Figure 3.9b), a similar decreasing trend could be found, however, its rate of decrease is smaller (the PL intensity dropped by ~50% in five weeks) compared with that of SiNCs from the 1-h reaction. The SiNCs from the 24-h reaction again show the best stability among the three samples; the PL intensity only dropped by ~16% after testing for five weeks.

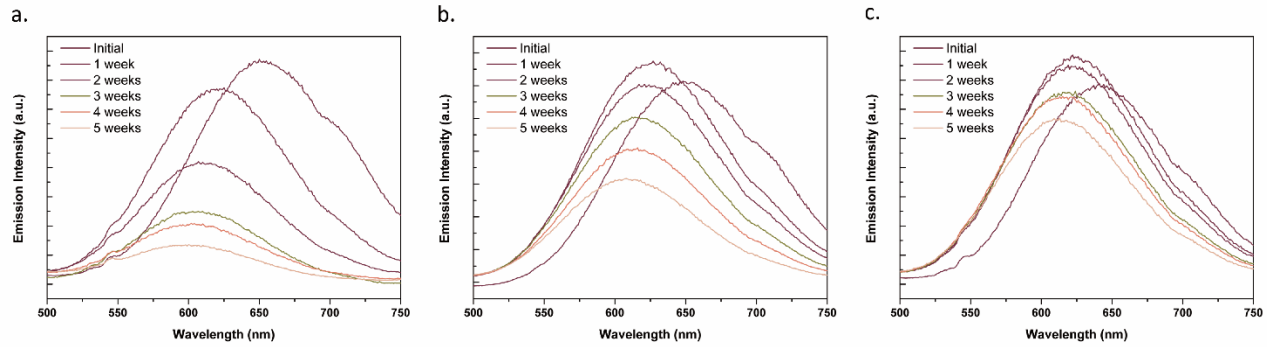

Figure 3.9. PL spectra as a function of exposure time (0–5 weeks) to SBF. The PL changes of (a) SiNCs from the 1-h reaction, (b) SiNCs from the 12-h reaction, and (c) SiNCs from the 24-h reaction.

Similar results were obtained in the case of AP-SiNCs in PBS or TBS, and the PL spectra are shown in Figure 3.10.

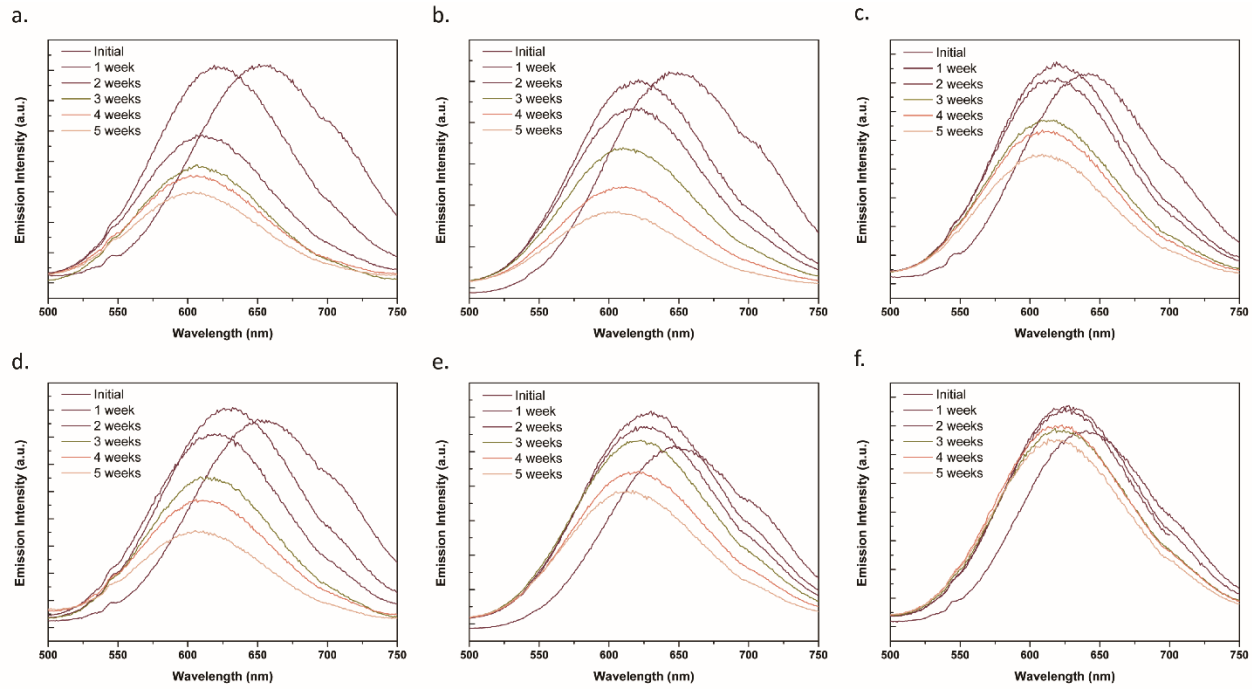

Figure 3.10. PL spectra as a function of exposure time (0–5 weeks) to PBS (a–c) or TBS (d–f). (a) and (d) show the PL changes of SiNCs from the 1-h reaction, (b) and (e) show the PL changes of SiNCs from the 12-h reaction, (c) and (f) show the PL changes of SiNCs from the 24-h reaction.

3.4 Conclusions

In this chapter, SiNCs with an amphiphilic property were prepared successfully by thermal hydrosilylation of H-SiNCs with the mixed ligands, allyloxy (polyethylene oxide) and methyl 10-undecenoate. The resulting AP-SiNCs show red/near-infrared photoluminescence, which can be separated from the autofluorescence of the organism's tissues. In order to extend the potential application in bio-systems, the stability of AP-SiNCs in different buffers was tested. Moreover, the stability of AP-SiNCs could be tuned by changing the duration of thermal hydrosilylation to adapt to the needs of the applications.

3.5 References

(1) Quarta, A.; Curcio, A.; Kakwere, H.; Pellegrino, T. Polymer Coated Inorganic Nanoparticles: Tailoring the Nanocrystal Surface for Designing Nanoprobes with Biological Implications. *Nanoscale* **2012**, *4* (11), 3319.

(2) Jańczewski, D.; Tomczak, N.; Han, M.-Y.; Vancso, G. J. Synthesis of Functionalized Amphiphilic Polymers for Coating Quantum Dots. *Nat. Protoc.* **2011**, *6* (10), 1546–1553.

(3) Park, J.; Yu, M. K.; Jeong, Y. Y.; Kim, J. W.; Lee, K.; Phan, V. N.; Jon, S. Antibiofouling Amphiphilic Polymer-Coated Superparamagnetic Iron Oxide Nanoparticles: Synthesis, Characterization, and Use in Cancer Imaging in Vivo. *J. Mater. Chem.* **2009**, *19* (35), 6412–6417.

(4) Niikura, K.; Kobayashi, K.; Takeuchi, C.; Fujitani, N.; Takahara, S.; Ninomiya, T.; Hagiwara, K.; Mitomo, H.; Ito, Y.; Osada, Y.; et al. Amphiphilic Gold Nanoparticles Displaying Flexible Bifurcated Ligands as a Carrier for SiRNA Delivery into the Cell Cytosol. *ACS Appl. Mater. Interfaces* **2014**, *6* (24), 22146–22154.

(5) Veinot, J. G. C. Synthesis, Surface Functionalization, and Properties of Freestanding Silicon Nanocrystals. *Chem. Commun.* **2006**, *0* (40), 4160–4168.

(6) Dasog, M.; Kehrle, J.; Rieger, B.; Veinot, J. G. C. Silicon Nanocrystals and Silicon-Polymer Hybrids: Synthesis, Surface Engineering, and Applications. *Angew. Chem. Int. Ed.* **2015**, *55* (7), 2322–2339.

(7) Qi, L.; Gao, X. Quantum Dot−Amphipol Nanocomplex for Intracellular Delivery and Real-Time Imaging of SiRNA. *ACS Nano* **2008**, *2* (7), 1403–1410.

(8) Zrazhevskiy, P.; Sena, M.; Gao, X. Designing Multifunctional Quantum Dots for Bioimaging, Detection, and Drug Delivery. *Chem. Soc. Rev.* **2010**, *39* (11), 4326–4354.

(9) Kim, D.; Yu, M. K.; Lee, T. S.; Park, J. J.; Jeong, Y. Y.; Jon, S. Amphiphilic Polymer-Coated Hybrid Nanoparticles as CT/MRI Dual Contrast Agents. *Nanotechnology* **2011**, *22* (15), 155101.

(10) Yezhelyev, M. V.; Qi, L.; O'Regan, R. M.; Nie, S.; Gao, X. Proton-Sponge Coated Quantum Dots for SiRNA Delivery and Intracellular Imaging. *J. Am. Chem. Soc.* **2008**, *130* (28), 9006–9012.

(11) Gao, X.; Cui, Y.; Levenson, R. M.; Chung, L. W. K.; Nie, S. In Vivo Cancer Targeting and Imaging with Semiconductor Quantum Dots. *Nat. Biotechnol.* **2004**, *22* (8), 969–976.

(12) Hessel, C. M.; Henderson, E. J.; Veinot, J. G. C. Hydrogen Silsesquioxane: A Molecular Precursor for Nanocrystalline Si−SiO^2 Composites and Freestanding Hydride-Surface-Terminated Silicon Nanoparticles. *Chem. Mater.* **2006**, *18* (26), 6139–6146.

(13) Yang, Z.; Iqbal, M.; Dobbie, A. R.; Veinot, J. G. Surface-Induced Alkene Oligomerization: Does Thermal Hydrosilylation Really Lead to Monolayer Protected Silicon Nanocrystals? *J. Am. Chem. Soc.* **2013**, *135* (46), 17595–17601.

(14) Phosphate-Buffered Saline (PBS). *Cold Spring Harb. Protoc.* **2006**, *2006* (1), pdb.rec8247.

(15) Tris-Buffered Saline (TBS; 10×, PH 7.5). *Cold Spring Harb. Protoc.* **2014**, *2014* (9), pdb.rec081265.
(16) Kokubo, T.; Takadama, H. How Useful Is SBF in Predicting in Vivo Bone Bioactivity? *Biomaterials* **2006**, *27* (15), 2907–2915.
(17) Webb, L. J.; Nemanick, E. J.; Biteen, J. S.; Knapp, D. W.; Michalak, D. J.; Traub, M. C.; Chan, A. S. Y.; Brunschwig, B. S.; Lewis, N. S. High-Resolution X-Ray Photoelectron Spectroscopic Studies of Alkylated Silicon(111) Surfaces. *J. Phys. Chem. B* **2005**, *109* (9), 3930–3937.
(18) Sudeep, P. K.; Page, Z.; Emrick, T. PEGylated Silicon Nanoparticles: Synthesis and Characterization. *Chem. Commun.* **2008**, *0* (46), 6126–6127.
(19) Yu, Y.; Hessel, C. M.; Bogart, T. D.; Panthani, M. G.; Rasch, M. R.; Korgel, B. A. Room Temperature Hydrosilylation of Silicon Nanocrystals with Bifunctional Terminal Alkenes. *Langmuir* **2013**, *29* (5), 1533–1540.
(20) Purkait, T. K.; Iqbal, M.; Islam, M. A.; Mobarok, M. H.; Gonzalez, C. M.; Hadidi, L.; Veinot, J. G. C. Alkoxy-Terminated Si Surfaces: A New Reactive Platform for the Functionalization and Derivatization of Silicon Quantum Dots. *J. Am. Chem. Soc.* **2016**, *138* (22), 7114–7120.
(21) Cheng, X.; Lowe, S. B.; Ciampi, S.; Magenau, A.; Gaus, K.; Reece, P. J.; Gooding, J. J. Versatile “Click Chemistry” Approach to Functionalizing Silicon Quantum Dots: Applications toward Fluorescent Cellular Imaging. *Langmuir* **2014**, *30* (18), 5209–5216.
(22) XPS Interpretation of Carbon https://xpssimplified.com/elements/carbon.php (accessed Nov 8, 2018).
(23) Lockwood, R.; McFarlane, S.; Rodríguez Núñez, J. R.; Wang, X. Y.; Veinot, J. G. C.; Meldrum, A. Photoactivation of Silicon Quantum Dots. *J. Lumin.* **2011**, *131* (7), 1530–1535.
(24) Park, J.-H.; Gu, L.; von Maltzahn, G.; Ruoslahti, E.; Bhatia, S. N.; Sailor, M. J. Biodegradable Luminescent Porous Silicon Nanoparticles for *in Vivo* Applications. *Nat. Mater.* **2009**, *8* (4), 331–336.

Chapter 4
Conclusions and Future Directions

4.1 Conclusions

The research work presented in this thesis foucuses on preparing SiNCs with a water-soluble property to adapt it to biomedical applications. Current results and possible future directions are summarized in this chapter.

In Chapter 2, a series of experiments were carried out to prepare dendrimer-coated SiNCs with the purpose of combining the complementary advantages of each material, e.g., water solubility and luminescent properties. Divergent and convergent methods were performed on the two kinds of core materials, SiNC-ester and SiNC-ammonium. In the divergent method, a series of stepwise reactions, the Michael addition and an amination reaction, were carried out successfully; this provided a promising path to build dendrimer structures on SiNCs. In the divergent methods, commercialized dendrons were used to conjugate with SiNCs, however, the reaction conditions need to be optimized.

In Chapter 3, we have demonstrated the synthesis and characterization of amphiphilic SiNCs prepared by thermal hydrosilylation of H-SiNCs with the mixed ligands, allyloxy (polyethylene oxide) and methyl 10-undecenoate. These particles showed distinctive red photoluminescence to the autofluorescence of the organism's tissues. Moreover, the stability of

AP-SiNCs in different buffers was tested by measuring the size and PL changes as a function of exposure time. The stability of AP-SiNCs could be tuned by changing the duration of thermal hydrosilylation to adapt the needs of various applications.

4.2 Future Directions

4.2.1 The Comparison of SiNC/SiO_2 Composite Prepared from Commercial HSQ and Synthesized HSQ

In Chapters 2 and 3, two kinds of HSQ from different sources were used to prepare the SiNC/SiO_2 composite. When two samples of HSQ were characterized by NMR (Figure 4.1), a notable difference could be found in the NMR spectra; more HSQ with a low degree of polymerization was found in the synthesized HSQ (sharp peaks at 4–4.5 ppm) than in the commercial HSQ. This can potentially affect the composition of the SiNC/SiO_2 composite or the final SiNCs. It is well worth carrying out a detailed comparison of the SiNC/SiO_2 composite prepared from commercial HSQ and synthesized HSQ so that we can have a better understanding of the formation of the SiNC/SiO_2 composite. Moreover, it will be useful for consistence with future experiments if we can separate the HSQs according to their degree of polymerization.

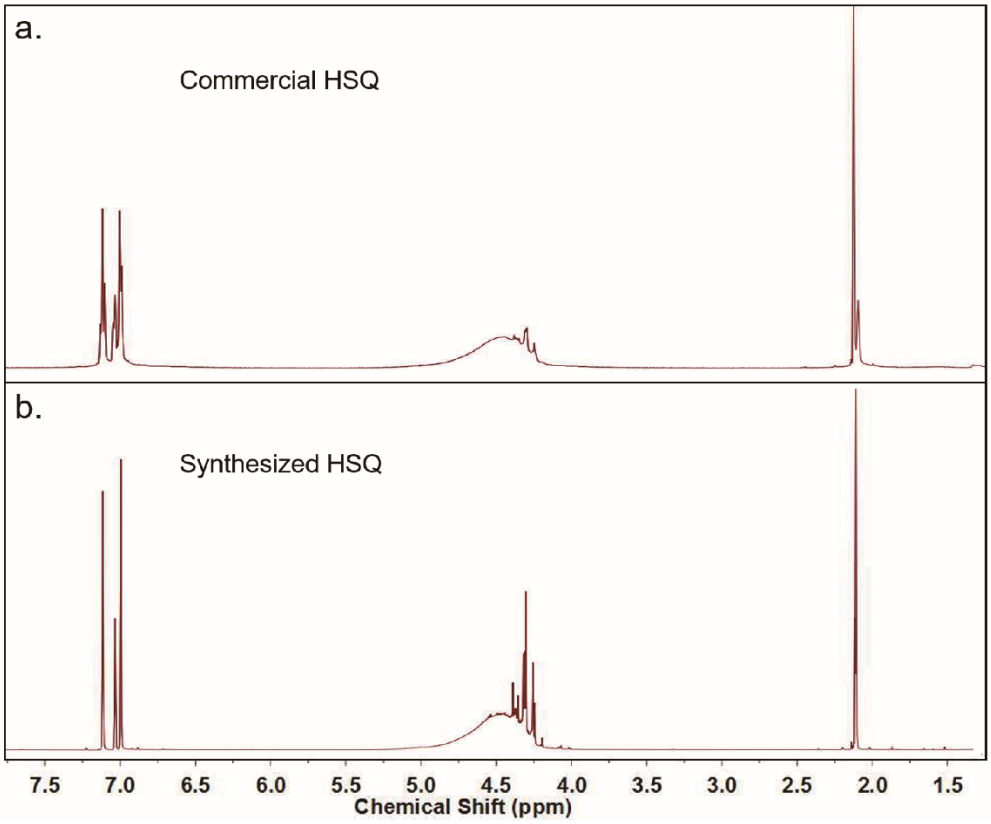

Figure 4.1. NMR spectra of (a) commercial HSQ and (b) synthesized HSQ in toluene-D_8.

4.2.2 Using the Divergent Method to Build Dendrimer Structures on SiNCs

In Sections 2.2.2 and 2.2.3, the divergent method was used to grow a PAMAM dendrimer on the surface of SiNCs, however, the reagents caused severe crosslinking during repetitive reactions. Besides optimizing the reaction conditions (lowering the concentration of reagents in the reaction or slowing down the reaction by lowering the reaction temperature) and optimizing the purification processes to get a purer product after each reaction (which helps to reduce the crosslinking),[1] another synthesis path without the use of a reagent that causes crosslinking could be used (Scheme 4.1). In this process, organic ammonium ion terminated SiNCs (SiNC-ammonium) as the core

materials were reacted with acrylonitrile through a Michael addition (coupling step), followed by the nitrile groups being reduced to amine groups (activation step).[2,3] These two steps were repeated to get a higher generation of SiNC@PPI.

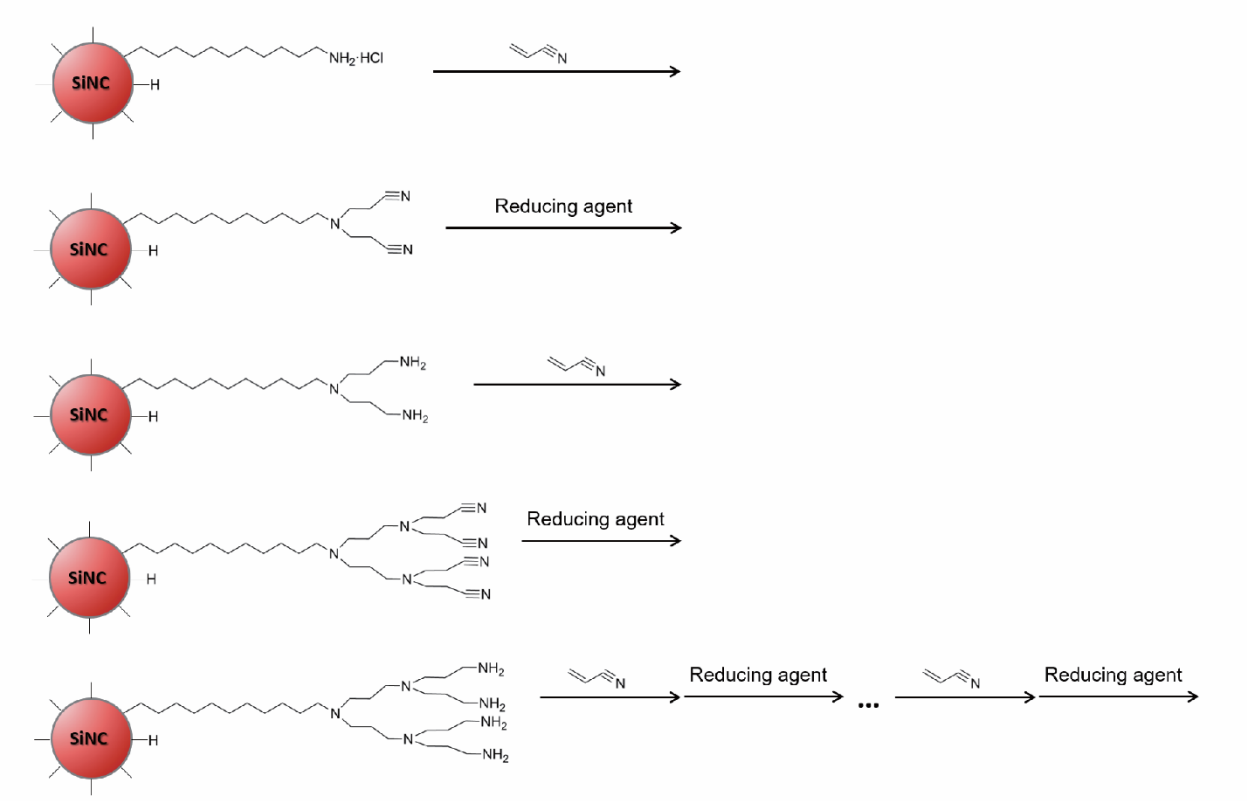

Scheme 4.1. A schematic representation of the synthesis of SiNC@PPI using organic ammonium ion terminated SiNCs (SiNC-ammonium) as the core material.

4.2.3 Using the Convergent Method to Couple SiNCs with Commercial Dendrons

In Section 2.2.4, the convergent method was used to couple SiNCs with commercial dendrons, however, the bulky structure of dendrons made them hard to approach the surfaces of SiNCs,

therefore, the ligands failed to provide enough protection from oxidation. Two possible strategies could be applied to overcome this problem. One method could be to introduce a linear linker molecule into the system. The linker molecule could be functionalized on H-SiNCs (Section 2.2.4.2 was performed with this strategy; however, optimizations need to be done to avoid side reactions) or on the dendron molecule to elongate the active sites, followed by reacting with a dendron or H-SiNCs, respectively. Another method could be to use mixed ligands to functionalize SiNCs.[4] In this work, the H-SiNCs were functionalized with the dendron molecule. After the reaction, another short chain ligand could be added into the system under inert conditions; this ligand could react with excess Si-H bonds to passivate the SiNCs fully.

4.2.4 Follow up Research on AP-SiNCs

In Chapter 3, SiNCs with an amphiphilic property were prepared and characterized by methods such as NMR, TGA, and DLS. In addition, the stability of the resulting particles was studied. However, there are still some unsolved puzzles about these SiNCs. First, the surface condition of SiNCs or the nature of the species on the surfaces can be complicated because of the existence of the two kinds of ligands with different chain lengths and hydrophilicities. Answering questions such as whether the ligand oligomers are formed during the reaction, what the ratio of the two ligands is, and how the reaction time and temperature will affect the properties of SiNCs,[5] is crucial for further modification of AP-SiNCs to adapt to the needs of various applications. Although some discussion about the nature of surface species was mentioned briefly, more work needs to be done.

A possible approach could be to use NMR or elemental analysis methods to analyze the ratio or the exact amount of each ligand on the surfaces of AP-SiNCs after getting purer samples (by optimizing the purification process) from a different reaction temperature and reaction time.[6–8] Another unsolved puzzle is the mechanism of degradation of AP-SiNCs. Based on the stability test, the stability of AP-SiNCs could be tuned by changing the duration of thermal hydrosilylation. In order to have a better understanding of their stabilities and a better control of these particles, it is worth studying the degradation process and the products from the degradation.[9] A possible approach could be to use high resolution mass spectrometry to analyze the composition of the fragments of AP-SiNCs obtained from the degradation.

4.3 References

(1) Tomalia, D. A.; Baker, H.; Dewald, J.; Hall, M.; Kallos, G.; Martin, S.; Roeck, J.; Ryder, J.; Smith, P. A New Class of Polymers: Starburst-Dendritic Macromolecules. *Polym. J.* **1985**, *17* (1), 117–132.

(2) Kaur, D.; Jain, K.; Mehra, N. K.; Kesharwani, P.; Jain, N. K. A Review on Comparative Study of PPI and PAMAM Dendrimers. *J. Nanoparticle Res.* **2016**, *18* (6), 146.

(3) Sowinska, M.; Urbanczyk-Lipkowska, Z. Advances in the Chemistry of Dendrimers. *New J. Chem.* **2014**, *38* (6), 2168–2203.

(4) Islam, M. A.; Sinelnikov, R.; Howlader, M. A.; Faramus, A.; Veinot, J. G. C. Mixed Surface Chemistry: An Approach to Highly Luminescent Biocompatible Amphiphilic Silicon Nanocrystals. *Chem. Mater.* **2018**.

(5) Yang, Z.; Iqbal, M.; Dobbie, A. R.; Veinot, J. G. Surface-Induced Alkene Oligomerization: Does Thermal Hydrosilylation Really Lead to Monolayer Protected Silicon Nanocrystals? *J. Am. Chem. Soc.* **2013**, *135* (46), 17595–17601.

(6) Lin, M.; Shapiro, M. J. Mixture Analysis by NMR Spectroscopy. *Anal. Chem.* **1997**, *69* (22), 4731–4733.

(7) Celik, H.; Shaka, A. J. A New Approach for Mixture Separation Using NMR Spectroscopy: Blind Iterative Source Identification. In *2012 38th Annual Northeast Bioengineering Conference (NEBEC)*; 2012; pp 149–150.
(8) Li, X.; Hu, K. Chapter Three - Quantitative NMR Studies of Multiple Compound Mixtures. In *Annual Reports on NMR Spectroscopy*; Webb, G. A., Ed.; Academic Press, 2017; Vol. 90, pp 85–143.
(9) Park, J.-H.; Gu, L.; von Maltzahn, G.; Ruoslahti, E.; Bhatia, S. N.; Sailor, M. J. Biodegradable Luminescent Porous Silicon Nanoparticles for *in Vivo* Applications. *Nat. Mater.* **2009**, *8* (4), 331–336.

Bibliography

(1) *Commission Recommendation of 18 October 2011 on the Definition of Nanomaterial Text with EEA Relevance*; 32011H0696; 2011.

(2) Buzea, C.; Pacheco, I. I.; Robbie, K. Nanomaterials and Nanoparticles: Sources and Toxicity. *Biointerphases* **2007**, *2* (4), MR17–MR71.

(3) Roduner, E. Size Matters: Why Nanomaterials Are Different. *Chem. Soc. Rev.* **2006**, *35* (7), 583–592.

(4) Isaeva, V. I.; Nefedov, O. M.; Kustov, L. M. Metal–Organic Frameworks-Based Catalysts for Biomass Processing. *Catalysts* **2018**, *8* (9), 368.

(5) Yang, Y.; Luo, M.; Zhang, W.; Sun, Y.; Chen, X.; Guo, S. Metal Surface and Interface Energy Electrocatalysis: Fundamentals, Performance Engineering, and Opportunities. *Chem* **2018**, *4* (9), 2054–2083.

(6) Saleem, A.; Imran, M.; Shahzadi, A.; Junaid, M.; Majeed, H.; Rafiq, A.; Shahzadi, I.; Ikram, M.; Naz, M.; Ali, S. Drastic Improvement in Catalytic, Optical and Visible-Light Photocatalytic Behavior of Cobalt and Nickel Doped TiO 2 Nanopowder. *Mater. Res. Express* **2019**, *6* (1), 015003.

(7) Wu, J.; Ran, P.; Zhu, S.; Mo, F.; Wang, C.; Fu, Y. A Highly Sensitive Electrochemiluminescence Sensor for the Detection of L-Cysteine Based on the Rhombus-Shaped Rubrene Microsheets and Platinum Nanoparticles. *Sens. Actuators B Chem.* **2019**, *278*, 97–102.

(8) Yang, Y.; Lu, L.; Tian, X.; Li, Y.; Yang, C.; Nie, Y.; Zhou, Z. Ratiometric Fluorescence Detection of Mercuric Ions by Sole Intrinsic Dual-Emitting Gold Nanoclusters. *Sens. Actuators B Chem.* **2019**, *278*, 82–87.

(9) Mehrzad-Samarin, M.; Faridbod, F.; Ganjali, M. R. A Luminescence Nanosensor for Ornidazole Detection Using Graphene Quantum Dots Entrapped in Silica Molecular Imprinted Polymer. *Spectrochim. Acta. A. Mol. Biomol. Spectrosc.* **2019**, *206*, 430–436.

(10) Wang, Y.; Zhou, X.; Yang, Z.; Wang, F.; Han, N.; Chen, Y.; Ho, J. C. GaAs Nanowires Grown by Catalyst Epitaxy for High Performance Photovoltaics. *Crystals* **2018**, *8* (9), 347.

(11) Xu, J.; Wang, H.; Yang, S.; Ni, G.; Zou, B. High-Sensitivity Broadband Colloidal Quantum Dot Heterojunction Photodetector for Night-Sky Radiation. *J. Alloys Compd.* **2018**, *764*, 446–451.

(12) Seoudi, R.; Althagafi, H. A. Dependence of Copper Phthalocyanine Photovoltaic Thin Film on the Sizes of Silver Nanoparticles. *Silicon* **2018**, *10* (5), 2165–2171.

(13) Huang, H.; Cui, Y.; Liu, M.; Chen, J.; Wan, Q.; Wen, Y.; Deng, F.; Zhou, N.; Zhang, X.; Wei, Y. A One-Step Ultrasonic Irradiation Assisted Strategy for the Preparation of Polymer-Functionalized Carbon Quantum Dots and Their Biological Imaging. *J. Colloid Interface Sci.* **2018**, *532*, 767–773.

(14) Zhao, W.; Li, A.; Zhang, A.; Zheng, Y.; Liu, J. Recent Advances in Functional-Polymer-Decorated Transition-Metal Nanomaterials for Bioimaging and Cancer Therapy. *ChemMedChem* **2018**, *13* (20), 2134–2149.

(15) Luo, Y.; Li, Z.; Zhu, C.; Cai, X.; Qu, L.; Du, D.; Lin, Y. Graphene-like Metal-Free 2D Nanosheets for Cancer Imaging and Theranostics. *Trends Biotechnol.* **2018**, *36* (11), 1145–1156.
(16) Moreira, A. F.; Rodrigues, C. F.; Reis, C. A.; Costa, E. C.; Correia, I. J. Gold-Core Silica Shell Nanoparticles Application in Imaging and Therapy: A Review. *Microporous Mesoporous Mater.* **2018**, *270*, 168–179.
(17) ISO/TS 80004-2:2015(en), Nanotechnologies — Vocabulary — Part 2: Nano-objects
(18) Reed, M. A.; Randall, J. N.; Aggarwal, R. J.; Matyi, R. J.; Moore, T. M.; Wetsel, A. E. Observation of Discrete Electronic States in a Zero-Dimensional Semiconductor Nanostructure. *Phys. Rev. Lett.* **1988**, *60* (6), 535–537.
(19) Bentolila, L. A. 5 - Photoluminescent Quantum Dots in Imaging, Diagnostics and Therapy. In *Applications of Nanoscience in Photomedicine*; Hamblin, M. R., Avci, P., Eds.; Chandos Publishing: Oxford, 2015; pp 77–104.
(20) Éfros, A. L. Density of States and Interband Absorption of Light in Strongly Doped Semiconductors. *Sov. Phys. Uspekhi* **1974**, *16* (6), 789.
(21) Ekimov, A. I.; Efros, A. L.; Onushchenko, A. A. Quantum Size Effect in Semiconductor Microcrystals. *Solid State Commun.* **1985**, *56* (11), 921–924.
(22) Takagahara, T.; Takeda, K. Theory of the Quantum Confinement Effect on Excitons in Quantum Dots of Indirect-Gap Materials. *Phys. Rev. B* **1992**, *46* (23), 15578–15581.
(23) Brus, L. E. Electron–Electron and Electron-hole Interactions in Small Semiconductor Crystallites: The Size Dependence of the Lowest Excited Electronic State. *J. Chem. Phys.* **1984**, *80* (9), 4403–4409.
(24) Rogach, A. L.; Talapin, D. V.; Shevchenko, E. V.; Kornowski, A.; Haase, M.; Weller, H. Organization of Matter on Different Size Scales: Monodisperse Nanocrystals and Their Superstructures. *Adv. Funct. Mater.* **2002**, *12* (10), 653–664.
(25) Rossetti, R.; Nakahara, S.; Brus, L. E. Quantum Size Effects in the Redox Potentials, Resonance Raman Spectra, and Electronic Spectra of CdS Crystallites in Aqueous Solution. *J. Chem. Phys.* **1983**, *79* (2), 1086–1088.
(26) Murray, C. B.; Norris, D. J.; Bawendi, M. G. Synthesis and Characterization of Nearly Monodisperse CdE (E = Sulfur, Selenium, Tellurium) Semiconductor Nanocrystallites. *J. Am. Chem. Soc.* **1993**, *115* (19), 8706–8715.
(27) T, H.; H, S.; I, K. Mechanism of Formation of CdS and ZnS Ultrafine Particles in Reverse Micelles. *Ind. Eng. Chem. Res.* **1994**, *33* (12), 3262–3266.
(28) Micic, O. I.; Curtis, C. J.; Jones, K. M.; Sprague, J. R.; Nozik, A. J. Synthesis and Characterization of InP Quantum Dots. *J. Phys. Chem.* **1994**, *98* (19), 4966–4969.
(29) Olshavsky, M. A.; Goldstein, A. N.; Alivisatos, A. P. Organometallic Synthesis of Gallium-Arsenide Crystallites, Exhibiting Quantum Confinement. *J. Am. Chem. Soc.* **1990**, *112* (25), 9438–9439.

(30) Veinot, J. G. C. Synthesis, Surface Functionalization, and Properties of Freestanding Silicon Nanocrystals. *Chem. Commun.* **2006**, *0* (40), 4160–4168.
(31) Dashiell, M. W.; Denker, U.; Müller, C.; Costantini, G.; Manzano, C.; Kern, K.; Schmidt, O. G. Photoluminescence of Ultrasmall Ge Quantum Dots Grown by Molecular-Beam Epitaxy at Low Temperatures. *Appl. Phys. Lett.* **2002**, *80* (7), 1279–1281.
(32) Protesescu, L.; Yakunin, S.; Bodnarchuk, M. I.; Krieg, F.; Caputo, R.; Hendon, C. H.; Yang, R. X.; Walsh, A.; Kovalenko, M. V. Nanocrystals of Cesium Lead Halide Perovskites (CsPbX3, X = Cl, Br, and I): Novel Optoelectronic Materials Showing Bright Emission with Wide Color Gamut. *Nano Lett.* **2015**, *15* (6), 3692–3696.
(33) Hines, M. A.; Guyot-Sionnest, P. Synthesis and Characterization of Strongly Luminescing ZnS-Capped CdSe Nanocrystals. *J. Phys. Chem.* **1996**, *100* (2), 468–471.
(34) Yuan, R.; Ding, L.; Shao, G.; Zhang, Z.; Liu, J.; Xiang, W.; Liang, X. Suitable Medium for $CsPbBr_3$ Quantum Dots toward Light-Emitting-Diodes Fabrication. *Mater. Lett.* **2019**, *234*, 275–278.
(35) Medintz, I. L.; Uyeda, H. T.; Goldman, E. R.; Mattoussi, H. Quantum Dot Bioconjugates for Imaging, Labelling and Sensing. *Nat. Mater.* **2005**, *4* (6), 435–446.
(36) David Wegner, K.; Hildebrandt, N. Quantum Dots: Bright and Versatile in Vitro and in Vivo Fluorescence Imaging Biosensors. *Chem. Soc. Rev.* **2015**, *44* (14), 4792–4834.
(37) Houston, M. C. The Role of Mercury and Cadmium Heavy Metals in Vascular Disease, Hypertension, Coronary Heart Disease, and Myocardial Infarction. *Altern. Ther. Health Med.* **2007**, *13* (2), S128-133.
(38) Graeme, K. A.; Pollack, C. V. Heavy Metal Toxicity, Part I: Arsenic and Mercury. *J. Emerg. Med.* **1998**, *16* (1), 45–56.
(39) Gordon, R. B.; Bertram, M.; Graedel, T. E. Metal Stocks and Sustainability. *Proc. Natl. Acad. Sci.* **2006**, *103* (5), 1209–1214.
(40) Dasog, M.; Kehrle, J.; Rieger, B.; Veinot, J. G. C. Silicon Nanocrystals and Silicon-Polymer Hybrids: Synthesis, Surface Engineering, and Applications. *Angew. Chem. Int. Ed.* **2015**, *55* (7), 2322–2339.
(41) Silicon. *Wikipedia*; 2018.
(42) Canham, L. T. Silicon Quantum Wire Array Fabrication by Electrochemical and Chemical Dissolution of Wafers. *Appl. Phys. Lett.* **1990**, *57* (10), 1046–1048.
(43) Buriak, J. M. Organometallic Chemistry on Silicon and Germanium Surfaces. *Chem. Rev.* **2002**, *102* (5), 1271–1308.
(44) Dohnalová, K.; Gregorkiewicz, T.; Kůsová, K. Silicon Quantum Dots: Surface Matters. *J. Phys. Condens. Matter* **2014**, *26* (17), 173201.
(45) Bayliss, S. C.; Heald, R.; Fletcher, D. I.; Buckberry, L. D. The Culture of Mammalian Cells on Nanostructured Silicon. *Adv. Mater.* **1999**, *11* (4), 318–321.

(46) Stewart, M. P.; Buriak, J. M. Chemical and Biological Applications of Porous Silicon Technology. *Adv. Mater.* **2000**, *12* (12), 859–869.
(47) Erogbogbo, F.; Yong, K.-T.; Roy, I.; Xu, G.; Prasad, P. N.; Swihart, M. T. Biocompatible Luminescent Silicon Quantum Dots for Imaging of Cancer Cells. *ACS Nano* **2008**, *2* (5), 873–878.
(48) Cheng, K.-Y.; Anthony, R.; Kortshagen, U. R.; Holmes, R. J. High-Efficiency Silicon Nanocrystal Light-Emitting Devices. *Nano Lett.* **2011**, *11* (5), 1952–1956.
(49) Liu, C.-Y.; Holman, Z. C.; Kortshagen, U. R. Hybrid Solar Cells from P3HT and Silicon Nanocrystals. *Nano Lett.* **2009**, *9* (1), 449–452.
(50) Germanenko, I. N.; Li, S.; El-Shall, M. S. Decay Dynamics and Quenching of Photoluminescence from Silicon Nanocrystals by Aromatic Nitro Compounds. *J. Phys. Chem. B* **2001**, *105* (1), 59–66.
(51) Content, S.; Trogler, W. C.; Sailor, M. J. Detection of Nitrobenzene, DNT, and TNT Vapors by Quenching of Porous Silicon Photoluminescence. *Chem. – Eur. J.* **2000**, *6* (12), 2205–2213.
(52) Park, J.-H.; Gu, L.; von Maltzahn, G.; Ruoslahti, E.; Bhatia, S. N.; Sailor, M. J. Biodegradable Luminescent Porous Silicon Nanoparticles for *in Vivo* Applications. *Nat. Mater.* **2009**, *8* (4), 331–336.
(53) Erogbogbo, F.; Yong, K.-T.; Roy, I.; Hu, R.; Law, W.-C.; Zhao, W.; Ding, H.; Wu, F.; Kumar, R.; Swihart, M. T. In Vivo Targeted Cancer Imaging, Sentinel Lymph Node Mapping and Multi-Channel Imaging with Biocompatible Silicon Nanocrystals. *ACS Nano* **2010**, *5* (1), 413–423.
(54) Xu, Z.; Wang, D.; Guan, M.; Liu, X.; Yang, Y.; Wei, D.; Zhao, C.; Zhang, H. Photoluminescent Silicon Nanocrystal-Based Multifunctional Carrier for PH-Regulated Drug Delivery. *ACS Appl. Mater. Interfaces* **2012**, *4* (7), 3424–3431.
(55) Anglin, E. J.; Cheng, L.; Freeman, W. R.; Sailor, M. J. Porous Silicon in Drug Delivery Devices and Materials. *Adv. Drug Deliv. Rev.* **2008**, *60* (11), 1266–1277.
(56) Sato, K.; Tsuji, H.; Hirakuri, K.; Fukata, N.; Yamauchi, Y. Controlled Chemical Etching for Silicon Nanocrystals with Wavelength-Tunable Photoluminescence. *Chem. Commun.* **2009**, *0* (25), 3759–3761.
(57) Shirahata, N.; R. Linford, M.; Furumi, S.; Pei, L.; Sakka, Y.; J. Gates, R.; C. Asplund, M. Laser-Derived One-Pot Synthesis of Silicon Nanocrystals Terminated with Organic Monolayers. *Chem. Commun.* **2009**, *0* (31), 4684–4686.
(58) Heintz, A. S.; Fink, M. J.; Mitchell, B. S. Mechanochemical Synthesis of Blue Luminescent Alkyl/Alkenyl-Passivated Silicon Nanoparticles. *Adv. Mater.* **2007**, *19* (22), 3984–3988.
(59) Ehbrecht, M.; Ferkel, H.; Huisken, F.; Holz, L.; Polivanov, Y. N.; Smirnov, V. V.; Stelmakh, O. M.; Schmidt, R. Deposition and Analysis of Silicon Clusters Generated by Laser-induced Gas Phase Reaction. *J. Appl. Phys.* **1995**, *78* (9), 5302–5306.

(60) Tamir, S.; Berger, S. Laser Induced Deposition of Nanocrystalline Si with Preferred Crystallographic Orientation. *Appl. Surf. Sci.* **1995**, *86* (1), 514–520.
(61) Ehbrecht, M.; Huisken, F. Gas-Phase Characterization of Silicon Nanoclusters Produced by Laser Pyrolysis of Silane. *Phys. Rev. B* **1999**, *59* (4), 2975–2985.
(62) Li, X.; He, Y.; Swihart, M. T. Surface Functionalization of Silicon Nanoparticles Produced by Laser-Driven Pyrolysis of Silane Followed by HF−HNO3 Etching. *Langmuir* **2004**, *20* (11), 4720–4727.
(63) Mangolini, L.; Thimsen, E.; Kortshagen, U. High-Yield Plasma Synthesis of Luminescent Silicon Nanocrystals. *Nano Lett.* **2005**, *5* (4), 655–659.
(64) Pi, X. D.; Liptak, R. W.; Campbell, S. A.; Kortshagen, U. In-Flight Dry Etching of Plasma-Synthesized Silicon Nanocrystals. *Appl. Phys. Lett.* **2007**, *91* (8), 083112.
(65) Pi, X. D.; Liptak, R. W.; Nowak, J. D.; Wells, N. P.; Carter, C. B.; Campbell, S. A.; Kortshagen, U. Air-Stable Full-Visible-Spectrum Emission from Silicon Nanocrystals Synthesized by an All-Gas-Phase Plasma Approach. *Nanotechnology* **2008**, *19* (24), 245603.
(66) Littau, K. A.; Szajowski, P. J.; Muller, A. J.; Kortan, A. R.; Brus, L. E. A Luminescent Silicon Nanocrystal Colloid via a High-Temperature Aerosol Reaction. *J. Phys. Chem.* **1993**, *97* (6), 1224–1230.
(67) Fojtik, A.; Henglein, A. Luminescent Colloidal Silicon Particles. *Chem. Phys. Lett.* **1994**, *221* (5), 363–367.
(68) Holmes, J. D.; Ziegler, K. J.; Doty, R. C.; Pell, L. E.; Johnston, K. P.; Korgel, B. A. Highly Luminescent Silicon Nanocrystals with Discrete Optical Transitions. *J. Am. Chem. Soc.* **2001**, *123* (16), 3743–3748.
(69) Heath, J. R. A Liquid-Solution-Phase Synthesis of Crystalline Silicon. *Science* **1992**, *258* (5085), 1131–1133.
(70) Bley, R. A.; Kauzlarich, S. M. A Low-Temperature Solution Phase Route for the Synthesis of Silicon Nanoclusters. *J. Am. Chem. Soc.* **1996**, *118* (49), 12461–12462.
(71) Yang, C.-S.; Bley, R. A.; Kauzlarich, S. M.; Lee, H. W. H.; Delgado, G. R. Synthesis of Alkyl-Terminated Silicon Nanoclusters by a Solution Route. *J. Am. Chem. Soc.* **1999**, *121* (22), 5191–5195.
(72) Warner, J. H.; Hoshino, A.; Yamamoto, K.; Tilley, R. D. Water-Soluble Photoluminescent Silicon Quantum Dots. *Angew. Chem. Int. Ed.* **2005**, *44* (29), 4550–4554.
(73) Tilley, R. D.; Warner, J. H.; Yamamoto, K.; Matsui, I.; Fujimori, H. Micro-Emulsion Synthesis of Monodisperse Surface Stabilized Silicon Nanocrystals. *Chem. Commun.* **2005**, *0* (14), 1833–1835.
(74) Liu, S.; Sato, S.; Kimura, K. Synthesis of Luminescent Silicon Nanopowders Redispersible to Various Solvents. *Langmuir* **2005**, *21* (14), 6324–6329.

(75) Hessel, C. M.; Henderson, E. J.; Veinot, J. G. C. Hydrogen Silsesquioxane: A Molecular Precursor for Nanocrystalline Si−SiO2 Composites and Freestanding Hydride-Surface-Terminated Silicon Nanoparticles. *Chem. Mater.* **2006**, *18* (26), 6139–6146.
(76) Sun, W.; Qian, C.; Chen, K. K.; Ozin, G. A. Silicon Nanocrystals: It's Simply a Matter of Size. *ChemNanoMat* **2016**, *2* (9), 847–855.
(77) Sorarù, G. D.; Modena, S.; Bettotti, P.; Das, G.; Mariotto, G.; Pavesi, L. Si Nanocrystals Obtained through Polymer Pyrolysis. *Appl. Phys. Lett.* **2003**, *83* (4), 749–751.
(78) Pauthe, M.; Bernstein, E.; Dumas, J.; Saviot, L.; Pradel, A.; Ribes, M. Preparation and Characterisation of Si Nanocrystallites Embedded in a Silica Matrix. *J. Mater. Chem.* **1999**, *9* (1), 187–191.
(79) Hessel, C. M.; Reid, D.; Panthani, M. G.; Rasch, M. R.; Goodfellow, B. W.; Wei, J.; Fujii, H.; Akhavan, V.; Korgel, B. A. Synthesis of Ligand-Stabilized Silicon Nanocrystals with Size-Dependent Photoluminescence Spanning Visible to Near-Infrared Wavelengths. *Chem. Mater.* **2012**, *24* (2), 393–401.
(80) Yang, Z.; Dobbie, A. R.; Cui, K.; Veinot, J. G. C. A Convenient Method for Preparing Alkyl-Functionalized Silicon Nanocubes. *J. Am. Chem. Soc.* **2012**, *134* (34), 13958–13961.
(81) Yang, Z.; Dobbie, A. R.; Veinot, J. G. C. Shape Evolution of Faceted Silicon Nanocrystals upon Thermal Annealing in an Oxide Matrix. *MRS Online Proc. Libr. Arch.* **2013**, *1536*, 207–212.
(82) Pavesi, L.; Dal Negro, L.; Mazzoleni, C.; Franzò, G.; Priolo, F. Optical Gain in Silicon Nanocrystals. *Nature* **2000**, *408* (6811), 440–444.
(83) Yang, L.; Lua, Y.-Y.; Lee, M. V.; Linford, M. R. Chemomechanical Functionalization and Patterning of Silicon. *Acc. Chem. Res.* **2005**, *38* (12), 933–942.
(84) Kůsová, K.; Cibulka, O.; Dohnalová, K.; Pelant, I.; Valenta, J.; Fučíková, A.; Žídek, K.; Lang, J.; Englich, J.; Matějka, P.; et al. Brightly Luminescent Organically Capped Silicon Nanocrystals Fabricated at Room Temperature and Atmospheric Pressure. *ACS Nano* **2010**, *4* (8), 4495–4504.
(85) Godefroo, S.; Hayne, M.; Jivanescu, M.; Stesmans, A.; Zacharias, M.; Lebedev, O. I.; Van Tendeloo, G.; Moshchalkov, V. V. Classification and Control of the Origin of Photoluminescence from Si Nanocrystals. *Nat. Nanotechnol.* **2008**, *3* (3), 174–178.
(86) Dasog, M.; De los Reyes, G. B.; Titova, L. V.; Hegmann, F. A.; Veinot, J. G. Size vs Surface: Tuning the Photoluminescence of Freestanding Silicon Nanocrystals across the Visible Spectrum via Surface Groups. *ACS Nano* **2014**, *8* (9), 9636–9648.
(87) Robidillo, C. J. T.; Islam, M. A.; Aghajamali, M.; Faramus, A.; Sinelnikov, R.; Zhang, X.; Boekhoven, J.; Veinot, J. G. C. Functional Bioinorganic Hybrids from Enzymes and Luminescent Silicon-Based Nanoparticles. *Langmuir* **2018**, *34* (22), 6556–6569.
(88) Buriak, J. M. Illuminating Silicon Surface Hydrosilylation: An Unexpected Plurality of Mechanisms. *Chem. Mater.* **2014**, *26* (1), 763–772.

(89) Yang, Z.; Iqbal, M.; Dobbie, A. R.; Veinot, J. G. Surface-Induced Alkene Oligomerization: Does Thermal Hydrosilylation Really Lead to Monolayer Protected Silicon Nanocrystals? *J. Am. Chem. Soc.* **2013**, *135* (46), 17595–17601.
(90) Pujari, S. P.; Driss, H.; Bannani, F.; van Lagen, B.; Zuilhof, H. One-Pot Gram-Scale Synthesis of Hydrogen-Terminated Silicon Nanoparticles. *Chem. Mater.* **2018**, *30* (18), 6503–6512.
(91) Hua, F.; Swihart, M. T.; Ruckenstein, E. Efficient Surface Grafting of Luminescent Silicon Quantum Dots by Photoinitiated Hydrosilylation. *Langmuir* **2005**, *21* (13), 6054–6062.
(92) Purkait, T. K.; Iqbal, M.; Wahl, M. H.; Gottschling, K.; Gonzalez, C. M.; Islam, M. A.; Veinot, J. G. C. Borane-Catalyzed Room-Temperature Hydrosilylation of Alkenes/Alkynes on Silicon Nanocrystal Surfaces. *J. Am. Chem. Soc.* **2014**, *136* (52), 17914–17917.
(93) Yang, Z.; Gonzalez, C. M.; Purkait, T. K.; Iqbal, M.; Meldrum, A.; Veinot, J. G. C. Radical Initiated Hydrosilylation on Silicon Nanocrystal Surfaces: An Evaluation of Functional Group Tolerance and Mechanistic Study. *Langmuir* **2015**, *31* (38), 10540–10548.
(94) Pankove, J. I. *Optical Processes in Semiconductors*; Courier Corporation, 1975.
(95) Chelikowsky, J. R.; Cohen, M. L. Electronic Structure of Silicon. *Phys. Rev. B* **1974**, *10* (12), 5095.
(96) Delley, B.; Steigmeier, E. F. Quantum Confinement in Si Nanocrystals. *Phys. Rev. B* **1993**, *47* (3), 1397–1400.
(97) Hybertsen, M. S. Absorption and Emission of Light in Nanoscale Silicon Structures. *Phys. Rev. Lett.* **1994**, *72* (10), 1514–1517.
(98) Cullis, A. G.; Canham, L. T.; Calcott, P. D. J. The Structural and Luminescence Properties of Porous Silicon. *J. Appl. Phys.* **1997**, *82* (3), 909–965.
(99) Daldosso, N.; Pavesi, L. Nanosilicon Photonics. *Laser Photonics Rev.* **2009**, *3* (6), 508–534.
(100) Delerue, C.; Allan, G.; Lannoo, M. Theoretical Aspects of the Luminescence of Porous Silicon. *Phys. Rev. B* **1993**, *48* (15), 11024–11036.
(101) Kůsová, K.; Hapala, P.; Valenta, J.; Jelínek, P.; Cibulka, O.; Ondič, L.; Pelant, I. Direct Bandgap Silicon: Tensile-Strained Silicon Nanocrystals. *Adv. Mater. Interfaces* **2014**, *1* (2), 1300042.
(102) Kůsová, K.; Pelant, I.; Humpolíčková, J.; Hof, M. Comprehensive Description of Blinking-Dynamics Regimes in Single Direct-Band-Gap Silicon Nanocrystals. *Phys. Rev. B* **2016**, *93* (3), 035412.
(103) Lockwood, R.; McFarlane, S.; Rodríguez Núñez, J. R.; Wang, X. Y.; Veinot, J. G. C.; Meldrum, A. Photoactivation of Silicon Quantum Dots. *J. Lumin.* **2011**, *131* (7), 1530–1535.
(104) Goguenheim, D.; Lannoo, M. Theoretical Calculation of the Electron-Capture Cross Section Due to a Dangling Bond at the Si(111)-SiO_2 Interface. *Phys. Rev. B* **1991**, *44* (4), 1724–1733.

(105) Almeida, A. J.; Sahu, A.; Riedinger, A.; Norris, D. J.; Brandt, M. S.; Stutzmann, M.; Pereira, R. N. Charge Trapping Defects in CdSe Nanocrystal Quantum Dots. *J. Phys. Chem. C* **2016**, *120* (25), 13763–13770.
(106) Puzder, A.; Williamson, A. J.; Grossman, J. C.; Galli, G. Surface Chemistry of Silicon Nanoclusters. *Phys. Rev. Lett.* **2002**, *88* (9), 097401.
(107) Luppi, M.; Ossicini, S. Oxygen Role on the Structural and Optoelectronic Properties of Silicon Nanodots. *Phys. Status Solidi A* **2003**, *197* (1), 251–256.
(108) Luppi, M.; Ossicini, S. Ab Initio Study on Oxidized Silicon Clusters and Silicon Nanocrystals Embedded in SiO_2: Beyond the Quantum Confinement Effect. *Phys. Rev. B* **2005**, *71* (3), 035340.
(109) Wolkin, M. V.; Jorne, J.; Fauchet, P. M.; Allan, G.; Delerue, C. Electronic States and Luminescence in Porous Silicon Quantum Dots: The Role of Oxygen. *Phys. Rev. Lett.* **1999**, *82* (1), 197–200.
(110) Biteen, J. S.; Lewis, N. S.; Atwater, H. A.; Polman, A. Size-Dependent Oxygen-Related Electronic States in Silicon Nanocrystals. *Appl. Phys. Lett.* **2004**, *84* (26), 5389–5391.
(111) Kang, Z.; Liu, Y.; Tsang, C. H. A.; Ma, D. D. D.; Fan, X.; Wong, N.-B.; Lee, S.-T. Water-Soluble Silicon Quantum Dots with Wavelength-Tunable Photoluminescence. *Adv. Mater.* **2009**, *21* (6), 661–664.
(112) Sinelnikov, R.; Dasog, M.; Beamish, J.; Meldrum, A.; Veinot, J. G. C. Revisiting an Ongoing Debate: What Role Do Surface Groups Play in Silicon Nanocrystal Photoluminescence? *ACS Photonics* **2017**, *4* (8), 1920–1929.
(113) Chen, S.; Yang, K.; Tuguntaev, R. G.; Mozhi, A.; Zhang, J.; Wang, P. C.; Liang, X.-J. Targeting Tumor Microenvironment with PEG-Based Amphiphilic Nanoparticles to Overcome Chemoresistance. *Nanomedicine Nanotechnol. Biol. Med.* **2016**, *12* (2), 269–286.
(114) Weissleder, R. A Clearer Vision for *in Vivo* Imaging. *Nat. Biotechnol.* **2001**, *19*, 316–317.
(115) Berezin, M. Y.; Achilefu, S. Fluorescence Lifetime Measurements and Biological Imaging. *Chem. Rev.* **2010**, *110* (5), 2641–2684.
(116) Cheng, X.; B. Lowe, S.; J. Reece, P.; Justin Gooding, J. Colloidal Silicon Quantum Dots: From Preparation to the Modification of Self-Assembled Monolayers (SAMs) for Bio-Applications. *Chem. Soc. Rev.* **2014**, *43* (8), 2680–2700.
(117) Barnes, T. J.; Prestidge, C. A. Recent Advances in Porous Silicon-Based Therapeutic Delivery. *Ther. Deliv.* **2015**, *6* (2), 97–100.
(118) Joo, J.; Liu, X.; Kotamraju, V. R.; Ruoslahti, E.; Nam, Y.; Sailor, M. J. Gated Luminescence Imaging of Silicon Nanoparticles. *ACS Nano* **2015**, *9* (6), 6233–6241.
(119) Mobarok, M. H.; Purkait, T. K.; Islam, M. A.; Miskolzie, M.; Veinot, J. G. Instantaneous Functionalization of Chemically Etched Silicon Nanocrystal Surfaces. *Angew. Chem. Int. Ed.* **2017**, *56* (22), 6073–6077.

(120) Atkins, T. M.; Cassidy, M. C.; Lee, M.; Ganguly, S.; Marcus, C. M.; Kauzlarich, S. M. Synthesis of Long T1 Silicon Nanoparticles for Hyperpolarized 29Si Magnetic Resonance Imaging. *ACS Nano* **2013**, *7* (2), 1609–1617.
(121) Thompson, K.; Booske, J.; Gianchandani, Y.; Cooper, R. RF and Microwave Rapid Magnetic Induction Heating of Silicon Wafers. In *Advances in Microwave and Radio Frequency Processing*; Willert-Porada, M., Ed.; Springer Berlin Heidelberg, 2006; pp 673–680.
(122) Thompson, K.; Gianchandani, Y. B.; Booske, J.; Cooper, R. F. Direct Silicon-Silicon Bonding by Electromagnetic Induction Heating. *J. Microelectromechanical Syst.* **2002**, *11* (4), 285–292.
(123) Chinnathambi, S.; Chen, S.; Ganesan, S.; Hanagata, N. Silicon Quantum Dots for Biological Applications. *Adv. Healthc. Mater.* **2014**, *3* (1), 10–29.
(124) Peng, F.; Su, Y.; Zhong, Y.; Fan, C.; Lee, S.-T.; He, Y. Silicon Nanomaterials Platform for Bioimaging, Biosensing, and Cancer Therapy. *Acc. Chem. Res.* **2014**, *47* (2), 612–623.
(125) McVey, B. F. P.; Tilley, R. D. Solution Synthesis, Optical Properties, and Bioimaging Applications of Silicon Nanocrystals. *Acc. Chem. Res.* **2014**, *47* (10), 3045–3051.
(126) Clark, R. J.; Dang, M. K. M.; Veinot, J. G. C. Exploration of Organic Acid Chain Length on Water-Soluble Silicon Quantum Dot Surfaces. *Langmuir* **2010**, *26* (19), 15657–15664.
(127) Shiohara, A.; Hanada, S.; Prabakar, S.; Fujioka, K.; Lim, T. H.; Yamamoto, K.; Northcote, P. T.; Tilley, R. D. Chemical Reactions on Surface Molecules Attached to Silicon Quantum Dots. *J. Am. Chem. Soc.* **2010**, *132* (1), 248–253.
(128) Zhai, Y.; Dasog, M.; B. Snitynsky, R.; K. Purkait, T.; Aghajamali, M.; H. Hahn, A.; B. Sturdy, C.; L. Lowary, T.; C. Veinot, J. G. Water-Soluble Photoluminescent d -Mannose and l -Alanine Functionalized Silicon Nanocrystals and Their Application to Cancer Cell Imaging. *J. Mater. Chem. B* **2014**, *2* (47), 8427–8433.
(129) Nakahara, Y.; Machiya, K.; Sato, T.; Nwe, N. T.; Furuike, T.; Tamura, H.; Kimura, K. Synthesis of Silicon Quantum Dots Functionalized Chemically with Monosaccharides and Their Use in Biological Fluorescence Imaging. *Chem. Lett.* **2013**, *42* (5), 498–500.
(130) Hessel, C. M.; Rasch, M. R.; Hueso, J. L.; Goodfellow, B. W.; Akhavan, V. A.; Puvanakrishnan, P.; Tunnel, J. W.; Korgel, B. A. Alkyl Passivation and Amphiphilic Polymer Coating of Silicon Nanocrystals for Diagnostic Imaging. *Small* **2010**, *6* (18), 2026–2034.
(131) Henderson, E. J.; Shuhendler, A. J.; Prasad, P.; Baumann, V.; Maier-Flaig, F.; Faulkner, D. O.; Lemmer, U.; Wu, X. Y.; Ozin, G. A. Colloidally Stable Silicon Nanocrystals with Near-Infrared Photoluminescence for Biological Fluorescence Imaging. *Small* **2011**, *7* (17), 2507–2516.
(132) Xu, Z.; Li, Y.; Zhang, B.; Purkait, T.; Alb, A.; Mitchell, B. S.; Grayson, S. M.; Fink, M. J. Water-Soluble PEGylated Silicon Nanoparticles and Their Assembly into Swellable Nanoparticle Aggregates. *J. Nanoparticle Res.* **2015**, *17* (1), 56.
(133) Choudhary, S.; Gupta, L.; Rani, S.; Dave, K.; Gupta, U. Impact of Dendrimers on Solubility of Hydrophobic Drug Molecules. *Front. Pharmacol.* **2017**, *8*.

(134) Sowinska, M.; Urbanczyk-Lipkowska, Z. Advances in the Chemistry of Dendrimers. *New J. Chem.* **2014**, *38* (6), 2168–2203.
(135) Khodadust, R.; Unsoy, G.; Yalcın, S.; Gunduz, G.; Gunduz, U. PAMAM Dendrimer-Coated Iron Oxide Nanoparticles: Synthesis and Characterization of Different Generations. *J. Nanoparticle Res.* **2013**, *15* (3), 1488.
(136) Zhang, A.; Shu, L.; Bo, Z.; Schlüter, A. D. Dendronized Polymers: Recent Progress in Synthesis. *Macromol. Chem. Phys.* **2003**, *204* (2), 328–339.
(137) Li, J.; Liang, H.; Liu, J.; Wang, Z. Poly (Amidoamine) (PAMAM) Dendrimer Mediated Delivery of Drug and PDNA/SiRNA for Cancer Therapy. *Int. J. Pharm.* **2018**, *546* (1), 215–225.
(138) Kojima, C.; Tsumura, S.; Harada, A.; Kono, K. A Collagen-Mimic Dendrimer Capable of Controlled Release. *J. Am. Chem. Soc.* **2009**, *131* (17), 6052–6053.
(139) Chung, Y.-M.; Rhee, H.-K. Pt-Pd Bimetallic Nanoparticles Encapsulated in Dendrimer Nanoreactor. *Catal. Lett.* **2003**, *85* (3), 159–164.
(140) Crooks, R. M.; Zhao, M.; Sun, L.; Chechik, V.; Yeung, L. K. Dendrimer-Encapsulated Metal Nanoparticles: Synthesis, Characterization, and Applications to Catalysis. *Acc. Chem. Res.* **2001**, *34* (3), 181–190.
(141) Zhou, Z.; Wang, Y.; Yan, Y.; Zhang, Q.; Cheng, Y. Dendrimer-Templated Ultrasmall and Multifunctional Photothermal Agents for Efficient Tumor Ablation. *ACS Nano* **2016**, *10* (4), 4863–4872.
(142) Lesniak, W. G.; Oskolkov, N.; Song, X.; Lal, B.; Yang, X.; Pomper, M.; Laterra, J.; Nimmagadda, S.; McMahon, M. T. Salicylic Acid Conjugated Dendrimers Are a Tunable, High Performance CEST MRI NanoPlatform. *Nano Lett.* **2016**, *16* (4), 2248–2253.
(143) Chang, H.; Lv, J.; Gao, X.; Wang, X.; Wang, H.; Chen, H.; He, X.; Li, L.; Cheng, Y. Rational Design of a Polymer with Robust Efficacy for Intracellular Protein and Peptide Delivery. *Nano Lett.* **2017**, *17* (3), 1678–1684.
(144) Li, P.; Zhang, M.; Sun, X.; Guan, S.; Zhang, G.; Baumgarten, M.; Müllen, K. A Dendrimer-Based Highly Sensitive and Selective Fluorescence-Quenching Sensor for Fe^{3+} Both in Solution and as Film. *Biosens. Bioelectron.* **2016**, *85*, 785–791.
(145) Wang, S. H.; Shen, C. Y.; Lin, Y. M.; Du, J. C. Piezoelectric Sensor for Sensitive Determination of Metal Ions Based on the Phosphate-Modified Dendrimer. *Smart Mater. Struct.* **2016**, *25* (8), 085018.
(146) Ye, R.; Zhukhovitskiy, A. V.; Deraedt, C. V.; Toste, F. D.; Somorjai, G. A. Supported Dendrimer-Encapsulated Metal Clusters: Toward Heterogenizing Homogeneous Catalysts. *Acc. Chem. Res.* **2017**, *50* (8), 1894–1901.
(147) Caminade, A.-M.; Ouali, A.; Laurent, R.; Turrin, C.-O.; Majoral, J.-P. Coordination Chemistry with Phosphorus Dendrimers. Applications as Catalysts, for Materials, and in Biology. *Coord. Chem. Rev.* **2016**, *308*, 478–497.

(148) Zhang, J.; Ling, L.; Wang, C.-F.; Chen, S.; Chen, L.; Y. Son, D. Versatile Dendrimer-Derived Nanocrystal Microreactors towards Fluorescence Colloidal Photonic Crystals. *J. Mater. Chem. C* **2014**, *2* (18), 3610–3616.
(149) Chen, M.; Tian, Y.; Zhang, J.; Hong, R.; Chen, L.; Chen, S.; Y. Son, D. Fabrication of Crack-Free Photonic Crystal Films via Coordination of Microsphere Terminated Dendrimers and Their Performance in Invisible Patterned Photonic Displays. *J. Mater. Chem. C* **2016**, *4* (37), 8765–8771.
(150) Vunain, E.; Mishra, A.; Mamba, B. Dendrimers, Mesoporous Silicas and Chitosan-Based Nanosorbents for the Removal of Heavy-Metal Ions: A Review. *Int. J. Biol. Macromol.* **2016**, *86*, 570–586.
(151) Lakew Mekuria, S.; Ayane Debele, T.; Tsai, H.-C. PAMAM Dendrimer Based Targeted Nano-Carrier for Bio-Imaging and Therapeutic Agents. *RSC Adv.* **2016**, *6* (68), 63761–63772.
(152) Janaszewska, A.; Studzian, M.; Petersen, J. F.; Ficker, M.; Paolucci, V.; Christensen, J. B.; Tomalia, D. A.; Klajnert-Maculewicz, B. Modified PAMAM Dendrimer with 4-Carbomethoxypyrrolidone Surface Groups-Its Uptake, Efflux, and Location in a Cell. *Colloids Surf. B Biointerfaces* **2017**, *159*, 211–216.
(153) Kesharwani, P.; Jain, K.; Jain, N. K. Dendrimer as Nanocarrier for Drug Delivery. *Prog. Polym. Sci.* **2014**, *39* (2), 268–307.
(154) Wang, H.; Huang, Q.; Chang, H.; Xiao, J.; Cheng, Y. Stimuli-Responsive Dendrimers in Drug Delivery. *Biomater. Sci.* **2016**, *4* (3), 375–390.
(155) Yang, J.; Zhang, Q.; Chang, H.; Cheng, Y. Surface-Engineered Dendrimers in Gene Delivery. *Chem. Rev.* **2015**, *115* (11), 5274–5300.
(156) Kesharwani, P.; Iyer, A. K. Recent Advances in Dendrimer-Based Nanovectors for Tumor-Targeted Drug and Gene Delivery. *Drug Discov. Today* **2015**, *20* (5), 536–547.
(157) Tomalia, D. A.; Baker, H.; Dewald, J.; Hall, M.; Kallos, G.; Martin, S.; Roeck, J.; Ryder, J.; Smith, P. A New Class of Polymers: Starburst-Dendritic Macromolecules. *Polym. J.* **1985**, *17* (1), 117–132.
(158) Kaur, D.; Jain, K.; Mehra, N. K.; Kesharwani, P.; Jain, N. K. A Review on Comparative Study of PPI and PAMAM Dendrimers. *J. Nanoparticle Res.* **2016**, *18* (6), 146.
(159) Grayson, S. M.; Fréchet, J. M. J. Convergent Dendrons and Dendrimers: From Synthesis to Applications. *Chem. Rev.* **2001**, *101* (12), 3819–3868.
(160) Shao, N.; Su, Y.; Hu, J.; Zhang, J.; Zhang, H.; Cheng, Y. Comparison of Generation 3 Polyamidoamine Dendrimer and Generation 4 Polypropylenimine Dendrimer on Drug Loading, Complex Structure, Release Behavior, and Cytotoxicity. *Int. J. Nanomedicine* **2011**, *6*, 3361–3372.
(161) A. Mintzer, M.; W. Grinstaff, M. Biomedical Applications of Dendrimers: A Tutorial. *Chem. Soc. Rev.* **2011**, *40* (1), 173–190.

(162) Devarakonda, B.; Hill, R. A.; de Villiers, M. M. The Effect of PAMAM Dendrimer Generation Size and Surface Functional Group on the Aqueous Solubility of Nifedipine. *Int. J. Pharm.* **2004**, *284* (1), 133–140.
(163) Boas, U.; H. Heegaard, P. M. Dendrimers in Drug Research. *Chem. Soc. Rev.* **2004**, *33* (1), 43–63.
(164) Gupta, U.; Agashe, H. B.; Asthana, A.; Jain, N. K. Dendrimers: Novel Polymeric Nanoarchitectures for Solubility Enhancement. *Biomacromolecules* **2006**, *7* (3), 649–658.
(165) Jevprasesphant, R.; Penny, J.; Jalal, R.; Attwood, D.; McKeown, N. B.; D'Emanuele, A. The Influence of Surface Modification on the Cytotoxicity of PAMAM Dendrimers. *Int. J. Pharm.* **2003**, *252* (1), 263–266.
(166) Sadekar, S.; Ghandehari, H. Transepithelial Transport and Toxicity of PAMAM Dendrimers: Implications for Oral Drug Delivery. *Adv. Drug Deliv. Rev.* **2012**, *64* (6), 571–588.
(167) Albertazzi, L.; Gherardini, L.; Brondi, M.; Sulis Sato, S.; Bifone, A.; Pizzorusso, T.; Ratto, G. M.; Bardi, G. In Vivo Distribution and Toxicity of PAMAM Dendrimers in the Central Nervous System Depend on Their Surface Chemistry. *Mol. Pharm.* **2013**, *10* (1), 249–260.
(168) Sun, W.; Mignani, S.; Shen, M.; Shi, X. Dendrimer-Based Magnetic Iron Oxide Nanoparticles: Their Synthesis and Biomedical Applications. *Drug Discov. Today* **2016**, *21* (12), 1873–1885.
(169) Roy Barman, S.; Nain, A.; Jain, S.; Punjabi, N.; Mukherji, S.; Satija, J. Dendrimer as a Multifunctional Capping Agent for Metal Nanoparticles for Use in Bioimaging, Drug Delivery and Sensor Applications. *J. Mater. Chem. B* **2018**, *6* (16), 2368–2384.
(170) M. Rossi, L.; L. Fiorio, J.; S. Garcia, M. A.; P. Ferraz, C. The Role and Fate of Capping Ligands in Colloidally Prepared Metal Nanoparticle Catalysts. *Dalton Trans.* **2018**, *47* (17), 5889–5915.
(171) Pooja; Barman, P. B.; Hazra, S. K. Role of Capping Agent in Palladium Nanoparticle Based Hydrogen Sensor. *J. Clust. Sci.* **2018**, *29* (6), 1209–1216.
(172) Jhonsi, M. A.; Thulasi, S.; Kathiravan, A. Impact of Capping Agent on the Electron Transfer Dynamics of CdTe QDs with Methyl Viologen. *J. Lumin.* **2016**, *178*, 356–361.
(173) Liu, J.; Wang, F.; Han, Y.; Sun, M.; Li, H.; Hua, H.; Chen, C.; Lin, Y. Polyamidoamine Functionalized CdTeSe Quantum Dots for Sensitive Detection of Cry1Ab Protein in Vitro and in Vivo. *Sens. Actuators B Chem.* **2015**, *206*, 8–13.
(174) Ciganda, R.; Gu, H.; Hernandez, R.; Escobar, A.; Martínez, A.; Yates, L.; Moya, S.; Ruiz, J.; Astruc, D. Electrostatic Assembly of Functional and Macromolecular Ferricinium Chloride-Stabilized Gold Nanoparticles. *Inorg. Chem.* **2017**, *56* (5), 2784–2791.
(175) Luong, D.; Sau, S.; Kesharwani, P.; Iyer, A. K. Polyvalent Folate-Dendrimer-Coated Iron Oxide Theranostic Nanoparticles for Simultaneous Magnetic Resonance Imaging and Precise Cancer Cell Targeting. *Biomacromolecules* **2017**, *18* (4), 1197–1209.

(176) Deraedt, C.; Melaet, G.; Ralston, W. T.; Ye, R.; Somorjai, G. A. Platinum and Other Transition Metal Nanoclusters (Pd, Rh) Stabilized by PAMAM Dendrimer as Excellent Heterogeneous Catalysts: Application to the Methylcyclopentane (MCP) Hydrogenative Isomerization. *Nano Lett.* **2017**, *17* (3), 1853–1862.
(177) Mekuria, S. L.; Debele, T. A.; Tsai, H.-C. Encapsulation of Gadolinium Oxide Nanoparticle (Gd_2O_3) Contrasting Agents in PAMAM Dendrimer Templates for Enhanced Magnetic Resonance Imaging in Vivo. *ACS Appl. Mater. Interfaces* **2017**, *9* (8), 6782–6795.
(178) Divsar, F.; Ju, H. Electrochemiluminescence Detection of near Single DNA Molecules by Using Quantum Dots–Dendrimer Nanocomposites for Signal Amplification. *Chem. Commun.* **2011**, *47* (35), 9879–9881.
(179) Yen, C.-H.; Lien, H.-L.; Chung, J.-S.; Yeh, H.-D. Adsorption of Precious Metals in Water by Dendrimer Modified Magnetic Nanoparticles. *J. Hazard. Mater.* **2017**, *322*, 215–222.
(180) Wang, T.; Yang, W.-L.; Hong, Y.; Hou, Y.-L. Magnetic Nanoparticles Grafted with Amino-Riched Dendrimer as Magnetic Flocculant for Efficient Harvesting of Oleaginous Microalgae. *Chem. Eng. J.* **2016**, *297*, 304–314.
(181) J. Daou, T.; Pourroy, G.; M. Greneche, J.; Bertin, A.; Felder-Flesch, D.; Begin-Colin, S. Water Soluble Dendronized Iron Oxide Nanoparticles. *Dalton Trans.* **2009**, *0* (23), 4442–4449.
(182) Lamanna, G.; Kueny-Stotz, M.; Mamlouk-Chaouachi, H.; Ghobril, C.; Basly, B.; Bertin, A.; Miladi, I.; Billotey, C.; Pourroy, G.; Begin-Colin, S.; et al. Dendronized Iron Oxide Nanoparticles for Multimodal Imaging. *Biomaterials* **2011**, *32* (33), 8562–8573.
(183) Rosario-Amorin, D.; Gaboyard, M.; Clérac, R.; Vellutini, L.; Nlate, S.; Heuzé, K. Metallodendritic Grafted Core–Shell γ-Fe_2O_3 Nanoparticles Used as Recoverable Catalysts in Suzuki C-C Coupling Reactions. *Chem. – Eur. J.* **2012**, *18* (11), 3305–3315.
(1) Astruc, D.; Boisselier, E.; Ornelas, C. Dendrimers Designed for Functions: From Physical, Photophysical, and Supramolecular Properties to Applications in Sensing, Catalysis, Molecular Electronics, Photonics, and Nanomedicine. *Chem. Rev.* **2010**, *110* (4), 1857–1959.
(2) Li, X.; Kono, K. Functional Dendrimer–Gold Nanoparticle Hybrids for Biomedical Applications. *Polym. Int.* **2018**, *67* (7), 840–852.
(3) Boas, U.; Christensen, J. B.; Heegaard, P. M. Dendrimers: Design, Synthesis and Chemical Properties. *J. Mater. Chem.* **2006**, *16* (38), 3785–3798.
(4) Kaur, D.; Jain, K.; Mehra, N. K.; Kesharwani, P.; Jain, N. K. A Review on Comparative Study of PPI and PAMAM Dendrimers. *J. Nanoparticle Res.* **2016**, *18* (6), 146.
(5) Liu, J.; Erogbogbo, F.; Yong, K.-T.; Ye, L.; Liu, J.; Hu, R.; Chen, H.; Hu, Y.; Yang, Y.; Yang, J. Assessing Clinical Prospects of Silicon Quantum Dots: Studies in Mice and Monkeys. *ACS Nano* **2013**, *7* (8), 7303–7310.
(6) Erogbogbo, F.; Yong, K.-T.; Roy, I.; Hu, R.; Law, W.-C.; Zhao, W.; Ding, H.; Wu, F.; Kumar, R.; Swihart, M. T. In Vivo Targeted Cancer Imaging, Sentinel Lymph Node Mapping and

Multi-Channel Imaging with Biocompatible Silicon Nanocrystals. *ACS Nano* **2010**, *5* (1), 413–423.
(7) McVey, B. F.; Tilley, R. D. Solution Synthesis, Optical Properties, and Bioimaging Applications of Silicon Nanocrystals. *Acc. Chem. Res.* **2014**, *47* (10), 3045–3051.
(8) Buriak, J. M. Organometallic Chemistry on Silicon and Germanium Surfaces. *Chem. Rev.* **2002**, *102* (5), 1271–1308.
(9) Dasog, M.; De los Reyes, G. B.; Titova, L. V.; Hegmann, F. A.; Veinot, J. G. Size vs Surface: Tuning the Photoluminescence of Freestanding Silicon Nanocrystals across the Visible Spectrum via Surface Groups. *ACS Nano* **2014**, *8* (9), 9636–9648.
(10) Maier-Flaig, F.; Rinck, J.; Stephan, M.; Bocksrocker, T.; Bruns, M.; Kübel, C.; Powell, A. K.; Ozin, G. A.; Lemmer, U. Multicolor Silicon Light-Emitting Diodes (SiLEDs). *Nano Lett.* **2013**, *13* (2), 475–480.
(11) Hessel, C. M.; Henderson, E. J.; Veinot, J. G. C. Hydrogen Silsesquioxane: A Molecular Precursor for Nanocrystalline Si−SiO_2 Composites and Freestanding Hydride-Surface-Terminated Silicon Nanoparticles. *Chem. Mater.* **2006**, *18* (26), 6139–6146.
(12) Yang, Z.; Iqbal, M.; Dobbie, A. R.; Veinot, J. G. Surface-Induced Alkene Oligomerization: Does Thermal Hydrosilylation Really Lead to Monolayer Protected Silicon Nanocrystals? *J. Am. Chem. Soc.* **2013**, *135* (46), 17595–17601.
(13) Kelly, J. A.; Veinot, J. G. C. An Investigation into Near-UV Hydrosilylation of Freestanding Silicon Nanocrystals. *ACS Nano* **2010**, *4* (8), 4645–4656.
(14) Mobarok, M. H.; Purkait, T. K.; Islam, M. A.; Miskolzie, M.; Veinot, J. G. Instantaneous Functionalization of Chemically Etched Silicon Nanocrystal Surfaces. *Angew. Chem. Int. Ed.* **2017**, *56* (22), 6073–6077.
(15) Yang, Z.; Gonzalez, C. M.; Purkait, T. K.; Iqbal, M.; Meldrum, A.; Veinot, J. G. Radical Initiated Hydrosilylation on Silicon Nanocrystal Surfaces: An Evaluation of Functional Group Tolerance and Mechanistic Study. *Langmuir* **2015**, *31* (38), 10540–10548.
(16) Pan, B.; Cui, D.; Gao, F.; He, R. Growth of Multi-Amine Terminated Poly (Amidoamine) Dendrimers on the Surface of Carbon Nanotubes. *Nanotechnology* **2006**, *17* (10), 2483.
(17) Abu-Reziq, R.; Alper, H.; Wang, D.; Post, M. L. Metal Supported on Dendronized Magnetic Nanoparticles: Highly Selective Hydroformylation Catalysts. *J. Am. Chem. Soc.* **2006**, *128* (15), 5279–5282.
(18) Khodadust, R.; Unsoy, G.; Yalcın, S.; Gunduz, G.; Gunduz, U. PAMAM Dendrimer-Coated Iron Oxide Nanoparticles: Synthesis and Characterization of Different Generations. *J. Nanoparticle Res.* **2013**, *15* (3), 1488.
(19) Schneider, M. J.; Schäfer, R.; Mülhaupt, R. Aminofunctional Linear Low Density Polyethylene via Metallocene-Catalysed Ethene Copolymerization with N,N-Bis(Trimethylsilyl)-1-Amino-10-Undecene. *Polymer* **1997**, *38* (10), 2455–2459.

(20) Zhang, M.; Kim, H. K.; Chalkova, E.; Mark, F.; Lvov, S. N.; Chung, T. M. New Polyethylene Based Anion Exchange Membranes (PE–AEMs) with High Ionic Conductivity. *Macromolecules* **2011**, *44* (15), 5937–5946.
(21) Luong, D.; Sau, S.; Kesharwani, P.; Iyer, A. K. Polyvalent Folate-Dendrimer-Coated Iron Oxide Theranostic Nanoparticles for Simultaneous Magnetic Resonance Imaging and Precise Cancer Cell Targeting. *Biomacromolecules* **2017**, *18* (4), 1197–1209.
(22) Webb, L. J.; Nemanick, E. J.; Biteen, J. S.; Knapp, D. W.; Michalak, D. J.; Traub, M. C.; Chan, A. S. Y.; Brunschwig, B. S.; Lewis, N. S. High-Resolution X-Ray Photoelectron Spectroscopic Studies of Alkylated Silicon(111) Surfaces. *J. Phys. Chem. B* **2005**, *109* (9), 3930–3937.
(23) Yu, X.; Wang, X.; Zhang, Q.; Li, J.; Liu, J. Oxidation-Resistant, Solution-Processed Plasmonic Ni Nanochain-SiOx (x < 2) Selective Solar Thermal Absorbers. *J. Appl. Phys.* **2014**, *116* (7), 073508.
(24) Purkait, T. K.; Iqbal, M.; Islam, M. A.; Mobarok, M. H.; Gonzalez, C. M.; Hadidi, L.; Veinot, J. G. C. Alkoxy-Terminated Si Surfaces: A New Reactive Platform for the Functionalization and Derivatization of Silicon Quantum Dots. *J. Am. Chem. Soc.* **2016**, *138* (22), 7114–7120.
(25) Cheng, X.; Lowe, S. B.; Ciampi, S.; Magenau, A.; Gaus, K.; Reece, P. J.; Gooding, J. J. Versatile "Click Chemistry" Approach to Functionalizing Silicon Quantum Dots: Applications toward Fluorescent Cellular Imaging. *Langmuir* **2014**, *30* (18), 5209–5216.
(26) Robidillo, C. J. T.; Islam, M. A.; Aghajamali, M.; Faramus, A.; Sinelnikov, R.; Zhang, X.; Boekhoven, J.; Veinot, J. G. C. Functional Bioinorganic Hybrids from Enzymes and Luminescent Silicon-Based Nanoparticles. *Langmuir* **2018**, *34* (22), 6556–6569.
(27) Jansen, R. J. J.; Van Bekkum, H. XPS of Nitrogen-Containing Functional Groups on Activated Carbon. *Carbon* **1995**, *33* (8), 1021–1027.
(28) Johnson, S. G. National Standard Reference Data Series https://www.nist.gov/srd/national-standard-reference-data-series (accessed Sep 28, 2018).
(29) Dasog, M.; Yang, Z.; Regli, S.; Atkins, T. M.; Faramus, A.; Singh, M. P.; Muthuswamy, E.; Kauzlarich, S. M.; Tilley, R. D.; Veinot, J. G. C. Chemical Insight into the Origin of Red and Blue Photoluminescence Arising from Freestanding Silicon Nanocrystals. *ACS Nano* **2013**, *7* (3), 2676–2685.
(1) Quarta, A.; Curcio, A.; Kakwere, H.; Pellegrino, T. Polymer Coated Inorganic Nanoparticles: Tailoring the Nanocrystal Surface for Designing Nanoprobes with Biological Implications. *Nanoscale* **2012**, *4* (11), 3319.
(2) Jańczewski, D.; Tomczak, N.; Han, M.-Y.; Vancso, G. J. Synthesis of Functionalized Amphiphilic Polymers for Coating Quantum Dots. *Nat. Protoc.* **2011**, *6* (10), 1546–1553.

(3) Park, J.; Yu, M. K.; Jeong, Y. Y.; Kim, J. W.; Lee, K.; Phan, V. N.; Jon, S. Antibiofouling Amphiphilic Polymer-Coated Superparamagnetic Iron Oxide Nanoparticles: Synthesis, Characterization, and Use in Cancer Imaging in Vivo. *J. Mater. Chem.* **2009**, *19* (35), 6412–6417.
(4) Niikura, K.; Kobayashi, K.; Takeuchi, C.; Fujitani, N.; Takahara, S.; Ninomiya, T.; Hagiwara, K.; Mitomo, H.; Ito, Y.; Osada, Y.; et al. Amphiphilic Gold Nanoparticles Displaying Flexible Bifurcated Ligands as a Carrier for SiRNA Delivery into the Cell Cytosol. *ACS Appl. Mater. Interfaces* **2014**, *6* (24), 22146–22154.
(5) Veinot, J. G. C. Synthesis, Surface Functionalization, and Properties of Freestanding Silicon Nanocrystals. *Chem. Commun.* **2006**, *0* (40), 4160–4168.
(6) Dasog, M.; Kehrle, J.; Rieger, B.; Veinot, J. G. C. Silicon Nanocrystals and Silicon-Polymer Hybrids: Synthesis, Surface Engineering, and Applications. *Angew. Chem. Int. Ed.* **2015**, *55* (7), 2322–2339.
(7) Qi, L.; Gao, X. Quantum Dot−Amphipol Nanocomplex for Intracellular Delivery and Real-Time Imaging of SiRNA. *ACS Nano* **2008**, *2* (7), 1403–1410.
(8) Zrazhevskiy, P.; Sena, M.; Gao, X. Designing Multifunctional Quantum Dots for Bioimaging, Detection, and Drug Delivery. *Chem. Soc. Rev.* **2010**, *39* (11), 4326–4354.
(9) Kim, D.; Yu, M. K.; Lee, T. S.; Park, J. J.; Jeong, Y. Y.; Jon, S. Amphiphilic Polymer-Coated Hybrid Nanoparticles as CT/MRI Dual Contrast Agents. *Nanotechnology* **2011**, *22* (15), 155101.
(10) Yezhelyev, M. V.; Qi, L.; O'Regan, R. M.; Nie, S.; Gao, X. Proton-Sponge Coated Quantum Dots for SiRNA Delivery and Intracellular Imaging. *J. Am. Chem. Soc.* **2008**, *130* (28), 9006–9012.
(11) Gao, X.; Cui, Y.; Levenson, R. M.; Chung, L. W. K.; Nie, S. In Vivo Cancer Targeting and Imaging with Semiconductor Quantum Dots. *Nat. Biotechnol.* **2004**, *22* (8), 969–976.
(12) Hessel, C. M.; Henderson, E. J.; Veinot, J. G. C. Hydrogen Silsesquioxane: A Molecular Precursor for Nanocrystalline Si−SiO^2 Composites and Freestanding Hydride-Surface-Terminated Silicon Nanoparticles. *Chem. Mater.* **2006**, *18* (26), 6139–6146.
(13) Yang, Z.; Iqbal, M.; Dobbie, A. R.; Veinot, J. G. Surface-Induced Alkene Oligomerization: Does Thermal Hydrosilylation Really Lead to Monolayer Protected Silicon Nanocrystals? *J. Am. Chem. Soc.* **2013**, *135* (46), 17595–17601.
(14) Phosphate-Buffered Saline (PBS). *Cold Spring Harb. Protoc.* **2006**, *2006* (1), pdb.rec8247.
(15) Tris-Buffered Saline (TBS; 10×, PH 7.5). *Cold Spring Harb. Protoc.* **2014**, *2014* (9), pdb.rec081265.
(16) Kokubo, T.; Takadama, H. How Useful Is SBF in Predicting in Vivo Bone Bioactivity? *Biomaterials* **2006**, *27* (15), 2907–2915.
(17) Webb, L. J.; Nemanick, E. J.; Biteen, J. S.; Knapp, D. W.; Michalak, D. J.; Traub, M. C.; Chan, A. S. Y.; Brunschwig, B. S.; Lewis, N. S. High-Resolution X-Ray Photoelectron

Spectroscopic Studies of Alkylated Silicon(111) Surfaces. *J. Phys. Chem. B* **2005**, *109* (9), 3930–3937.
(18) Sudeep, P. K.; Page, Z.; Emrick, T. PEGylated Silicon Nanoparticles: Synthesis and Characterization. *Chem. Commun.* **2008**, *0* (46), 6126–6127.
(19) Yu, Y.; Hessel, C. M.; Bogart, T. D.; Panthani, M. G.; Rasch, M. R.; Korgel, B. A. Room Temperature Hydrosilylation of Silicon Nanocrystals with Bifunctional Terminal Alkenes. *Langmuir* **2013**, *29* (5), 1533–1540.
(20) Purkait, T. K.; Iqbal, M.; Islam, M. A.; Mobarok, M. H.; Gonzalez, C. M.; Hadidi, L.; Veinot, J. G. C. Alkoxy-Terminated Si Surfaces: A New Reactive Platform for the Functionalization and Derivatization of Silicon Quantum Dots. *J. Am. Chem. Soc.* **2016**, *138* (22), 7114–7120.
(21) Cheng, X.; Lowe, S. B.; Ciampi, S.; Magenau, A.; Gaus, K.; Reece, P. J.; Gooding, J. J. Versatile "Click Chemistry" Approach to Functionalizing Silicon Quantum Dots: Applications toward Fluorescent Cellular Imaging. *Langmuir* **2014**, *30* (18), 5209–5216.
(22) XPS Interpretation of Carbon https://xpssimplified.com/elements/carbon.php (accessed Nov 8, 2018).
(23) Lockwood, R.; McFarlane, S.; Rodríguez Núñez, J. R.; Wang, X. Y.; Veinot, J. G. C.; Meldrum, A. Photoactivation of Silicon Quantum Dots. *J. Lumin.* **2011**, *131* (7), 1530–1535.
(24) Park, J.-H.; Gu, L.; von Maltzahn, G.; Ruoslahti, E.; Bhatia, S. N.; Sailor, M. J. Biodegradable Luminescent Porous Silicon Nanoparticles for *in Vivo* Applications. *Nat. Mater.* **2009**, *8* (4), 331–336.
(1) Tomalia, D. A.; Baker, H.; Dewald, J.; Hall, M.; Kallos, G.; Martin, S.; Roeck, J.; Ryder, J.; Smith, P. A New Class of Polymers: Starburst-Dendritic Macromolecules. *Polym. J.* **1985**, *17* (1), 117–132.
(2) Kaur, D.; Jain, K.; Mehra, N. K.; Kesharwani, P.; Jain, N. K. A Review on Comparative Study of PPI and PAMAM Dendrimers. *J. Nanoparticle Res.* **2016**, *18* (6), 146.
(3) Sowinska, M.; Urbanczyk-Lipkowska, Z. Advances in the Chemistry of Dendrimers. *New J. Chem.* **2014**, *38* (6), 2168–2203.
(4) Islam, M. A.; Sinelnikov, R.; Howlader, M. A.; Faramus, A.; Veinot, J. G. C. Mixed Surface Chemistry: An Approach to Highly Luminescent Biocompatible Amphiphilic Silicon Nanocrystals. *Chem. Mater.* **2018**.
(5) Yang, Z.; Iqbal, M.; Dobbie, A. R.; Veinot, J. G. Surface-Induced Alkene Oligomerization: Does Thermal Hydrosilylation Really Lead to Monolayer Protected Silicon Nanocrystals? *J. Am. Chem. Soc.* **2013**, *135* (46), 17595–17601.
(6) Lin, M.; Shapiro, M. J. Mixture Analysis by NMR Spectroscopy. *Anal. Chem.* **1997**, *69* (22), 4731–4733.

(7) Celik, H.; Shaka, A. J. A New Approach for Mixture Separation Using NMR Spectroscopy: Blind Iterative Source Identification. In *2012 38th Annual Northeast Bioengineering Conference (NEBEC)*; 2012; pp 149–150.
(8) Li, X.; Hu, K. Chapter Three - Quantitative NMR Studies of Multiple Compound Mixtures. In *Annual Reports on NMR Spectroscopy*; Webb, G. A., Ed.; Academic Press, 2017; Vol. 90, pp 85–143.
(9) Park, J.-H.; Gu, L.; von Maltzahn, G.; Ruoslahti, E.; Bhatia, S. N.; Sailor, M. J. Biodegradable Luminescent Porous Silicon Nanoparticles for *in Vivo* Applications. *Nat. Mater.* **2009**, *8* (4), 331–336.